Universitá degli Studi di Palermo
Dipartimento di Chimica “S. Cannizzaro”

Dottorato in Scienze Chimiche XXIII ciclo
Settore scientifico disciplinare CHIM/03

Studio computazionale di catalizzatori nanostrutturati

IRMOF-3: indagine computazionale

Autore:
Remedios Cortese

Supervisore:
Prof. D. Duca

Coordinatore:
Prof. M. Gruttadauria

Non, rien de rien, je ne regrette rien.

Edith Piaf Non je ne regrette rien

A zio Mario amico di scienza

RINGRAZIAMENTI

Le cose terminano ed è inevitabile dover fare dei bilanci....vorrei essere seria in questa pagina ma io non lo sono, sarò precisa e testarda forse profonda...ma non seria. Quindi comincio da chi mi ha dato la possibilità di essere quì oggi in tutti i sensi: i miei genitori. Li ringrazio per tutte quelle volte che mi hanno sostenuto ma sopratutto per tutte quelle volte che mi hanno fatto notare i miei sbagli, per aver sopportato tutti i colori dei miei capelli e delle mie emozioni. Ringrazio le mie sorelle e Annarita che è come una sorella per me, per tutto ciò che mi hanno dato e sopratutto per quello che sono sicura mi daranno. Ringrazio Laura e Valentina che mi hanno accompagnato in giro per il mondo. Ringrazio tutti gli abitanti di Casa Mazzola che non so spiegare bene quanto siano stati importante nel mio divenire, quindi mi limito a dire che sono stati il mio rifugio e la mia forza anche quando ero ai confini del mondo, li ringrazio per aver sopportato tutte le transizioni del mio ego tra gli anfratti delle parole che finiscono in –ista, da nichilista ad avanguardista, insomma per avermi amato per dieci lunghi anni. Ringrazio Nerina e Teresa per aver condiviso con me i deliri quotidiani ed aver reso questa vita fatta di *segmentation fault* e *SCF confused* più sopportabile, a tal proposito non posso non ringraziare Valerio che ha quasi sempre aggiustato tutti i miei *kernel panic*. Ringrazio Odette ed Josè per essere stati la mia famiglia finlandese pur essendo venezuelani ed in particolare Odette per avermi illuminata riguardo ad alcune questioni su Gandalf. Ringrazio tutte le persone che io ritengo amiche di scienza, quelle che mi hanno insegnato ad essere curiosa nel modo giusto, quelle che mi hanno insegnato ad avere il coraggio delle proprie scelte, scientifiche e non, e quelle che mi hanno svelato che prima viene la sostanza e poi l'eleganza nelle cose. Ringrazio tutto coloro che mi ha dato ispirazione, da Dervis Fontecedro a Paul Erdös passando per Schiele. Finale con i fuochi di artificio: Ringrazio le mie due N, semplicemente per il fatto di essere parte di me, quindi in fondo in fondo ringrazio un pò anche me stessa per aver tenuto duro in tutti i momenti di sconforto. Purtroppo non tutti quelli a cui sono rivolti questi ringraziamenti potranno leggerli, perchè le cose stanno così: tutto inizia e prima o poi finisce.

SOMMARIO

La reazione di Knoevenagel consiste nella condensazione di un composto contenente un gruppo carbonilico, in presenza di una base, con una specie avente α idrogeni acidi attivati per produrre alcheni; viene impiegata nell'ambito industriale per la produzione di intermedi nella sintesi di profumi, farmaci e polimeri; è noto che la condensazione di Knoevenagel può essere catalizzata da una vasta gamma di basi e perciò viene utilizzata come reazione di testing per la basicità di un catalizzatore. Il lavoro di tesi di seguito descritto è stato incentrato sull'analisi delle proprietà catalitiche, manifestate nella reazione di condensazione di Knoevenagel, di un composto basico di nuova generazione: l'IRMOF-3 (IsoReticular Metal Organic Framework). Questo solido cristallino è il terzo membro di una famiglia di solidi ibridi organici–inorganici basati sulla medesima topologia reticolare cubica e composti da cluster di Zn_4O e leganti politopici derivanti dalla funzionalizzazione del 1,4 benzendicarbossilato. Generalmente, i catalizzatori eterogenei basici vengono sintetizzati a partire da supporti con elevata area superficiale che vengono funzionalizzati con basi organiche. La funzionalizzazione di questi solidi è però affetta da fenomeni di rilascio del gruppo chimico responsabile dell'attività catalitica e ciò ovviamente ne limita l'impiego e lo sviluppo. Alla luce di queste problematiche, la presenza di una funzionalità amminica come parte integrante della struttura cristallina dell'IRMOF-3 lo rende un buon candidato come catalizzatore eterogeneo basico. Il coinvolgimento della funzionalità amminica dell'IRMOF-3 nella condensazione di Knoevenagel è stato studiato in dettaglio in un recente lavoro sperimentale di Gascon; sulla base dei risultati è stata attribuita, in questa reazione, al gruppo amminico aromatico presente nell'IRMOF-3 un'eccezionale attività catalitica soprattutto se confrontata con quella delle comuni ammine aromatiche; ciò induce a pensare che si stabiliscano all'interno del reticolo delle interazioni che aumentano la basicità del gruppo amminico attivandone la funzione di catalizzatore nella reazione di condensazione. La tesi è stata articolata in quattro fasi che possono essere riassunte in: i) scelta di metodi e modelli, ii) caratterizzazione della struttura e della basicità del catalizzatore iii) analisi del ciclo catalitico e dei possibili meccanismi di disattivazione di questo, iv) analisi dell'effetto dei prodotti secondari del ciclo sull'attività del catalizzatore. L'interesse di questa tesi risiede non solo nelle sue implicazioni dal punto di vista chimico ma anche nelle informazioni ottenute più strettamente connesse al lavoro di modellizzazione dei materiali nanostrutturati ibridi e quindi relative all'impiego di tecniche teorico computazionali nell'analisi di sistemi

complessi di interesse catalitico. In letteratura si riportano pochi lavori riguardanti la modellizzazione delle proprietà catalitiche dei MOF, risulta dunque chiaro che questo lavoro di tesi va inquadarato in un ottica a lungo termine tesa a formulare un protocollo computazionale efficace per lo studio dei suddetti sistemi. Dal punto di vista chimico, è stato possibile ottenere molte informazioni riguardanti la reattività dei sistemi analizzati anche se la visione d'insieme, proprio perchè trattasi di sistemi alquanto complessi, non è ancora del tutto chiara. In primo luogo, sono state chiarite le origini della maggiore basicità dell'IRMOF-3, quindi sono stati formulati vari meccanismi di reazione per la condensazione di Knoevenagel fra cianoacetato di etile e benzaldeide catalizzata da anilina, dimetil–2–ammino–tereftalato e IRMOF-3 e sulla base dei risultati ottenuti si è ipotizzato che basicità e attività non siano direttamente connesse; quindi sono stati analizzati vari meccanismi di disattivazione del ciclo tra cui anche l'avvelenamento dei siti catalitici amminici, dei tre catalizzatori analizzati, da parte di prodotti secondari del ciclo. Inoltre è stato considerato il coinvolgimento nel ciclo catalitico degli atomi metallici del vertice inorganico, nominalmente saturi, ipotesi riportata in letteratura in lavori di tipo sperimentale ma mai proposta in uno studio teorico. Quest'ultima ipotesi davvero interessante non solo riporta alla mente una serie di analogie tra questi sistemi complessi e la cinetica enzimatica ma è anche oggetto di possibili sviluppi futuri della tesi di seguito esposta.

LIST OF ABBREVIATIONS

1,4 BDC	1,4 Benzendicarboxylate
2A-1,4-BDC	2-Amino-1,4-benzenedicarboxylate
AIM	Atoms in molecule
AM1	Austin Model 1
AO	Atomic Orbital
BSSE	Basis Set Superposition Error
CHelpG	CHarges from Electrostatic Potentials using a Grid
COF	Covalent-Organic Framework
CP	Coordination Polymer
CSD	Cambridge Structure Database
CSRT	Continuous–Flow Stirred Tank Reactor
DFT	Density Functional Theory
DM2AT	dimethyl 2-amino-terephthalate
DMAN	1,8-bis(dimethylamino)naphthalene
DOE	The U.S. Department of Energy
G03	Gaussian 03
GCMC	Grand Canonical Monte Carlo
GGA	Generalized–Gradient–Approximation
GTO	gaussian–type orbitals
HF	Hartree–Fock
HKUST	Hong-Kong University of Science and Technology
IB	Intrinsic Basicity
IRMOF	IsoReticular Metal–Organic Framework
KS	Khon–Sham
MD	Molecular Dynamics
MEP	Molecular Electrostatic Potential

MIL	Materiaux de l'Institut Lavoisier
MK	Merz–Singh–Kolmann charge partition scheme
MM	Molecular Mechanics
MO	Molecular Orbital
MOF	Metal–Organic Framework
MOM	Metal–Organic Material
MP2	Second order Møller–Plesset perturbation theory
MPF	Metal–Peptide Framework
ONIOM	Our own n-layered integrated molecular orbital and molecular mechanics
PA	Proton Affinity
PCP	Porous Coordination Polymers
PES	Potential Energy Surface
PFR	Plug Flow Reactor
PM3	Parametrized Model 3
QM	Quantum mechanics
RMSD	Root-Mean-Standard Deviation
RPF	Rare–Earth Polymeric Framework
SBU	Secondary–Buildings Units
SCF	Self–Consistent–Field
SWNT	Single–Walled Nanotube
TGA	Thermogravimetric Analysis
TS	Transition states
UFF	Universal Force Field
ZIF	Zeolitic Imidazolate Framework
ZPE	Zero point vibrational energy

CONTENTS

1 INTRODUCTION

> Don't get any big ideas, the're not gonna happen, you paint your smile and fill the holes. There'll be something missing just when you found it.
>
> Radiohead "Nude"

CONTENTS

1.1 WHY DO WE NEED MODELING IN CATALYSIS ?

Industrially, catalysis can be mostly subdivided into two main branches, namely heterogeneous and homogeneous catalysis. The former includes a process where the phase of the catalyst and that of the reactants and products is the same, on the contrary in the latter the phase of the catalyst and that of the reactants and products is different.

Catalysis is ubiquitous in all the industrial processes and nowadays heterogeneous catalysts in most of them are employed. The use of heterogeneous catalysts is mainly due to their easy separation from reactants and products hence to their lower environmental impact, if compared to the homogeneous one; nevertheless, homogeneous catalysts are usually more active and selective. Therefore, since the early eighties the need of recyclable catalysts has more and more encouraged research on the development of new heterogenization techniques of homogeneous catalysts [1, 2].

One of the most important employment in the industry of the heterogeneous catalysts is, without any doubts, the production of transportation fuels. Moreover, the number of processes by which fossil resources are converted into fuels and chemicals is almost endless [3]. Currently, there is a significant drive to diminish our dependence on fossil fuels and to minimize the emission of carbon dioxide. Reducing environmental impact will require entirely new catalysts, more active and selective operating in mild conditions. Indeed, nowadays there is a strong and growing effort in what is called the Bioindustrial Revolution [4]. The current goal is to design catalysts that can convert bio–based feedstocks into chemicals and fuels [5]. It is clear that

catalysis plays an important role in society today and will be a critical technology for advancing our future.

The core issue for the progress of this area is mainly related to the development of new highly selective and active catalysts and in addition the improvement of the old ones is required. Unfortunately, the microscopical processes occurring during a catalyzed reaction are not always well understood. Generally this is due to the high complexity of catalyzed processes and this implicates that even if a catalyst is active and selective, the whole molecular process is not really improvable on a molecular scale because of the lack of knowledge on the molecular working level of the catalysts. For long time catalysis has been considered nearly as a "black art" and the dominion in this corner of science was almost prerogative of experimentalists. Murray Raney, an american mechanical engineer, developer of a nickel catalyst that became known as Raney nickel, said concerning the synthesis of a catalyst: *"It is in the preparation of catalysts that the chemist is most likely to revert to type and to employ alchemical methods. The work should be approached with humility and supplication and the production of a good catalyst received with rejoicing and thanksgiving"*.

Nevertheless, with the growing of both computational performances and theoretical development the application of molecular modeling in heterogeneous catalysis research as a complement to experimental studies has grown rapidly [6]. Computational modeling has the potential to provide new insights into the reaction pathways, to predict properties of catalysts that have not yet been synthesized and to bring information for a given system from many different experimental techniques into a coherent picture [7]. Especially in this field, theory and experiment, need to be strictly connected and community of interests for both experimental results explanation and computational model validation has to be achieved. Therefore new modeling techniques must be carefully validated against experiment. The need for such molecular–level understanding is greater today than ever before with industry under increasing economic and environmental pressure to develop more precise control of catalytic processes [8].

1.2 CATALYTIC PHENOMENA: HOW TO INVESTIGATE THEM ?

Heterogeneous catalytic reactivity is controlled by the combination of intrinsic chemical reactivity and the extrinsic heat and mass transfer effects related to the catalyst morphology and reactor configuration. Considering these two phenomena uncoupled two main issues can influence the intrinsic chemical reactivity and therefore the kinetics of a catalytic system:

- nature of the complexes formed along with the interaction between the catalyst and the catalytic substrate;

- nature of the reaction environment.

The former concerns the modeling of the catalytic sites either in a Langmuir [9] or in a Taylor [10] model and is thus related to a local description of the active sites. Moreover, during the formulation of the model, the description of the active site can be both statical or dynamic. The latter deals with all the external influences as solvent, support, defects at the catalyst surface and lateral interactions between surface adsorbates.

Catalysis is a complex process and a comprehensive understanding can be achieved taking into account at least four issues that can be analyzed with a multiscale approach as showed in Figure 1:

- structural and electronic changes driving the intrinsic reactivity;
- dynamical behaviour of adsorbates on the layers and on the catalytic surface;
- kinetics of the adsorption–desorption, diffusion and reaction processes;
- fluid dynamic due to heat and mass transfer inside the reactor.

All the events described above occur on different length scales – ranging from the catalytic site (10^{-10} m) up to the size of the reactor (1 m)– and time scales – spanning from femtoseconds up to hours – therefore it is not straightforward to model a catalyzed reaction taking into account all the variables that can influence the catalytic mechanism.

In principle, macroscopic observables are directly computable solving the microscopic equations, however in practice, it will never be feasible to do this directly. Quantum mechanical calculations, even with today fastest computers, can only be carried out for hundreds of atoms and the time scales of interest are many orders of magnitude beyond current capabilities. This implies that for a whole comprehension of a catalytic process a multiscale approach is needed. Four principal categories of computation can be identified as methods to elucidate catalytic systems and everyone of these describes phenomena on a different time or length scale. The multiscale approach integrates together information from different computational techniques as:

- quantum mechanics;
- atomistic simulation and statistical mechanical theories;
- continuum engineering models.

QUANTUM MECHANICS Quantum mechanical calculations are based on the solution of the Schrödinger equation [11]. The goal of quantum mechanics (QM) based methods is to predict the structure and energy of an N–particle system, where N refers to both the electrons

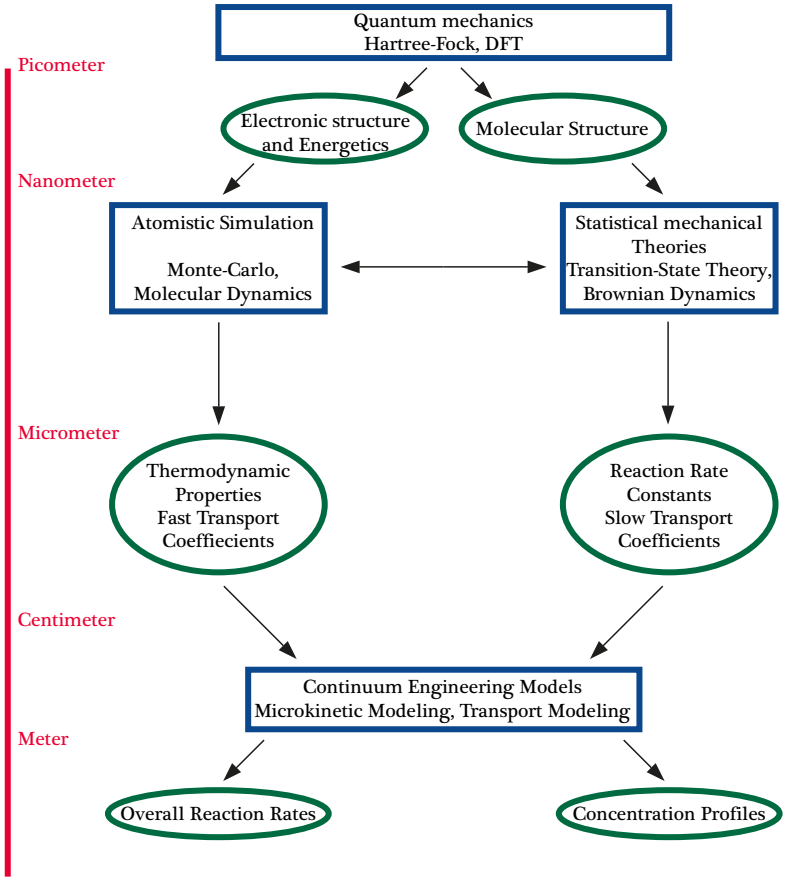

Figure 1.: Flow–chart concerning the multiscale approach designed for the analysis of catalytic processes by computational modeling techniques.

and the nuclei. Among all the possible quantum mechanical based methods ranging from semiempirical to *ab-initio* methods, those based on the density functional theory (DFT) [12] has had a strong impact on modeling heterogeneous catalytic systems [7]. The relative accuracy of DFT [13, 14] along with the size of systems that can handle make it attractive for modeling heterogeneous catalytic systems. The inferable information from this kind of analysis is related to molecular properties ranging from the geometries to the energetics and to the distribution of the electron density of the analyzed systems.

These methods can be applied in different fashion to model catalytic processes. Mainly three approaches can be identified:

- cluster models;
- embedding schemes;
- slab methods.

The former concerns the use of small atoms *ensamble* that can, in a way, be representative of the whole catalyst [15, 16, 17]; embedded cluster calculations are hybrid calculations employing both QM and Molecular mechanics based methods (MM). QM/MM or QM/QM approaches are based on the individuation of a region of the entire model suitable of an high level of theory description and other regions treated classically or with a lower level of theory [18]. The latter deals with the use of periodic calculations based codes and it is very often employed in the description of oxide and metallic surfaces [19, 20]. Information achievable employing these methods are mainly:

- activation energies;
- spectroscopic information;
- molecular description of all the species involved in a given catalytic cycle.

ATOMISTIC SIMULATION AND STATISTICAL MECHANICAL THEORIES The ability to model chemical reactions requires the full accounting of the electronic structure of the system, on the other hand modeling the atomic structure in microporous materials namely sites of adsorption, adsorption isotherms and adsorbate diffusion requires the ability to simulate much larger systems and longer time scales. This can be important in a full catalytic cycle because in addition to the events at the active site, adsorption desorption and diffusion can influence the kinetics and in some cases it is necessary take them into account.

Atomistic simulations are based on force fields and are often well suited for modeling weak interactions characterizing diffusion processes, since they are parametrized to handle such systems [21]. Dispersion, repulsion, and electrostatic forces are typically accounted,

as well as intramolecular forces such as torsion energies, for flexible adsorbates. The results depend not only on the parameter set (obtainable by experimental data or quantum mechanical calculations), but also on the assignment of atoms types to the atoms in a particular chemical environment typical of the selected force field. Atomistic simulation calculates the time–dependent behaviour of a molecular system by integrating their classical equations of motion. Molecular dynamics (MD) simulations generate information at the microscopic level, which are: atomic positions, velocities, forces [22]. The conversion of this microscopic information to macroscopic observables, such as pressure, stress tensor, strain tensor, energy, heat capacities requires theories and strategies developed in the realm of statistical mechanics. Complete isotherms are typically computed using grand canonical Monte Carlo (GCMC) simulations [23, 24]. In a GCMC simulation the volume, temperature and chemical potential are fixed, and the number of molecules in the system can change. During the simulation the average number of molecules in the system is calculated, yielding the amount adsorbed that corresponds to given gas phase conditions. Summarizing information achievable from such kind of studies can be:

- adsorption isotherms;
- heats of adsorption;
- diffusion coefficients;
- activation energy for diffusion.

CONTINUUM ENGINEERING MODEL At the longest time and length scales, continuum engineering modeling approaches such as microkinetic modeling are used to calculate reaction rates, reactant conversion, and product yields and selectivities, using model parameters predicted by the other levels of the multiscale approach. Microkinetic modeling is an ideal framework for assembling the microscopic information provided by atomistic simulations and electronic structure calculations to obtain macroscopic predictions of physical and chemical phenomena in systems involving chemical transformations [25]. The microkinetic analysis includes:

- the combination of available experimental data, theoretical principles and appropriate correlations relevant to the catalytic process in a quantitative fashion;
- a starting point usually, corresponding to the formulation of the elementary chemical reaction steps that capture the essential surface chemistry;
- a working tool that must be adapted continually to new results from experiments.

The typical parameters employed to perform a microkinetic analysis are:

- sticking coefficients;
- surface bond energies;
- pre–exponential factors for surface reactions;
- activation energies for surface reactions;
- surface bonding geometries;
- active site densities and ensemble sizes.

These parameters are described mainly within the framework of two theories able to describe the catalytic phenomenon: i) the collision theory and ii) the transition state theory. Moreover all these information have to be included within the description of the reactors. General types of ideal reactors are: batch reactor, continuous–flow stirred tank reactor (CSTR) and plug flow reactor (PFR).

The fundamental principle in microkinetic analysis is the use of kinetic parameters in the rate expressions that have physical meaning and, as much as possible, that can be estimated theoretically or experimentally. Therefore it represents a framework for quantitative interpretation, generalization, and extrapolation of experimental data and theoretical concepts for catalytic processes.

1.3 AIM OF THIS WORK

This investigation was conceived on the ground of the enormous developments in the field of synthesis and application of the metal–organic framework (MOF) compounds. Heterogeneous catalysis was one of the earliest proposed applications for MOF materials as well as one of the earliest demonstrated. Considering the lack of information in the literature about the theoretical description of the role of metal–organic frameworks involved in catalysis one of the driving idea of the whole study was to rationalize the behaviour of these new generation compounds as catalysts. This investigation was devised in a long term perspective aimed at creating a kind of computational protocol to study the MOF materials involved in catalysis. The source of inspiration was an experimental work of Gascon et. al. [26] and most of the study was aimed at understanding the role of IRMOF-3 (IsoReticular Metal–Organic Framework) as catalyst in the Knoevenagel condensation of benzaldehyde and ethyl cyanoacetate (Figure 2). Moreover this investigation includes the comparison between the IRMOF-3 behaviour and that of other basic catalysts involved in the Knoevenagel condensation. The study presented here can be summarized into five key issues:

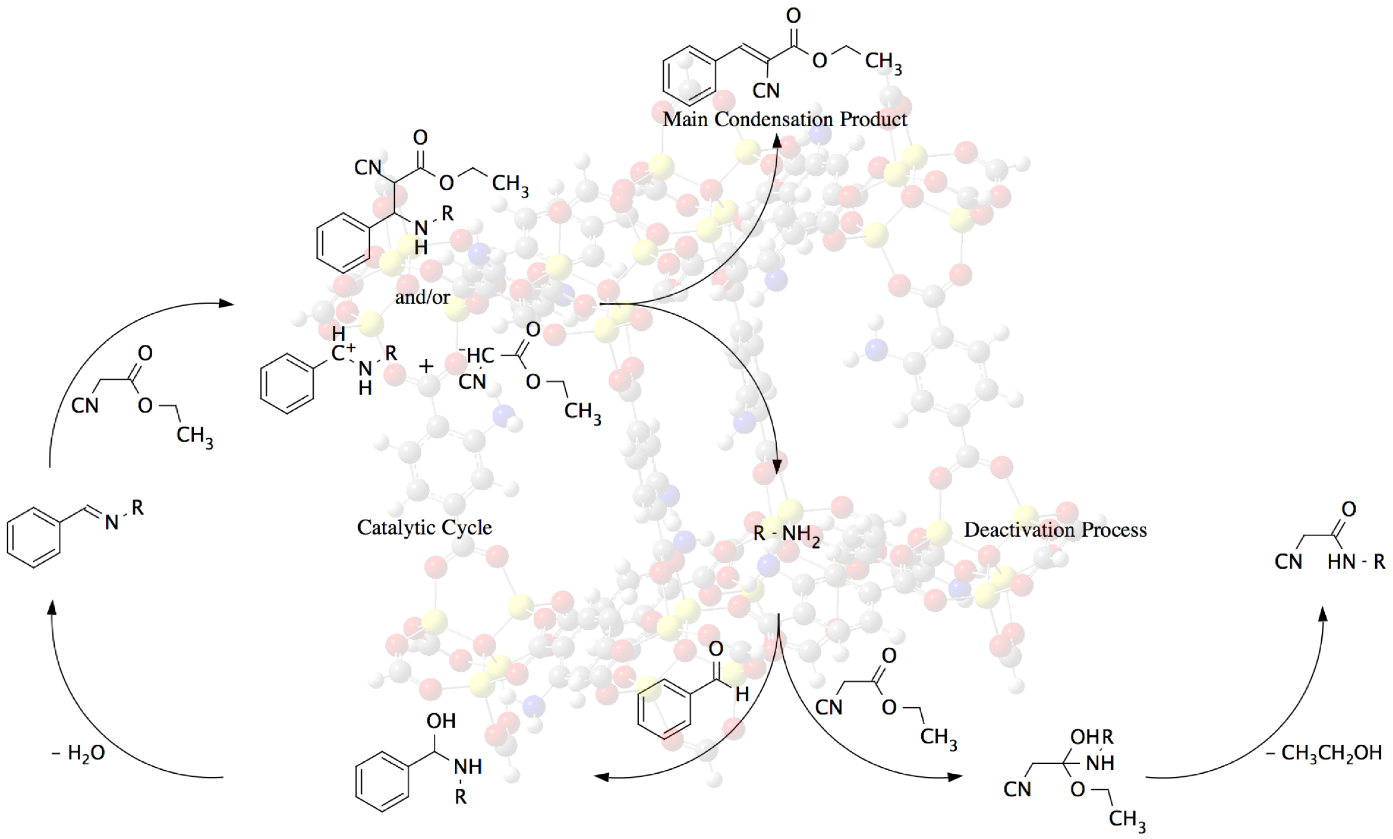

Figure 2.: Hypothesized catalytic cycle and deactivation route for Knoevenagel condensation of benzaldehyde and ethyl cyanoacetate catalyzed by IRMOF-3.

- selection of method and model for the IRMOF-3 computational description;
- evaluation of IRMOF-3 basic properties;
- analysis of kinetics of the catalytic cycle of the IRMOF-3 catalyzed Knoevenagel condensation;
- analysis of kinetics concerning the deactivation mechanism;
- analysis of the confinement effects both on the catalytic cycle and deactivation mechanism.

The elucidation of these issues would increase the understanding of the MOF role in catalysis at a molecular level and would help in predicting the performance of other similar types of catalytic systems. Beyond this introductory chapter aimed at framing the scientific context of this work, this thesis is structured as follows:

THE II CHAPTER summarizes the main features of the metal–organic framework compounds. An overall view of their peculiar application is given and the state of the art dealing with theoretical studies on the topic is presented.

THE III CHAPTER gives a short overview of the computational methods used and it includes choice of methods and models employed in this thesis.

THE IV CHAPTER deals with the investigation by computational methods of the structural features and properties of IRMOF-3. Comparisons with other aminic catalysts are presented and the energetics of the investigated catalytic cycle is reported. Moreover the kinetics and the poison and deactivation effects present in the catalytic cycle of the title system are elucidated.

THE V CHAPTER lists the main conclusions and suggestions for future investigations.

2

METAL–ORGANIC FRAMEWORKS

> On candystripe legs the spiderman
> comes softly through the shadow of
> the evening sun stealing past.
>
> The Cure "Lullaby"

CONTENTS

2.1 INTRODUCTION

2.1.1 *Linking organic and inorganic realms*

MOM (Metal–organic material) are composed by metal moieties and organic ligands and are exemplified by different groups of discrete or polymeric structures. Whereas MOMs have existed for several decades [27, 28, 29, 30, 31, 32, 33] it was not until the early 1990's that they captured broad attention as it becames evident that these materials are typically *facile* to prepare and are adaptable to crystal engineering design strategies [34, 35, 36, 37, 38, 39, 40, 41, 42, 43].

In 1989 Hoskins and Robson demonstrated that networks with predictable architectures can be engineered by a related strategy based on the interaction of metals with ligands containing multiple sites of coordination [44, 45]. Mostly, their research was based on a strategy involving coordination of linear ditopic organic molecules such as 4,4′–bipyridyl to transition metal cations [46, 47, 48]. The resulting compounds can exist as 1–periodic, 2–periodic or 3–periodic nets that are at the very least rational based upon the geometry of the node and the node:spacer stoichiometry. Since 1990's crystal engineering,

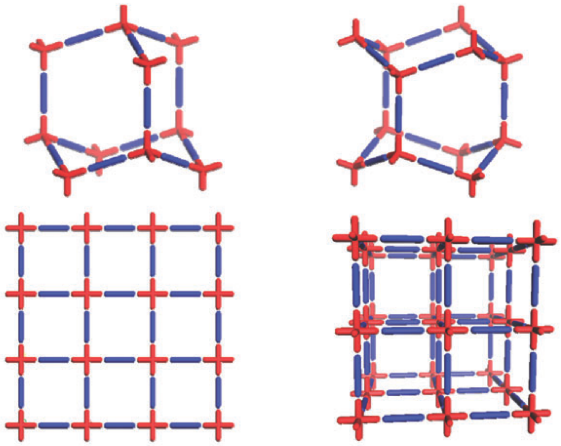

Figure 3.: Schematic illustration of the node (red) and linear (blue) approach based upon tetrahedral or octahedral metal nodes [51].

especially network based materials design, has emerged as a promising field of research. The approaches elaborated in this field were based on the "node and spacer" conceptual scheme by A. F. Wells who introduced the *idea* that inorganic crystal can be described as networks defined by metal ions (nodes) linked together via bonds (spacer) to generate coordination polymers (CP) [49, 50]. A very important concept arising from this strategy concerns the role of both the geometry and coordination environment of the nodes that establish the network topology as the spacer is only a linear connection between adjacent nodes. For instance, considering metals usually adopting the tetrahedral coordination mixed with two equivalents of a linear bifunctional ligand likely, a cubic or hexagonal diamondoid network will arise; in the same fashion a metal adopting an octahedral geometry can sustain octahedral nets or square grids as shown in Figure 3. The node and spacer approach has been remarkably successful at producing predictable network architectures. Even if in the early nineties many 3D hybrid organic–inorganic lattice were produced, most of them were not able to survive to guest exchange [52], therefore they could not cogency be considered porous compounds; this limitation widely influenced the application of these solids. Thus, one of the main goal of the crystal engineering design based research was to find 3D MOMs able to survive to guest exchange. In the late 1990's O. M. Yaghi and S. Kitagawa reported the first examples of MOMs that exhibit permanent porosity [53, 54]; these porous hybrid solids will be matter of discussion in this thesis. These materials could be considered as second generation MOMs for which Yaghi and Kitagawa coined the term metal–organic frameworks (MOFs) [55, 56], already introduced, and porous coordination polymers (PCPs), respectively [57, 58].

2.1.2 *Prediction or design of solids ?*

"One of the continuing scandals in the physical sciences is that it remains in general impossible to predict the structure of even the simplest crystalline solids from knowledge of their chemical composition" [59]. These words used by Maddox are suggestive and illustrative of one of the most pressing issue in material science and solid state chemistry. As a matter of fact, to achieve the fine properties tunability of a solid a total and direct control on the structure is needed. Indeed, the key issue for the obtaining of solids with the designed properties is the comprehension of the intimate relationship between molecular structure and properties. The crystal engineering is based on this concept.

The term crystal engineering was first coined in a contribution by G. M. J. Schmidt concerning the subject of organic solid state photochemistry [60]. In this work he implicitly assumes that in appropriate circumstances crystal could be thought as a sum of a series of molecular events rather than the results of the need to "avoid vacuum". A useful modern definition is that provided by G. R. Desiraju, who in 1988 defined crystal engineering as *"the understanding of intermolecular interactions in the context of crystal packing and the utilization of such understanding in the design of new solids with desired physical and chemical properties"* [61]. To achieve specificity in the solid design strategy it is necessary to understand the fundamentals controlling processes between molecular units resulting into the formation of frameworks. Concerning this, the concept of molecular self–assembly is primal as the physical process relying on the constitution of solids designed by the crystal engineering.

CP and hydrogen bonded structures with multiple complementary components can be regarded as being the consequence of modular self–assembly. By the way, it should be remembered that the final aim of structure prediction according to Hawthorne is: i) predict the stoichiometry of the stable compounds, ii) predict the bond topology, iii) calculate, given the bond topology, accurate static and dynamic properties of the crystal [62]. Regarding this it is important to stress that crystal engineering is still not crystal structure prediction; in fact as stated by Zaworotko *"the raison d'etre and strategies of crystal engineering are somewhat different from those of crystal structure prediction since the former is primarly concerned with design and, although more restrictive in terms of molecular components that might be employed is becoming increasingly synonymous with the concept of supramolecular synthesis of new solid-state structures"* [51].

With the discovery, by Yaghi and his research group, of the permanent porous MOFs, the broad concept of crystal engineering was recast and the new concept of reticular synthesis arose. According to Yaghi crystal engineering is a term which has mutated over the years

	MOF-5	$Zn(L)_2(ClO_4)_2$
Joint(SBU)	Polyatomic (Zn_4O)	Monoatomic (Zn)
Framework	Neutral	Charged
Pores	Can be empty	Must contain counterions
Zn-X bond to break per SBU	12	4
Energy to excise SBU kJ mol^{-1}	2200	400-600

Table 1.: Some distinctions between a typical MOF (MOF-5) and a typical CP ($Zn(L)_2(ClO_4)_2$). L is N,N′-bis-(4-pyridil)urea [65].

and which is rather broadly defined, on the contrary the concept of reticular synthesis is more precise because it concerns the logical approach to the synthesis of robust materials with predesigned building blocks, extended structures, and properties [63]. Thus, it might be considered as a subclass of crystal engineering.

2.1.3 *Nomenclature*

In most of his papers Yaghi points out some clarification concerning the name and the classification of metal–organic materials. As a matter of fact, for a long time metal–organic compounds were classified vaguely; various names for the identification of these kind of solids can be found in the literature like MOFs, CPs, hybrid inorganic–organic materials and organic zeolites analogues. Each term was coined in order to emphasize some characteristics respect to others and was used in an interchangeable way. The term CP is the most general and was applied to all those compounds formed by a metal center and an organic linker capable to realize extended connections and, according to Yaghi, no particular relevance with this term is assigned to the resultant topology of the extended solid. Whereas MOF is a name that identify a solid with peculiar characteristics: i) strong bonds, which characterize robust networks, ii) linkers, which can undergo post-synthetic changes and iii) well defined geometric structures [64]. Some relevant differences between CPs and MOFs are reported in the Table 1 and these distinctions are enough important, according to Yaghi, to assign a different name to MOFs [65]. Very often to indicate a MOF a descriptive name is used; usually it consists of an acronym followed by a number that represents the chronological order of preparation of the compound. The acronym can be indicative of i) the type of components of the materials, like in the series MOF-n (Metal–Organic Framework) [66], COF-n (Covalent-Organic Framework) [67], RPF-n (Rare-Earth Polymeric Framework) [68], or MPF-n (Metal–Peptide Framework) [69] ii) the type of structure, like in the series ZIF-n (Zeolitic Imidazolate Framework) [70] or iii) the laboratory

in which the material was prepared, like for instance the series MIL-n (Materiaux de l'Institut Lavoisier) [71] or HKUST-n (Hong-Kong University of Science and Technology) [72]. A systematic terminology has been proposed to rationalize the known structures, and it is based on the structure of the crystalline nets adopted by the material [73, 74]. These 3D nets are represented by either a three-letter symbol (as in sod, rho, gis etc.) or a three–letter symbol with an extension (such as in pcu-c or bcu-k). This methods allows one to describe and classify the known structures as well as new potential MOF structures as a function of their net topology.

However, there is no consensus in the scientific literature about the definitions of the terms CP and MOF. As reported above some authors suggest definitions based on chemical bonding others propose that the terms CP and MOF are synonyms. An IUPAC project was initiated in 2009 to address the terminology issues in this area and will deliver its final report in the current year (2011).

2.2 STRUCTURAL FEATURES

The Cambridge Structure Database (CSD) reports the crystal structures of more than 11,000 extended metal–organic compounds in which a metal ion or cluster has been linked by an organic moiety in which the linking functionality is a cyanide, pyridyl, phosphate or carboxylate. Of these nearly 3,000 compounds have 3D structures and about 6,000 have 2D structures.

A large variety of metal atoms (alkaline, alkaline–earth, transition, rare–earth and main group metals) in their stable oxidation states, have been successfully used in the synthesis of MOFs. Depending on the metal and its oxidation state, coordination numbers can range from 2 to 7 giving raise to various geometries, which can be linear, T- or Y-shaped, tetrahedral, square-planar, square-pyramidal, trigonal-prismatic, pentagonal bipyramidal and the correspondent distorted forms.

In order to synthesize crystalline porous stable MOFs, rigid conjugated aromatic molecules are usually preferred over flexible ones as organic components or linker. The most widely used linker are polycarboxylates aromatic molecules, bipyridines and polyazaheterocycles and their derivatives [75]. Organic linkers provides to the resulting network a high degree of chemical and structural properties, that can be selected during the design process of the solid in order to achieve predetermined properties. Depending on the connector and on its coordination number, periodic chains, arrays and nets are obtainable; thus the periodicity can be tuned according to the choice of the metal. The framework structure is, thus, controlled by the number of bonds involving the bridging linker and the coordination number of the

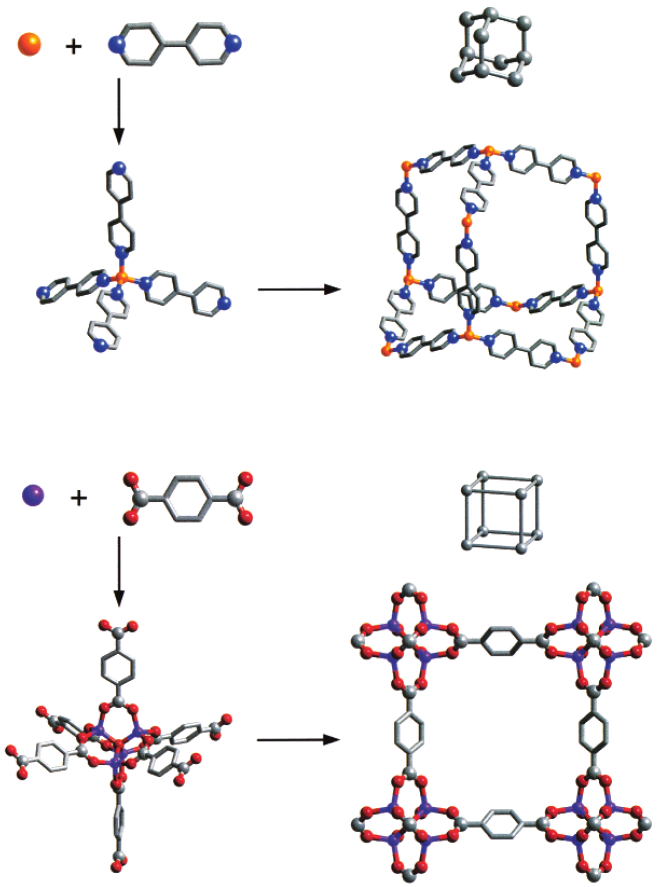

Figure 4.: Exemplification of an expanded metal–organic framework and a decorated expanded framework [64].

metal. Therefore, the remarkable properties of linker and connectors are the coordination numbers and coordination geometries.

The research on metal–organic frameworks address mainly two key issues: i) to understand which topologies, depending on the reaction environments, are preferred ii) to design robust and permanent porous networks. The *a priori* synthesis of structures from simply a metal and an organic linker is very difficult because ions do not have directional information and this lack of directionality is the reason of a high flexibility around the metal ion and a lack of control on the resulting structure. Instead of a naked metal ion, the use of metal–complex connectors have the advantage of offering control of the bond angles and restricting the number of coordination sites; indeed sites that are not required can be blocked by either chelating or macrocyclic ligands that are directly bound to a metal connector, and thus leave specific sites free for linkers [76]. This concept is well demonstrated comparing frameworks containing as linker $4,4'$–bipyridine and other containing carboxylates. Synthesis of open framework by assembly of metal ions with di-, tri-, and polytopic N-bound organic linkers produced

many cationic framework structures but the attempt of remove guests molecules determines the collapse of the framework; whereas the use of carboxylate results in robust decorated expanded frameworks permanent porous because of the multiple coordination to the metal as shown in Figure 4 [77, 78]. Which framework topology can be expected to form is of extremely importance because the number of possible structure for each geometrical shape is very high and predictability of the framework is one of the ultimate goal of the research on MOFs. For example, more than 100 different topologies are possible for linking tetrahedral building blocks together into structure with just one kind of vertex. Recently Yaghi and co–workers stated that generally only a small number of simple high symmetry structures would be expected to commonly form and they call them default structures [63, 79].

2.2.1 *Secondary–Buildings Units*

General lack of control over the structure of solids produced through the traditional synthetic methods is directly related to the fact that the reactants do not retain their structure during the assembling process. The design of robust extended network can be realized by starting with well–defined and rigid molecular building blocks that will retain their structural integrity throughout the construction process. The concept of secondary–building unit (SBU) is indispensable in order to classify and design the directionality of MOFs [65]. SBUs are simple geometric figures representing the inorganic cluster or coordination spheres that are linked by the organic components to form the framework; the reticulation of SBUs involves self–assembly steps able to connect building units into molecular lattices by very strong bonds. Due to this, there is a direct connection between starting molecular units and resulting frameworks. A hierarchy of information is incorporated into the building blocks that make them sufficiently unique for the construction of a target network. Two essential elements of this approach are i) the knowledge of the possible networks that could be formed based on a given building block and ii) the determination of the geometric attributes that uniquely define the network targeted for the design. In principle, it is, therefore, possible to tune the MOFs growth processes hence their reticular topologies, designing and employing SBUs, formed by metal clusters and organic ligands (see Figure 7). The achievement of a well designed open framework starting from a particular SBU relies both on its rigidity and directionality of bonding. Metal–containing namely cationic SBUs are not isolable entities, and so it has been essential to establish the exact chemical conditions that will determine the formation of a specific SBU *in situ* [80]. In order to individuate the shape of the SBU in a given metal–organic frameworks, the overall shape adopted by its points of extension has to be considered. For instance, the carboxylate carbon atoms, as illustrated

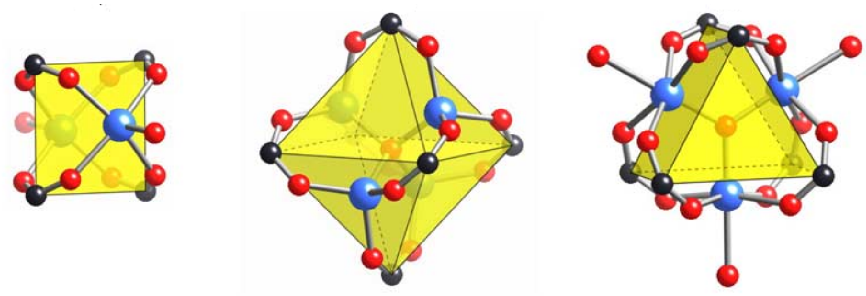

Figure 5.: Inorganic SBUs commonly occurring in metal–carboxylates include the square "paddle–wheel", with two terminal ligand sites, the octahedral basic zinc acetate cluster, and the trigonal prismatic oxo–centered trimer, with three terminal ligand sites [80].

in Figure 5, form respectively a square, an octahedron and a trigonal prism. The SBUs are reticulated into metal–organic frameworks by linking the carboxylate carbons with organic units, but may also be linked by replacement of the terminal ligands. It is important to illustrate also the *caveat* perspective of Biradha dealing with the nature and the role of SBUs. He states that in the case of MOFs there is no experimental evidence that SBUs are synthetic intermediates during the growth of a crystalline phase [81]. Due to such limitations, the role of SBUs should be limited to the understanding of the topology of a given architecture rather than be extended to their use in the synthetic design strategy. Regarding this, Ramanan and Whittingham proposed that MOFs are formed by point zero charge molecules as true building units and the topology of the resulting solid should be rationalized on the ground of these real building units [82].

2.2.2 *Non–carboxylated based MOFs*

The carboxylate and pyridyl based compounds represent the most studied family of MOFs and also the study reported here concerns carboxylate based MOF but for the sake of completeness there will be briefly described also metal–organic compounds based on phosphonate, porphyrin and zeolitic imidazolate frameworks.

POSPHONATES Phosphonate ligands present some difficulties due to the i) formation of simple phosphonate structures as dense layered materials, ii) the rapid precipitation of the phosphonate phase as not ordered phase, iii) the complexity of the phosphonate coordination chemistry. Nevertheless these ligands are attractive to prepare interesting compounds with different structures and properties [83]. The organo phosphonic acids generally require mild synthetic conditions to form the metal–phosphonates therefore many researchers have been interested into the formation of frameworks based on this linker. The first three dimensional metal–phosphonate with one dimensional chan-

nels have been observed in b—Cu—(O_3PCH_3) [84]. Phosphonate framework structures are now known with a variety of transition metals , p–block elements as well as lanthanide elements [85, 86, 87, 88, 89, 90].

PORPHYRINS Porphyrins are well suited as building units because of their rigidity and the large possibilities of functionalization. Moreover, the opportunity of accommodating different metal ions inside the porphyrin ring open up the feasibility of tuning the electronic behaviour of these extended structures. The use of meso–tetraarylporphyrins, such as the meso–tetra (4–pyridil) porphyrin, as ligands resulted in a number of porphyrin based metal–organic compounds with 3D structures [91, 92, 93]. Particularly notable is the tetra (4–carboxyphenyl) zinc porphyrin moiety, which was used in the formation of a nanoporous solid with nanosized channels (1.5 nm) [94]. Multiporphyrin assembly based on interlinked arrays of tetra (4–carboxyphenyl) zinc porphyrin and 4,4′–bipyridyl ligands were also synthesized resulting in an open three–dimensional framework in which the individual metalloporphyrin units are cross–linked both axially as well as equatorially by ion–pairing interactions, metal–ligand coordination and hydrogen bonding. This lattice is fully sustained by specific intermolecular interactions and not by virtue of van der Waals forces. This solid presents a zeolite–like framework which is crossed by wide channels in two perpendicular directions [95].

IMIDAZOLATE Traditionally microporous solids have been associated with aluminosilicate zeolites. Between all the metal–organic compounds recently developed, ZIF based structures have attracted much interest due to their unusual thermal and chemical stability. These solids are constructed from tetrahedral metal ions (usually Zn^{2+} and Co^{2+}) bridged by imidazolate (Im). Interestingly, the angle M-Im-M is similar to the Si–O–Si angle (145°), this analogy has led to the synthesis of a large number of ZIFs with zeolite–type tetrahedral topologies (Figure 6) [96]. ZIFs present permanent porosity and high thermal and chemical stability therefore these solids are ideal platforms for performing useful organic transformations under strong reaction conditions. In the last years more than 90 new ZIF structures has been reported and now it is also possible to make ZIFs with topologies previously unknown in zeolites, in addition to mimicking known structures. The exceptional robustness of their frameworks and the reproducible nature of their synthesis has led to a series of isoreticular materials with controlled pore metrics. Among the novel synthesized ZIFs, two of them are very attractive because of their uncommon structures and properties: ZIF-95 and ZIF-100. These ZIFs have immense and complex cages in particular the most notable aspect of the ZIF-100 structure is a giant cage with 264 vertices assembled from 7524 atoms: 264 Zn, 3604 C, 2085 H, 26 O, 1030 N and 515 Cl.

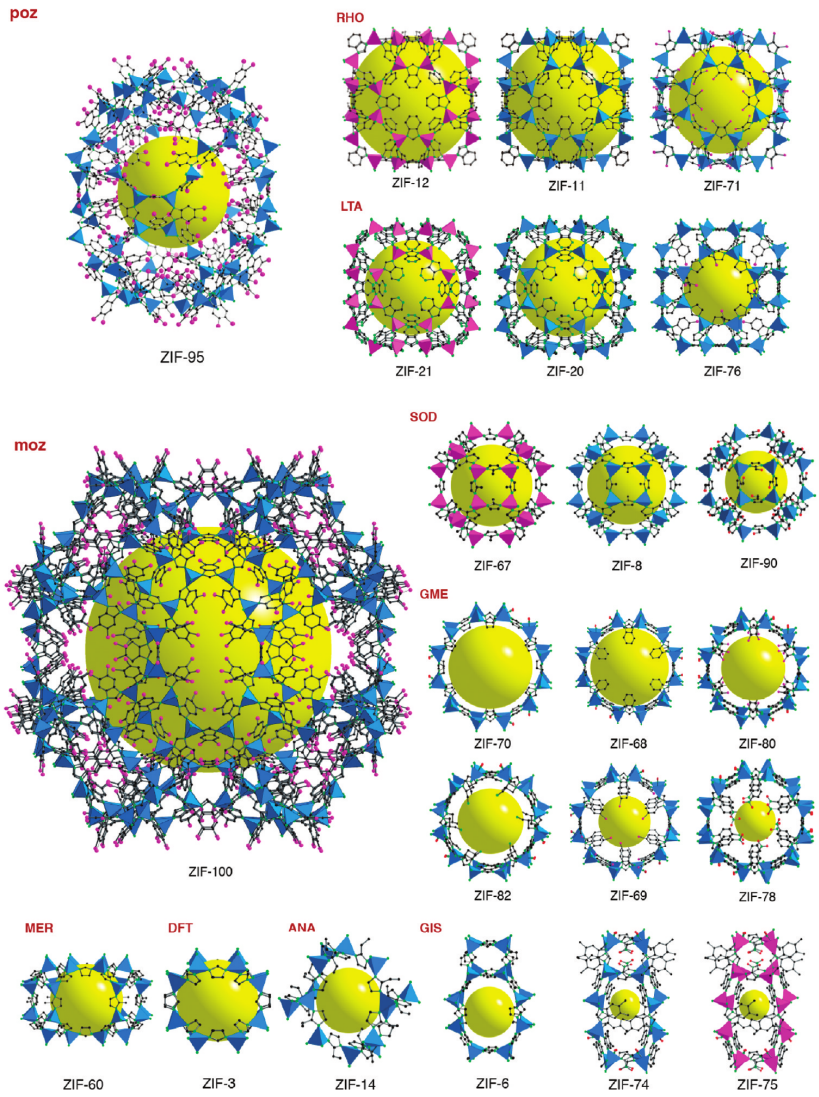

Figure 6.: Crystal structures of ZIFs grouped according to their topology. The largest cage in each ZIF is shown by ZnN_4 blue and CoN_4pink polyhedra. The yellow ball indicates space in the cage [96].

The outer and inner sphere diameters measure 67.2 Å and 35.6 Å respectively; in comparison the corresponding distances in the faujasite supercage of zeolite are 18.1 Å and 14.1 Å and the diameter of C_{60} is 10.5 Å [97].

2.2.3 *Carboxylate based MOFs*

Without any doubt among the linkers that can be used in the synthesis of metal–organic frameworks, the most promising and employed are the carboxylates. The use of multidentate carboxylate functionalities was addressed to chelate metal ions and lock them into rigid and thus directional metal–oxygen–carbon clusters, with the points of

extension defining geometrical shapes referred to as SBUs (Figure 7). Design of frameworks based on these kind of SBUs is fruitful in

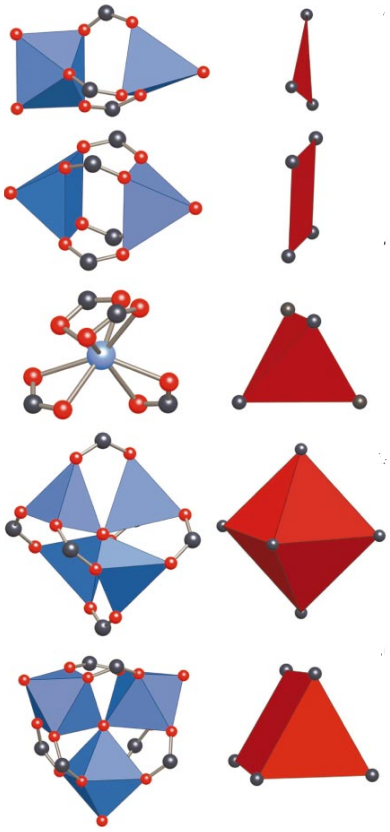

Figure 7.: Examples of SBUs for carboxylate MOFs [63].

order to accomplish rigid and permanent porous solids. The use of rigid carboxylates yielded neutral, non interpenetrated networks that were shown to retain crystallinity during desorption and resorption of guest molecules. As observed by thermogravimetric analysis (TGA) these compounds present decomposition temperatures in a range in between of 300 – 500°C [80]. The strength of these frameworks arises from the metal–carboxylates bonds and clearly from the presence of geometrically defined clusters due to chelation and bridging properties of carboxylates.

Carboxylates, currently used in synthesis are bidentate and tridentate linkers and the respective derivatives. Typically, preparation of carboxylated MOFs is performed combining the metal salt with the acid form of the organic carboxylate at room temperature under aerobic or under solvo(hydro)thermal conditions. The use of triethylamine as noncoordinating base for the deprotonation of the carboxylic acid was shown to be critically important in achieving 3D porous framework [98]. It was in fact reported that the use of both solvent and–or deprotonating agents needed for the formation of the carboxylates

from the carboxylic acids results in 1D and 2D structures while the formation of a 3D framework is prevented.

In the review of Tranchemontagne et al. [65] 131 different geometries for carboxylates based SBUs, their connectivity and their composition can be found. For sure, among all these SBUs the two most representative examples of carboxylates based SBUs are the square paddle–wheel and the octahedral shaped clusters.

The former is one of the most common SBU formed by metals and carboxylates; two metal atoms are bridged in a syn–syn fashion by four carboxylates as in the second SBU example of Figure 7. The square SBU is generated *in situ* by the combination of four carboxylates with two cations such as Cu^{2+}, Zn^{2+}, Fe^{2+}, Mo^{2+}, Rh^{2+}. In most examples, heteroatom containing ligands are on the apical positions. A typical example of paddle–wheel complex is copper (II) acetate hydrate, in which four acetate–anions are each coordinated as dimonodentate ligands to two copper (II) ions forming the D_{4h}-symmetry structure having the shape of a paddle–wheel with four blades, in axial position of which the molecules of water are coordinated [99, 100]. The similar construction employing different bridging carboxylates are known for nearly all metal ions in periodic system [101]. For metal of the 5–th and 6–th periods the paddle–wheel structures with lowered symmetry are also known. The symmetry lowering to C_{2v} and D_{2h} can arise, for instance, when two different bridging ligands are used for constructing the paddle–wheel geometry [102] whereas C_{4v} SBUs will occur if the axial ligands are not equivalent or if the oxidation states of metal ions are different [103]. For lanthanides even higher lowering of the symmetry can occur due to the increase of the coordination sphere characterizing these ions. 1D, 2D and 3D arrangement with paddle–wheel based SBUs are known [104]. The occurrence of a structural periodic arrangement based on this SBU is strictly related to the linker fashion employed in connecting two SBUs. For instance if two SBUs are connected by a 1,4 benzendicarboxylate (1,4 BDC) molecule it is straightforward to note that the squares individuated by the SBUs are related by simple translations. Continuation of this structure with the same link produces the 2D periodic planar structure as shown in the Figure 8 [76]. For instance, MOF-2 and MOF-46 are solid based on the combination of linear linker and paddle–wheel SBUs. If linkers are distorted, different structural organization will occur. Depending on the bent in the plane of the original linker, different periodic organization of linked paddle–wheels will arise as shown in Figure 8.

The octahedral SBU, as shown in the fourth SBU example of Figure 7, has the structure of the basic acetate zinc [105, 106, 107]. This consists of a single O atom bonded to four metal atoms to form a M_4O tetrahedron. The edges of the tetrahedron are capped by carboxylates to form the octahedron. This structure has been observed for Zn, Co

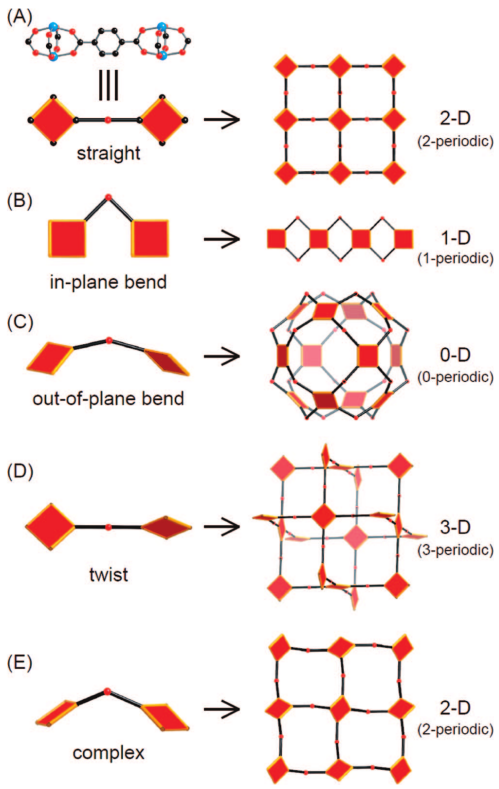

Figure 8.: Schematic representation of ditopic organic links connected between two square paddle–wheels on the left and the corresponding expecting default structures expected to results employing organic links with the appropriate angles between two squares [76].

and Be. Based on this arrangement a large number of metal–organic frameworks are known but MOF-5 is surely one of the most representative and studied; its synthesis was first reported in a letter to Nature in 1999 by Yaghi and co–workers [98]. The synthesis, as also stated by the authors, was achieved by borrowing ideas from metal carboxylate chemistry, where an inorganic dicarboxylate linker is used in a reaction that gives supertetrahedron clusters when capped with monocarboxylates. The tetranuclear supertetrahedral cluster motif is adopted by a number of metal–carboxylates where combination of Zn^{2+} and the appropriate carboxylic acid yields the oxide center cluster as a distinct and well defined unit. As suggested by the authors the structure may be derived from a simple cubic six–connected net in two stages: first the nodes of the net are replaced by cluster of SBUs; second, the linker of the net are replaced by finite rods of BDC molecules. This solid presents a cubic porous lattice, consisting of Zn_4O tetrahedra linked by 1,4 benzenedicarboxylate (1,4-BDC) groups, and as SBU the octahedral $Zn_4O(CO_2)_6$ moiety. This structure is synthesized from a solution of Zn^{2+} and 1,4-BDC acid under conditions that generate the tetrazinc cluster *in situ*. After the identification of the synthetic conditions necessary for the generation of the SBU a

series of 16 isoreticular metal–organic frameworks were produced in crystalline form. MOF-5 became the first member of a IRMOFs family where each member shares the same cubic topology [108]. IRMOF lattices are based on Zn_4O clusters and polytopic linkers derived by functionalizing the 1,4-BDC moieties as shown in Figure 9. By using different 1,4-BDC derivatives it is possible to obtain frameworks with equal topology but different pore sizes and, as a consequence, different chemical properties; this family is unique because is the only instance where a very high level of control has been exerted in molecular–based solids.

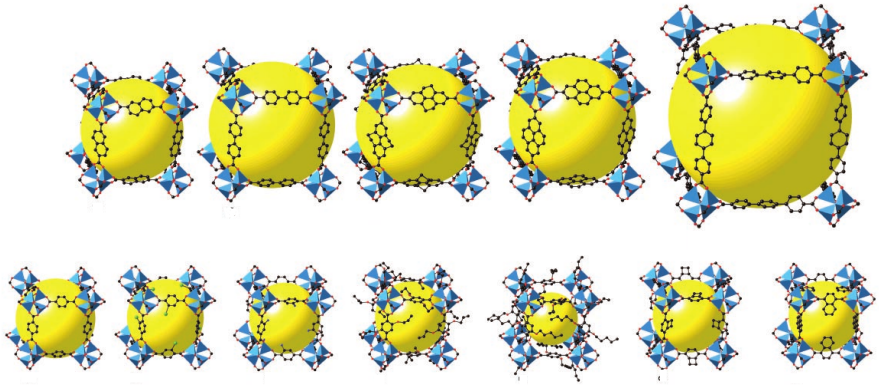

Figure 9.: Family of Iso-Reticular MOF-5 Frameworks. The large yellow spheres represent the largest van der Waals spheres that would fit in the cavities without touching the frameworks [108].

2.3 PROPERTIES

MOFs have been recognized to be very promising materials in different fields because of their high versatility. This characteristic is due to the unique structural features of these solids that, in principle, allow to design and synthesize them depending on the target application. These new class of porous compounds with variable reticular topology, have shown potential use in many fields and consequently their application as gas carriers, sensors, molecular sieves and catalysts has been suggested in the recent literature. Three main issues are considered as obstacles in metal–organic frameworks synthesis: i) stability ii) permanent porosity and ii) interpenetration. All these problems are limiting in their applications. Nevertheless, among all the synthesized MOFs a large part of them show stability in respect of the loss of the solvent guest and therefore permanent porosity; moreover, nowadays a high control on the phenomenon of interpenetration has been reached.

2.3.1 *Adsorption*

To establish the attainment of permanent porosity after guest removal, as stressed by Yaghi, the measurement of gas isotherms is indispensable [80]. The measurement of nitrogen or argon isotherms allows to calculate the apparent surface areas of these materials, typically assuming Langmuir-type coverage. As shown in Figure 10 through the design of solids by reticular synthesis it is possible to improve desired properties; this exemplify the high control on the structure that it is possible to obtain with the rational approach of reticular synthesis.

Microporous metal–organic frameworks are promising candidates for gas storage applications because they can be synthesized in high purity and at low cost, high crystallinity and potentially large quantities [109, 110, 111, 112, 113]. MOF materials has been proposed to be active in methane, hydrogen and carbon dioxide storage. All these applications have unquestionable impact on different aspects of our life. Methane storage by adsorption is important as an alternative to compressed natural gas storage for natural–gas–powered vehicles, while effective removal of CO_2 from the flue exhaust of power plants is undoubtedly a challenge and in addition it is widely accepted that the most crucial goals for hydrogen transportation application involve hydrogen storage. MOFs seems to be well suited in order to be apply in these research areas especially thanks to i) their large apparent surface area and ii) their flexibility with which chemical functionalization and molecular–level fine–tuning can be achieved for optimized uptake capacities.

Uptake of methane was studied for the IRMOFs [108]. IRMOF-6 was the first solid studied because of the exceptional high surface area and the appropriate designed aperture for methane storage. It was found that this solid has a methane uptake of 240 cm^3 at 298 K and 36 atm. The uptake was evaluated also for other member of the Iso-reticular family namely IRMOF-1 and IRMOF-3, under the same conditions, and it was found to be lower than that of IRMOF-6. The difference in the uptake value, as suggested by the authors, relies in the linkers. The fundamental concept of solid design outstands clear in this findings, in fact changing the linker and retaining the same topology it is possible to improve the desired property.

The U.S. Department of Energy (DOE) has established a series of targets of hydrogen storage for automotive applications [116]. The 2010 goals for system gravimetric and volumetric densities were 6 wt % and 45 kg H_2 m^{-3}; the ultimate targets are more demanding at 9 wt % and 81 kg H_2 m^{-3}. Rosi et al. [109], first proposed hydrogen storage in MOFs, they reported the hydrogen adsorption in IRMOF-1 at 78 K and 298 K. The highest pressures investigated were about 0.75 bar at 78 K, with a reported uptake of 4.5 wt% and 20 bar at 298 K

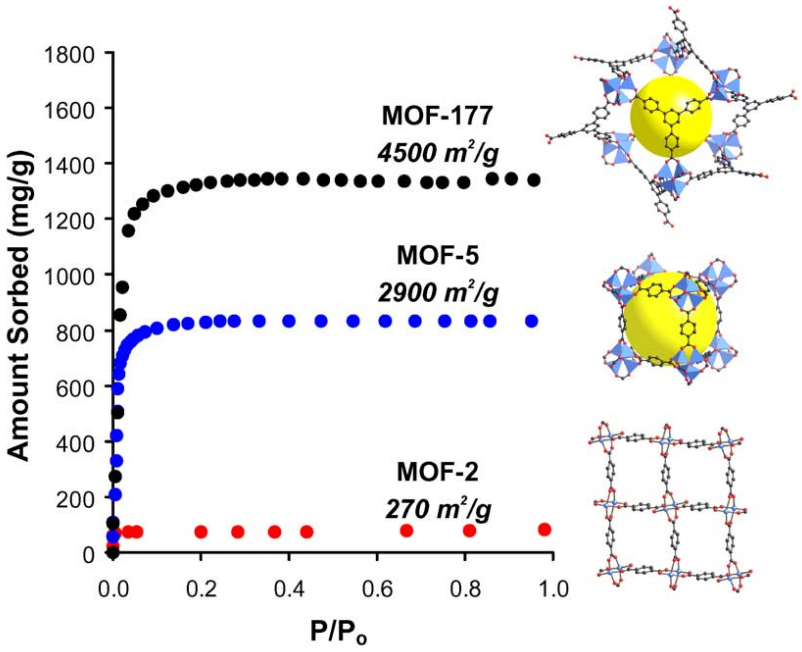

Figure 10.: MOFs have displayed impressive increases in their apparent surface areas since the measurement of the first low temperature isotherm for these materials [98, 114, 115]. The nitrogen adsorption isotherms were measured at 77 K and display Type I behaviour, as expected for compounds with uniform micropores [80].

which gave about 1 wt %. They include in their study also the effect due to the change of the linker with the investigation of IRMOF-6 and IRMOF-8. They demonstrated that the change in linker leads to an improvement in the uptake, to a level of 2.0 wt % in IRMOF-8 at 293 K and 10 bar. Roswell et al. [117], reported H_2 uptake in five different MOF materials and the largest uptake was about 1.5 wt % at 77 K and 1 atm. While these values are far short of the DOE targets, they are larger than adsorption reported for typical activated carbons and some reports of hydrogen storage on SWNTs (Single–Walled Nanotubes). Even if the measured uptakes are far from the desired targets, the most relevant inference related to these studies was the evidence of the feasible improvement of the uptake capacity by tuning the structural features.

The first attempt to employ MOF in CO_2 removal was reported in 2005 by the group of Yaghi [118]. Various compound were tested in order to examine a range of structural and porous attributes. Among the investigated solids, IRMOF-177 was the most effective in CO_2 removal. However the discovery of ZIFs made them more suitable candidates in order to capture CO_2 [119]; in fact, the main industrial applications of ZIFs are related to their exceptional uptake capacities for CO_2 [96]. These solids are also very selective towards CO_2. It was reported the examination of a series of ZIFs (ZIF-68, -69, -70, -78, -79,

-81, -82, -95, -100) for their potential to separate CO_2 from CH_4, CO, O_2 and N_2. The CO_2 adsorption isotherms of ZIF-68, -69, and -70 show steep uptakes in the low pressure regions indicating a high gas affinity [97]. Some uptake capacity comparison were carried out also between MOFs and ZIFs and these studies have been shown that ZIFs have a higher affinity for CO_2, indeed at 298 K and 1 atm, IRMOF-177 has a maximum uptake of 7.60 L/L CO_2 while ZIF-69 has a capacity of 82.6 L/L CO_2 [120]. These findings, the flexibility with which ZIF structures can be made and functionalized coupled to their stability, make these compounds very attractive not only in capturing carbon dioxide but also in transforming it into a fuel.

2.3.2 *Catalysis*

One of the first proposed application of MOFs was catalysis [121]. Intuitively, due to their peculiar features MOFs could be thought as a bridge between homogeneous and heterogeneous catalysis. MOFs catalytic potential has been also compared to enzime catlysis by Lee et al. [122]. However, in spite of the outstanding textural properties and high metal contents of MOFs, their use in catalysis has been very limited up to now.

MOFs have been identified as very promising heterogeneous catalyst candidates, considering that i) they may contain any organic functional groups, ii) their post–synthetic functionalization may consistently be performed and iii) their functional groups may, in principle, be spread without undergoing leaching phenomena on very different, but always large, surface areas. One of the most employed, and in some fashion useful, comparison has been that of MOFs and zeolites. This association arises because of the community of relevant catalytic features between these two crystalline porous solids. Both of them have large internal surface area and uniform pore and cavity sizes; however, they differ mainly in three important points: i) MOFs contain also organic species and therefore they can be synthesized in a larger variety than zeolites, ii) MOFs are not as stable as zeolites while iii) many MOFs exhibit permanent microporosity after solvent evaporation, others collapse when solvent is removed. MOF–based catalysis was proposed 20 years ago and demonstrated nearly 15 years ago but only recently there has been an extensive experimental research; this because of the lack of a well established procedure for MOFs synthesis; however, during the years a more aware knowledge about MOFs structural features and synthesis protocol has been gained. Among the possible application of MOFs in the field of catalysis at least: i) heterogenization of well–defined homogeneous catalysts [123], ii) framework stabilization of otherwise short-lived catalysts [123], iii) framework encapsulation of molecular catalysts [124], iv) coupling of catalysis to chemical separations – demonstration of adventitious

catalysis by nominally coordinatively saturated nodes (metal ions or cluster)– [121], v) post-synthesis incorporation of catalytic metal sites [125, 126, 127] and iv) substrate–size–selective catalysis have been demonstrated [128]. It has to be point out that literature about the catalytic properties of MOFs is still not very founded.

In all MOFs compounds, three different parts can be clearly differentiated: i) the metallic component ii) the organic ligand and iii) the pore system. It is, therefore, possible to think three different types of catalysts as suggested by Corma and co–workers based on MOFs and in practice, all of them have been described in the literature [129].

The first group of MOF based catalysts includes materials with only a type of metal centre, which is involved at the same time as structural component and as catalytic active site. Other MOFs belonging to the same class can contain two different types of metal: one of them is responsible for the catalytic activity, while the second has only a structural role and it is not directly involved in the catalytic process. The active metal can be both a single metal atom or a metal cluster. One of the earliest report about the catalytic activity of a MOM was a study of Fujita et al. in 1994 dealing with the cyanosilylation of aldehydes by a 2D MOF of formula $Cd(4,4'-bpy)_2(NO)_3$ [121]. The active sites are Cd (II) ions, with Lewis–acid catalysis. Other important examples reported in this field are those of Llabrés i Xamena et al. concerning the catalytic activity of a 2D square grid MOM containing single Pd (II) ions as nodes and 2-hydroxypyrimidinolates as linkers [130]. Despite initial coordinative saturation, the palladium centers in this MOM proved capable of catalyzing alcohol oxidation, olefin hydrogenation, and Suzuki C–C coupling. Ravon et al. reported the catalysis by MOF-5 of the Friedel–Crafts alkylation ascribing the catalytic activity probably to the Zn_4O vertices [131]. Up to now MOFs with metal catalytic active sites have been investigated in different reactions such as: hydrogenation, isomerization, cyanosilylation, polimerization, oxidation and enantioselective epoxidation. For a comprehensive list of reactions catalyzed by MOMs and MOFs see reviews [122, 129]

The second group of MOF based catalysts have functional groups in the organic linkers that are able to catalyze a given reaction. It is important that the linker employed in the construction of the MOF present both the coordinative groups ensuring the structural stability and the reactive group which is responsible of the reactivity. The number of MOFs belonging to this category with demonstrated catalytic activity is untill now very limited. This lack can be explained considering that metal atoms tend to coordinate all the reactive organic groups and these prevent the possibility of a free reactive organic group inside a solid. Seo et al. reported in 2000 the first example describing the catalytic activity of a MOF containing ligands with reactive groups. This compound was synthesized by Zn^{2+} and a chiral molecule containing carboxylic acid and a pyridine group; the author showed that

the resulting solid was active in the transterification reaction because of the presence of uncoordinated pyridyl groups [132]. Gascon et al. have studied the basic properties of IRMOF-3 and MIL-53(NH_2) [26]. Both materials contain 2–amino-1,4–benzenedicarboxylate (2A–1,4–BDC) as the organic linkers which coordinated to the metal ions only through the carboxylic oxygen atoms, thus leaving free the amino group. IRMOF-3 was found to be an active and stable catalyst in Knoevenagel condensation. Catalytic activity due to the linker can also arise after a post–synthetic modification. These kinds of modifications occur transforming the linker without changing the topology of the solid.

The third group consists of solids not directly involved in catalysis. In fact, the porous system of the material provides physical space where the catalysis occurs or act as a cage where the catalytic centers are encapsulated. Fischer and co–workers have studied the inclusion from the vapor phase of a series of ten organometallic compounds inside the MOF-5 [133]. Under *vacuum* and dry argon, it was observed that both the crystal structure and the organometallic moieties remain unchanged after the inclusion. Once the organometallic compounds are incorporated, it is possible to generate small metal nanoparticles in a weakly coordinating environment. These naked nanoparticles are highly reactive and extremely air sensitive.

2.4 COMPUTATIONAL MODELING

It is widely accepted that computational chemistry has a sound impact in the elucidation of structure and properties of materials and processes. With respect of this, it is in the following reported a selection of works that summarize topics of interest and that recall seminal works in the field.

Molecular simulations had and still have a strong impact on the research of meso–, micro–, and nanoporous materials [134]. Investigations dealing with diffusion and adsorption properties of molecules within the pores helped in understanding the transport and binding mechanism on a macroscopic level. Numerous theoretical investigations have been performed on structure, properties and catalytic activity of porous compounds as, for instance zeolites, using periodic DFT calculations [135, 136]. In accordance with that, periodic QM methods are thus well suited in order to analyze MOFs solids and according to Tafipolsky et al. neither the variability nor the flexibility of MOFs pose a principle problem [137]. Nevertheless for a first principle treatment of a general MOF still a substantial computational effort is needed. All periodic plane–wave based DFT investigations focused on static properties, with the two exceptions of the work by Mueller et al. [138] and Mulder et al. [139] who performed short first principles MD simulations of hydrogen in the 106 atom primitive cell

of MOF-5. Civalleri et al. have used MOF-5 as benchmark to test their implementation to calculate second derivatives of the atomic coordinates within the periodic QM code CRYSTAL, which uses atom centered basis functions. Moreover they compared the periodic MOF-5 with non–periodic cluster models using an exactly identical level of theory and a very important inference arises from this investigation: non–periodic clusters can well be employed to model the periodic system. Agreement between the bond lengths and bond angles from their calculations tend to be within 1.5 % of those observed from experiment [140].

Gao [141] and Braga et al. [142] have examined clusters representing portions of IRMOF-1, establishing that geometric aspects of these clusters agree well with experimental data for the full material when appropriate basis sets are chosen. Other examples of cluster calculations for MOFs include the analysis of linker groups of IRMOF-3, -6, -8, -12, -14, -18, and -993 [143], linkers of IRMOF-2 and -3 [142] and fragments of IRMOF-105 [144].

Most of the computational studies present in the literature dealing with MOFs concerns the study of gas adsorption on them *e.g.* H_2 [145] and CO_2 [146, 147]. The main attention was addressed to the possibility of using MOF as hydrogen carriers [148]. The related works can be divided into three broad categories: i) studies useful for predicting adsorption energies and favorite sites in the interaction with hydrogen [145], ii) studies aimed at determining the maximum amount of hydrogen that MOF can store [149], iii) studies devoted at evaluating hydrogen diffusion into MOF [150]. The H_2 adsorption sites in MOFs are very often analyzed by quantum mechanical calculations either wave-function and density functional based methods. Hydrogen storage capacity can be predicted in these porous materials using CGMC simulations [151, 152]. Moreover kinetic properties of H_2 can be predicted by MD simulations. Below seminal works dealing with QM methods applications will be recall more in detail.

The first study reported on the issue of hydrogen adsorption in MOFs was the investigation of Hüber et al.; in this paper the analysis is focused on the H_2 interaction with the aromatic system and second order Møller–Plesset calculations (MP2) [153] were performed [154]. The key point of this study was the relationship between adsorption strength and size of the aromatic system; in fact, they demonstrated that the adsorption energy between the hydrogen molecule and the aromatic system increases according to the dimension of the benzene–like system. Similar works were reported by Sagara et al. and Hamel and Côtè [155, 156]. Sagara et al. reported a study where the interaction of H_2 with both the organic linker as well as with the $Zn_4O(HCO_2)_6$ cluster were considered. Using the MP2 methodology they showed that the zinc oxide cluster has a higher H_2 binding energy than the organic linker. After 2005, several MP2 or DFT works on H_2 interaction with

organic linkers of various MOFs were reported. The DFT application to MOF-5 crystal, as recalled above, was tried by Mulder et al. and Mueller et al. They, indeed, showed that the strongest interactions with hydrogen are located near the Zn_4O clusters although they reported different H_2 binding energies to the Zn_4O clusters [138, 139]. Recently it was reported by Sillar et al. a study concerning the hydrogen adsorption by using a MP2:DFT hybrid scheme; this paper also contains an accurate overview about the current status of knowledge on the binding energy of hydrogen in MOF-5 [157].

Beyond hydrogen, also larger guest molecules in MOFs have been studied with periodic QM calculations. Devi et al., as an example, have accurately reproduced the experimental crystal structures of the zinc 2,6-naphthalene host framework (isostructural with MOF-105) using periodic DFT Generalized–Gradient–Approximation (GGA) energy minimizations, allowing both the atomic coordinates and the lattice parameters to change [158]. By calculating the binding energies of various aromatic hydrocarbons within the MOF, they were able to explain the selectivity of the crystallizing structure for the uptake of p-xylene compared to other xylene isomers. Hamel et al. showed, on the basis of static geometry optimizations within the periodic DFT–GGA, that MOF-5 can be utilized as a rigid host matrix for the encapsulation of C_{60}, and that in this way the density of states of a fullerene crystal can be finely tuned [159].

To our knowledge only few papers have been up to now published, which concerned modeling of catalytic properties. It is interesting to recall i) that of Choomwattana et al. [160], in which it was employed a combination of a high-level method, DFT–GGA, and a generic force field, UFF (Universal Force Field), in order to elucidate the mechanism of the carbonylene reaction occurring between formaldehyde and propylene encapsulated in MOF-11 and ii) that of Braga et al. [161],in which a conformational analysis of protonated cyclo-[(S)–phenylalanyl–(S)–histidyl] and its complex with benzaldehyde (C_6H_5CHO) within MOFs is carried out.

3

METHODS AND MODELS

> And we would go on as though nothing was wrong. And hide from these days we remained all alone. Staying in the same place, just staying out the time.
>
> Joy Division "Transmission"

CONTENTS

3.1 COMPUTATIONAL DETAILS

All the quantum mechanical calculations were performed by the Gaussian 03 (G03) suite of programs [162, 163]. Pure QM and hybrid QM/QM calculations were carried out on different IRMOF-3 and IRMOF-1 models reported in Figure 11 and 12. QM/QM calculations were performed within "our own n-layered integrated molecular orbital and molecular mechanics" (ONIOM) approach [18, 164]. DFT [13, 14] was employed, as higher level, and either AM1 (Austin Model 1) [165] or PM3 (Parametrized Model 3) [166, 167], as lower levels. In the following, the hybrid applications are collectively indicated as QM/QM and singularly as DFT/AM1 and DFT/PM3 approach. Pure QM calculations were also run within the DFT paradigm, being BP86 [168, 169], B3LYP [170, 171] and MPWB1K [172, 173] the tested functionals of exchange and correlation. Irrespective of the considered pure or hybrid applications, when the DFT paradigm was employed, Zn atoms were described by the basis set LANL2DZ [174, 175, 176], with an effective core potential for the inner electrons and its associated double-ζ basis set for the outer ones and the $6-31G(d,p)$ basis set [177, 178] was utilized for the H, N, C and O atoms. Each optimized structure was further characterized by subsequent frequency calculations, employing the vibration analysis within the harmonic approximation [163] and the basis-set scheme described above, thus obtaining even a full characterization of the transition state

(TS) species, involved in the investigated reactions. The DFT energy values here reported have been always corrected for the zero point vibrational energy (ZPE) contribution. Frequency calculations allowed us to evaluate also thermochemical properties of interest for the title system. Wherever the acronym BSSE (Basis Set Superposition Error) is reported it means that the Boys and Bernardi method has been used to correct the interaction energy [179].

3.2 BENCHMARK CALCULATIONS ON IRMOF-1

The model-size for IRMOF-3 and the theoretical methods employed in this investigation were chosen based on the results obtained for IRMOF-1 models reported in Figure 11a and Figure 12a12b. This was possible because the structures of these systems share the same reticular topology and their SBUs present analogous geometrical shape. The only difference is related to the presence in the IRMOF-3 of 2A-1,4-BDC moieties instead of the 1,4-BDC ones, which characterize the IRMOF-1 derivatives, see Figure 11b and Figure 12c. All the benchmark calculations were carried out on the IRMOF-1 models because in the literature a larger amount of structural experimental data about this porous solid can be found. Inferences reported below deal with i) the size of the models and ii) the theoretical methods employed in this investigation.

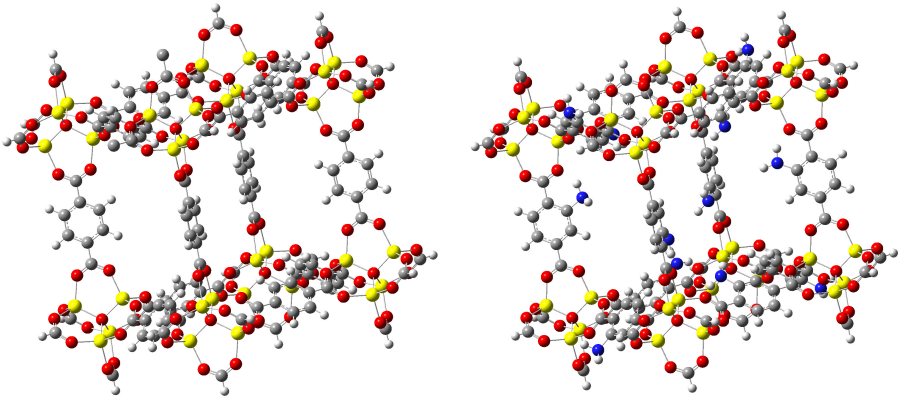

(a) IRMOF-1 (b) IRMOF-3

Figure 11.: Optimized IRMOF-1 (model 11a) and IRMOF-3 (model 11b) cubic fragments; these are formed by carbon atoms (grey), oxygen atoms (red), nitrogen atoms (blue), hydrogen atoms (white), zinc atoms (yellow); models 11a and 11b both contain, as corners, Zn_4O tetrahedral units saturated by formate moieties and, as edges, respectively, 1,4-BDC and 2A-1,4-BDC moieties. Details on corners and edges are given in Figure 12.

Considering the findings illustrated by Civalleri et al. [140] and inferring that only a small portion of the framework influences the

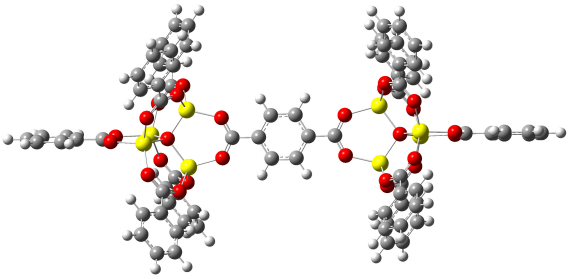

(a) *b*-1,4-BDC

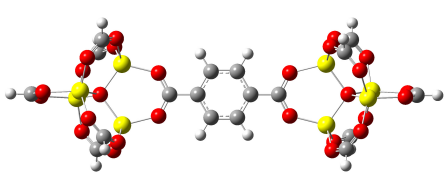

(b) *f*-1,4-BDC

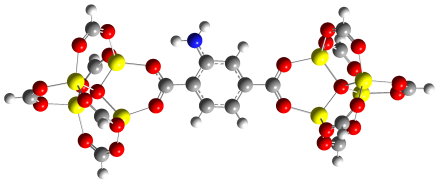

(c) *f*-2A-1,4-BDC

Figure 12.: Optimized IRMOF-1 (models 12a and 12b) and IRMOF-3 (model 12c) moieties; they contain, as corners, Zn_4O tetrahedral units saturated by benzoate (*b*-derivatives) or formate (*f*-derivatives) groups and, as mid residuals, either 1,4-BDC or 2A-1,4-BDC.

electronic properties of the catalytic site, it was assumed that a cluster treatment of the framework could be representative of the local properties of the solid [16, 180, 181]. As a consequence, differently sized fragments were initially cut out from the IRMOF-1 lattice and optimized, in order to find the most favorable ratio between reliability of the method and computational cost. Smaller IRMOF-1 models (moieties 12a and 12b), formed by one 1,4-BDC unit linked to two tetrahedral ZnO_4 units, saturated by benzoate (model 12a: *b*-1,4-BDC) or formate (model 12b: *f*-1,4-BDC) groups, were optimized at DFT level employing the three functional of exchange and correlation cited above. Whereas, in order to take into account confinement effects eventually produced by the lattice, the QM/QM approach described in section 3.1, was applied to optimize the IRMOF-1 fragment of Figure 11a. The model system and the real system for the QM/QM calculation within the ONIOM paradigm employed in the study are shown in Figure 13. Root-Mean-Standard Deviation (RMSD) analysis of IRMOF-1 structural parameters (selected parameters are shown in Figure 14), obtained comparing computational values and neutron-diffraction results obtained at 3.5 K [182] was employed to select models and calculation methods. Taking into consideration the *b*-1,4-BDC and *f*-1,4-BDC models it was found that the RMSD for the considered distances and angles was not sensitive to the size of the models, therefore the model with the minimum size that obviously is the less expensive in terms of computational costs was selected. Regarding the choice of the functional of exchange and correlation all

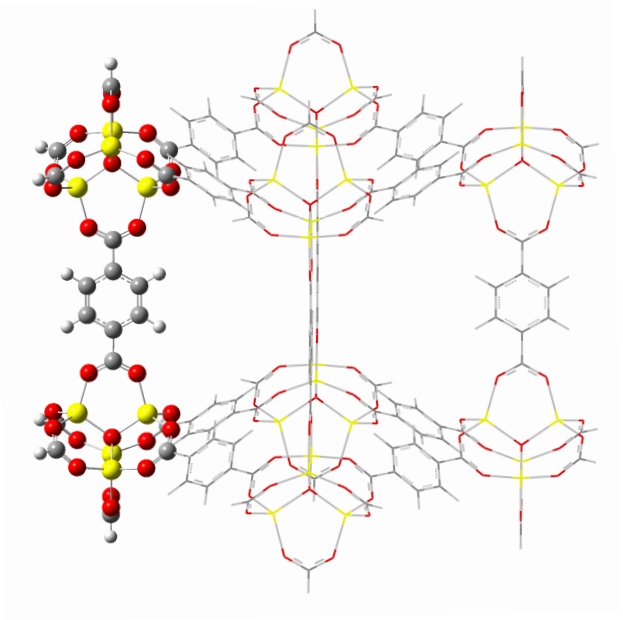

Figure 13.: IRMOF-1 cubic cell. Selected model and real systems within the ONIOM approach. The model system is reported in ball and stick whereas the rest of the model has been considered as real system.

the analyzed functionals were able to give results in the same range of accuracy for distances and angles (B3LYP 2/pm – 1.2/°, MPWB1K 1/pm – 1.2/°, BP86 2/pm – 0.7/°), however, the calculations with the BP86 were appreciably faster therefore this functional was employed in all the DFT calculation.

The QM/QM ONIOM higher level, in the treatment of the largest IRMOF-1 model, was selected according to the previous finding and therefore the calculation was performed at BP86 level of theory. The chosen model system for the ONIOM approach was one *f*-1,4-BDC moiety framed in the cubic cell of IRMOF-1 as shown in Figure 13. The DFT/AM1 and DFT/PM3 RMSD evaluations addressed to prefer PM3 with respect of AM1 as lower level in the same QM/QM ONIOM treatment. In fact, the RMSD distance and angle values for the IRMOF-1 fragment resulted 130 vs. 4pm and 3.4 vs. 0.08°, using AM1 and PM3 semi-empirical level, respectively.

3.3 IRMOF-3 MODELS

Hence, for the following catalytic applications, *f*-derivatives and BP86 were always taken into consideration as IRMOF-3 running models and DFT functional, respectively. In particular, the smallest IRMOF-3 model (model 12c: *f*-2A-1,4-BDC), successively optimized at BP86 level, was obtained inserting one amino group in the 1,4-BDC unit, present in the BP86 optimized *f*-1,4-BDC model, while the largest IRMOF-3 model, see Figure 11b, successively optimized at DFT/PM3

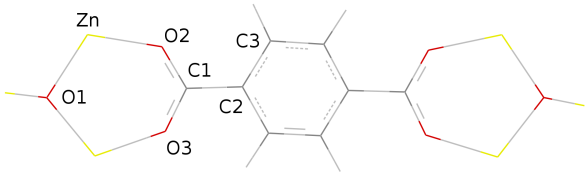

Figure 14.: Structural parameters employed for the RMSD analysis of the IRMOF-1 models, namely used for individuating the calculation level further exerted in the IRMOF-3 applications; distances and angles taken into consideration, respectively, were: O1–Zn, O2–Zn, O2–C1, C1–C2, C2–C3, and Zn–O2–C1, O2–C1–O3, O2–C1–C2, C1–C2–C3.

level, was obtained substituting, in the DFT/PM3 optimized IRMOF-1 model, all the 1,4-BDC edges by 2A-1,4-BDC edges and placing the amino groups of neighboring edges each other at the largest possible distance. Hereinafter, the largest model is named IRMOF-3c. A final

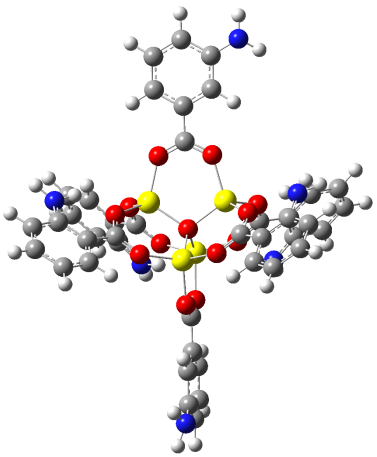

Figure 15.: Model 2A-B containing a Zn_4O cluster saturates with 2-amino benzoate moieties.

model identified as 2A-B and simulating a corner fragment of IRMOF-3 was also considered (Figure 15). This model was selected in order to investigate the interaction of a water molecule, byproduct of the catalytic cycle, with a Zn atom of the inorganic vertex.

3.4 CHARACTERIZATION OF IRMOF-3

Considering the experimentally proved basic properties of the IRMOF-3, a computational study aiming at characterizing these features of the investigated solids was performed. Here below will be recall the theory behind the quantities employed as descriptors of the basicity in the following of this investigation. Theoretical backgrounds dealing with Proton Affinity (PA), Intrinsic Basicity (IB) and charge partitioning

schemes will be reported, moreover some additional information concerning the calibration of the method will be provided.

3.4.1 *Proton Affinity and Intrinsic Basicity*

The reliability of the BP86 functional of exchange and correlation was benchmarked with the structural features of the investigated system. Moreover other benchmark calculation were needed in order to state the reliability of the selected functional of exchange and correlation towards the calculation of the properties chosen in order to describe the basicity of the analyzed catalyst. Proton Affinity and Intrinsic Basicity were selected as descriptors of the basicity of the title system. These two quantities are the opposite, respectively, of the enthalpy and Gibbs free energy-differences, occurring along with a given base (B) protonation, as represented in the following:

$$B + H^+ \rightarrow BH^+ \qquad [1]$$

The used standard PA and IB expressions are detailed below:

$$PA = \frac{5}{2}RT - [\Delta E_{SCF} + \Delta E_{vib}] \qquad (3.1)$$

$$IB = PA + T\Delta S^\circ \qquad (3.2)$$

Referring to the base protonation above, ΔE_{SCF} is the optimized self–consistent–field (SCF) energy-difference while ΔE_{vib} is the ZPE difference that includes the temperature corrections to the vibrational enthalpy while the $\frac{5}{2}RT$ term takes into account the translational energy of the proton that includes the $\Delta(PV)$ energy bit. Finally, ΔS° evaluates the standard entropy difference, being the standard entropy of the proton, having mass m, defined as in the following:

$$S^\circ(H^+) = R\left\{\frac{3}{2}\ln\left(\frac{2\pi m}{h^2}\right) + \frac{5}{2}\left[1 + \ln(kT)\right]\right\} \qquad (3.3)$$

Considering the lack of experimental data concerning PA and/or IB for the IRMOF-3, the molecules involved in the benchmark calculations concerning the reliability of the selected theoretical method with respect of the calculation of basic porperties were all containing nitrogen moieities namely ammonia, methylamine, dimethylamine, trimethylamine, pyridine and aniline. For all these molecules experimental data of PA are available. Second-order Møller-Plesset [153] perturbation theory calculations – as implemented in the G03 program package [183, 184] – were carried out to study proton affinity of the nitrogen containing moieties. The values obtained within the DFT were compared with those calculated at a MP2 level of theory in order to test the reliability of the PA results obtained with the BP86. The RMSD calculated between the PA experimental values and respectively the

quantities calculated by DFT and MP2, results in 22 and 30 kJmol^{-1}. It is conclusively underlined that BP86 does stand comparison also with MP2 methods, showing to be more performing in calculating PA values for the analyzed containing nitrogen molecules .

3.4.2 *Population Partition schemes*

The concept of a partial atomic charge is ambiguous because within the framework of quantum mechanics the atomic partial charge is not a quantum mechanical observable. Many different decompositions have been proposed, each leading to a different definition of the atom in the molecule. These methods can be broadly divided into two categories:

- separation of one particle density matrix in the Hilbert space;
- separation of the electron density in real space.

There is no universally agreement upon the "best" procedure for computing partial atomic charge. Mulliken population analysis [185], Löwdin population analysis [186, 187], Morokuma analysis [188] and natural bond orbital analysis [189] belong to the first class. Whereas the second class includes Hirshfeld population analysis [190], as well as atomic decomposition schemes based on the topology of the electron localization function of Becke or molecular electrostatic potential [191]. The method of atoms in molecule (AIM), as proposed by Bader [192] was originally formulated as belonging to the second class, but it can also be formulated as a "generalized population analysis" because the characteristics functions of the AIM regions are projectors; in this sense it is AIM in both classes. Below the three population partition schemes, namely Mulliken, Merz–Singh–Kolmann (MK) [193] and CHelpG (CHarges from Electrostatic Potentials using a Grid) [194] employed in this work are detailed.

MULLIKEN SCHEME This method involves a direct partioning of the molecular wave function into atomic contributions, following a orbital-based scheme. It was the first scheme ever proposed and is based on the concept that electrons can be divided up amongst the atoms according to the degree to which different atomic AO (Atomic Orbital) basis functions contribute to the overall wave function. Expanding the wave function in its AO basis set:

$$\begin{aligned} N &= \sum_{j}^{electrons} \int \psi_j(\mathbf{r}_j)\psi_j(\mathbf{r}_j)\partial\mathbf{r}_j \\ &= \sum_{j}^{electrons} \sum_{r,s} \int c_{jr}\phi_r(\mathbf{r}_j)c_{js}\phi_s(\mathbf{r}_j)\partial\mathbf{r}_j \\ &= \sum_{j}^{electrons} \left(\sum_{r} c_{jr}^2 + \sum_{r\neq s} c_{jr}c_{js}S_{rs} \right) \end{aligned} \tag{3.4}$$

where r and s are index of the AO basis function ϕ, c_{jr} is the coefficient of basis function r in MO j and S is the overlap matrix defined as:

$$S_{ij} = \int \phi_i\phi_j\partial\mathbf{r} \tag{3.5}$$

Electrons associated with only a single basis function should be thought as belonging entirely to the atom on which that basis function resides. For electrons "shared" between basis functions, Mulliken suggested that one might divide the former between the two atoms on which basis functions r and s reside. This corresponds to divide the basis functions up over k atoms to compute the atomic population so as to compute the atomic population N_k becomes:

$$N_k = \sum_{j}^{electrons} \left(\sum_{r\in k} c_{jr}^2 + \sum_{r,s\in k, r\neq s} c_{jr}c_{js}S_{rs} + \sum_{r\in k, s\notin k} c_{jr}c_{js}S_{rs} \right) \tag{3.6}$$

The Mulliken partial atomic charge is then defined as

$$q_k = Z_k - N_k \tag{3.7}$$

where Z is the nuclear charge and N_k is computed according to Eq. 3.6.

CHELPG SCHEME The degree to which a positive or negative test charge is attracted to or repelled by the molecule is represented by a quantity that can be computed exactly for any position $\mathbf{r}$, the V_{MEP}

$$V_{MEP}(\mathbf{r}) = \sum_{k}^{nuclei} \frac{Z_k}{|\mathbf{r}-\mathbf{r_k}|} - \int \psi(\mathbf{r}')\frac{1}{|\mathbf{r}-\mathbf{r_k}|}\psi(\mathbf{r}')d\mathbf{r}' \tag{3.8}$$

This assumes no polarization of the molecule in response to the test charge. The Molecular Electrostatic Potential (MEP) is an observable, although in practice it is rather difficult to design appropriate experiments to measure it. The MEP is pheraps the most obvious property to reproduce if one wants partial atomic charges that will be useful in

modeling molecule. MEP charge fitting schemes involve determining atomic partial charges q_k that when used as monopole expansion according to

$$V_{MEP}(\mathbf{r}) = \sum_{k}^{nuclei} \frac{q_k}{|\mathbf{r} - \mathbf{r_k}|} \tag{3.9}$$

minimize the difference between the value calculated by Eq. 3.9 and the correct one obtained by Eq. 3.8. Typical alghoritms select a large number of points spaced evenly on a cubic grid surrounding the van der Waals surface of the molecule. In the CHELPG (CHarges from ELectrostatic Potentials using a Grid based method) scheme by Breneman and Wiberg [194], atomic charges are fitted to reproduce the molecular electrostatic potential (MEP) at a number of points around the molecule. As a first step of the fitting procedure, the MEP is calculated at a number of gridpoints spaced 3.0 pm apart and distributed regularly in a cube. The dimensions of the cube are chosen such that the molecule is located at the center of the cube, adding 28.0 pm headspace between the molecule and the end of the box in all three dimensions. All points falling inside the van-der-Waals radius of the molecule are discarded from the fitting procedure. After evaluating the MEP at all valid grid points, atomic charges are derived that reproduce the MEP in the most optimum way. The only additional constraint in the fitting procedure is that the sum of all atomic charges equals that of the overall charge of the system.

MK SCHEME In the MK scheme by U. C. Singh and P. A. Kollman [193], atomic charges are fitted to reproduce the MEP at a number of points around the molecule. As a first step of the fitting procedure, the MEP is calculated at a number of gridpoints located on several layers around the molecule. The layers are constructed as an overlay of van der Waals spheres around each atom. All points located inside the van der Waals volume are discarded. Best results are achieved by sampling points not too close to the van der Waals surface and the van der Waals radii are therefore modified through scaling factors. The smallest layer is obtained by scaling all radii with a factor of 1.4. The default MK scheme then adds three more layers constructed with scaling factors of 1.6, 1.8, and 2.0. After evaluating the MEP at all valid grid points located on all four layers, atomic charges are derived that reproduce the MEP as closely as possible. The only additional constraint in the fitting procedure is that the sum of all atomic charges equals that of the overall charge of the system.

4

RESULTS AND DISCUSSION

> We passed upon the stair, we spoke in was and when. Although I wasn't there, he said I was his friend. Which came as a surprise, I spoke into his eyes.
>
> David Bowie "The man who sold the world"

CONTENTS

As already recalled, Gascon et al. [26] during the study concerning the Knoevenagel condensation, found a lower activity of aniline with respect of the corresponding aniline–like groups of IRMOF-3. This phenomenon should be related both to electronic and steric effects, influencing the chemistry of the aromatic aminic moieties framed in the IRMOF-3 structure. In order to deepen this issue and to find local correlations between placement and reactivity of the catalytic sites, it was preliminarily studied how the basicity of the catalytic sites in IRMOF-3 fragment derivatives could be affected by structural changes. IRMOF-3 presents an aromatic aminic group in the edge of the cubic cell; obviously this group is responsible for the IRMOF-3 basic properties. In the paper of Gascon et al. the aniline and IRMOF-3 performances were compared in the Knoevenagel condensation. The most relevant finding of this investigation concerns the reported activity trend of the two catalysts, in fact, it was established that IRMOF-3 is more active as catalyst in Knoevenagel condensation with

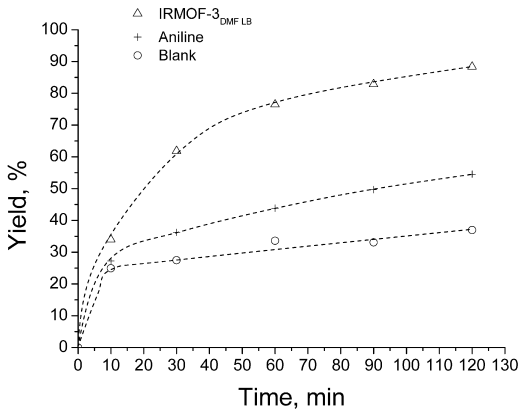

Figure 16.: Knoevenagel condensation of benzaldehyde and ethyl cyanoacetate; comparison between the IRMOF-3 and the aniline performances as catalysts [26].

respect of aniline, as reported in Figure 16. To deeply understand this issue also other basic molecules containing the aminic group and different model sizes of the IRMOF-3 were considered in order to elucidate:

- changes in reactivity of the aminic group caused by local changes of the chemical environment;
- confinement effects.

The former aspect deals with the variations of the aminic group chemistry in correspondence with local structural changes, whereas the latter considers the effect of an increase of the model on the calculated properties. In principle, a larger model is more realistic and moreover it is well known that i) important kinetics and energetics influences could arise in confined environments and ii) long range correlation effects could be relevant. Nevertheless, it is important to put on evidence that the general aim of a model is to be representative of the investigated system and at the same time not expensive in terms of computational cost.

4.1 BASIC PROPERTIES OF IRMOF-3

The first attempt to explain the behaviour of IRMOF-3 in the Knoevenagel condensation, as suggested by Gascon et al. was addressed to relate basicity with the activity. In order to check this inference basic properties of IRMOF-3 and aniline were investigated theoretically, employing:

- thermodynamic descriptors as PA and IB;
- comparative analysis on selected structural parameters.

4.1.1 *Effects of the local environment variations on the catalyst*

Aniline, dimethyl 2-amino-terephthalate (DM2AT) and *f*-2A-1,4-BDC, which will be collectively indicated as R-NH_2, were chosen to model the effect of an increasing local complexity, surrounding basic sites of interest for the IRMOF-3 systems. DM2AT and *f*-2A-1,4-BDC are, in fact, singly obtained substituting in the aniline molecule two hydrogen atoms in position 2 and 5 of the aromatic ring, with two methyl carboxylate or two SBUs with formula $Zn_4O(CO_2)_6$ saturated with hydrogen atoms as shown in Figure 17. The comparison of these three moieties was devised as a regular increase of complexity surrounding the aminic group aimed at understanding, which structural features are directly connected with the basicity. In Table 2 PA and IB for the investigated compounds are reported; basicity according to the employed descriptors increases going from aniline to *f*-2A-1,4-BDC fragment. This order is indicative of a pronounced basicity of the investigated catalyst but it does not explain why IRMOF-3 is more basic then aniline and DM2AT. Two reference basic compounds are also reported in Table 2 namely ammonia and 1,8-bis(dimethylamino)naphthalene (DMAN). The comparison with these reference molecules is aimed at building up both a PA and IB scale within the level of theory selected to perform such calculations. It is interesting to recall that DMAN is one of those compounds named "proton sponges" [195, 196], therefore it can be considered as an upper

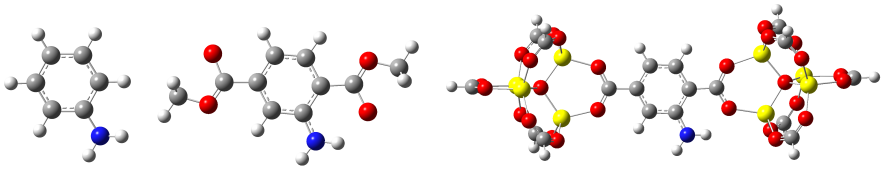

(a) Aniline (b) DM2AT (c) *f*-2A-1,4-BDC

Figure 17.: Optimized aniline 17a, DM2AT 17b and *f*-2A-1,4-BDC 17c.

Table 2.: Ammonia, Aniline, DM2AT, *f*-2A-1,4-BDC and DMAN calculated PA and IB values.

R-NH_2 model species	IB / kJmol^{-1}	PA / kJmol^{-1}
Aniline	869.8	897.6
DM2AT	873.8	908.2
f-2A-1,4-BDC	915.6	939.7
Reference compounds		
Ammonia	753.7	880.3
DMAN	1023.7	1056.1

limit for the calculated properties. In order to elucidate the trend reported above two explanations have been considered: i) variation of electronic density on the nitrogen atom due to the substituting effects on the aromatic ring or ii) structural effects that stabilize the resulting conjugate acid. The strategy adopted in order to understand the origin of the basicity trend reported above was based on i) the population analysis providing a means of estimating partial atomic charges from calculations and on the ii) analysis of the structural features of the investigated basic compound and their conjugate acids. Population analysis was performed employing the partition schemes reported in section 3.4.2. Table 3 shows the partial atomic charge of nitrogen

Table 3.: Partial atomic charge for the nitrogen atom calculated with different partition schemes.

R-NH_2 model species	MPA / a.u.	CHelpG / a.u.	MK / a.u.
Aniline	-0.7	-0.7	-0.7
DM2AT	-0.8	-0.8	-0.8
f-2A-1,4-BDC	-0.8	-0.8	-0.8

atom framed in the three different catalysts. Despite the employed partition schemes no difference arises between the considered species. This implies that the reported augmented basicity for the IRMOF-3 is not due to an electronic effect on the nitrogen atom of the aminic group. As it is well established, the reason of an increased basicity could also lie in the stabilization of the conjugated acid. Therefore relevant structural features of the catalyst and its conjugate acid were analyzed.

Table 4.: Significant calculated structural parameters of unprotonated and protonated aniline, DM2AT and *f*-2A-1,4-BDC. Numbering in the Table 4 is coherent with that reported in Figure 18. Vertibars separate structural parameters concerning unprotonated and protonated systems (unprotonated | protonated).

distance / pm	Aniline	DM2AT	*f*-2A-1,4-BDC
C2–C3	141 | 140	143 | 141	144 | 142
C3–N	140 | 150	138 | 150	137 | 149
N–H1	102 | 103	103 | 107	103 | 111
N–H2	102 | 103	102 | 103	102 | 103
H1···O2	— | —	194 | 164	191 | 147
angle / °	Aniline	DM2AT	*f*-2A-1,4-BDC
O2–C1–C2	— | —	113.8 | 112.8	118.6 | 116.9
C2–C3–N–H1	-26.2 | -1.7	14.5 | 0.0	-10.2 | -0.9

Table 4 shows that the homonym structural parameters of the three

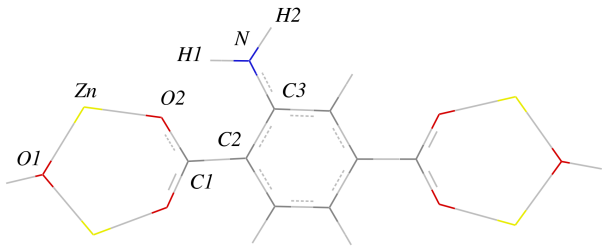

Figure 18.: Numbering employed in the structural features analysis.

considered species are substantially not different, the only differences being related to distances and angles concerning one hydrogen atom of the amino group of the protonated systems when interested in hydrogen–bonds, namely occurring in the DM2AT and *f*-2A-1,4-BDC species. In these, N–H1 and H1···O2 distances are increased and decreased, respectively while the C2–C3–N–H1 dihedral angle is approaching to zero. The formation of a 6–members ring occurs along with the structural changes above. Therefore, the increased basicity going from aniline through DM2AT to *f*-2A-1,4-BDC could be attributable to the formation of protonated forms, involving hydrogen-bonds and 6–terms *quasi*–planar rings (see Figure 19). The studies

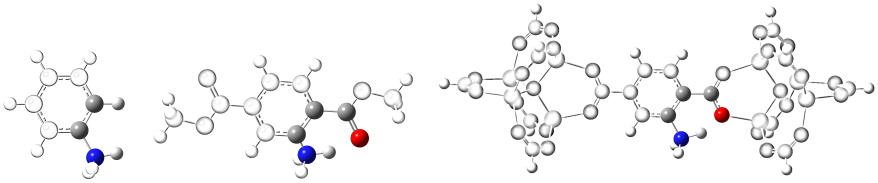

(a) (b) (c)

Figure 19.: Optimized protonated aniline 19a, DM2AT 19b and *f*-2A-1,4-BDC 19c. The evidenced part highlights the 6–terms *quasi*–planar ring responsible of the increased basicity of IRMOF-3.

reported in the literature by Kim et al. [197] concerning the structure and the properties of IRMOF systems were focused on the attribution of the basic enhanced properties of the IRMOF-3 to the hydrogen bond formed in the unprotonated species, nevertheless it is clear on the ground of the results previously reported that this establishment is not in agreement with our findings; however, in the following will be shown that the orientation of the hydrogen H1 due to the presence of the O2 atom also in the unprotonated species has some energetics implications in the catalytic cycle. To account possible confinement and long range order effects on the calculated properties, QM/QM calculations were carried out at the level of theory described in section 3.1. Thermodynamic descriptors were calculated also for the model IRMOF-3c shown in Figure 11b. Calculated values for PA and IB were

respectively, 927.3 kJ mol^{-1} and 897.9 kJ mol^{-1} whereas the structural parameters for the protonated species indicative of the presence of a 6–terms *quasi*–planar ring, namely H1···O2 distance and C2–C3–N–H1 were found to be respectively 148 pm and -1.2 °. Based on these results it is possible to state that at this stage of the investigation no further information were added by using a larger model and a QM/QM approach. This may imply that for the studied quantities confinement effects are not relevant. It is interesting to notice that, as already recalled in section 2.4, for MOFs the equivalence between smaller model containing all the chemical and geometrical features of the lattice and the periodic solid has been already proposed in the literature [140].

4.2 BUILDING UP A REACTION MECHANISM

The evaluation of the basic properties of IRMOF-3 was devised as a preliminary investigation for the reaction mechanism of the Knoevenagel condensation catalyzed by IRMOF-3. Different pathways were taken into account and considering the computational cost of a full transition state characterization, some routes were discarded on the ground of their energetics. Therefore, it is interesting to report the logical process that it was used in order to build up the catalytic cycle. The two sections here below concern the approach that was followed in the rationalization of the catalytic cycle.

4.2.1 *Framing the chemical context: two key issues*

In order to figure out the overall chemical context of these study two key points have to be put on evidence. One concerns the different pathways of the Knoevenagel condensation mechanism depending on the employed base, while the second deals with the tautomeric equilibrium of the species containing α acidic hydrogen.

I ISSUE Knoevenagel condensation is a reaction between one aldehyde and an α acidic hydrogen containing compound where α, β conjugated enone is produced. This condensation reaction is widely used in organic synthesis to produce important intermediates and end–products, and it can be catalyzed by a wide variety of bases from weak to strong basicities and has proven to be a very adequate test reaction for base catalyst [198, 199]. As it is well known two main mechanism exist for the Knoevenagel condensation, i) strong base and the ii) weak base catalyzed mechanism as reported respectively in Figure 20 and 21. The former includes:

1. acid-base reaction between the catalyst and the α acidic hydrogen containing compound;

2. nucleophilic addition of the carbanion to the carbonyl group;
3. elimination of a water molecule and formation of the product.

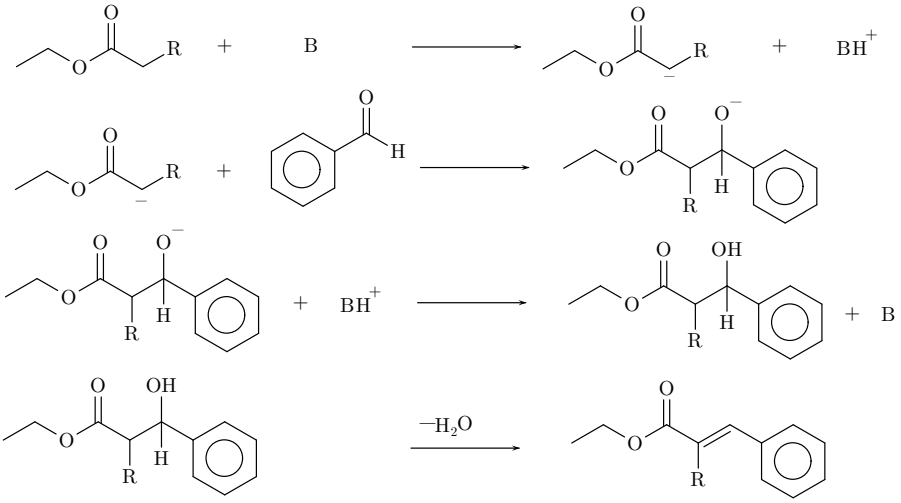

Figure 20.: Strong base catalyzed Knoevenagel condensation reaction steps. R is a generic electron–attractor group.

while the latter, usually carried out by aminic based catalysts is characterized by:

1. nucleophilic addition of the catalyst to the carbonyl group;
2. elimination of a water molecule and formation of an iminic derivative intermediate;
3. reaction of the iminic derivative with the α acidic hydrogen containing compound and formation of the product.

This two general mechanisms were evaluated for all the catalysts investigated in this study namely aniline, DM2AT and *f*-2A-1,4-BDC. Energetics implications originated by the comparisons of these two possible pathways were highlighted and employed in the selection of the more plausible reaction mechanism for the Knoevenagel condensation catalyzed by the above cited catalysts.

II ISSUE The second key issue concerns the tautomers of the α acidic hydrogen containing compound. It is well known that the tautomeric equilibrium for this species is a relevant feature of their chemistry. In fact, in order to understand the intrinsic chemical reactivity of this species, the three tautomers were considered namely the ketonic, *cis*–enolic and *trans*–enolic form as shown in Figure 22. Ketonic form is, in general, more stable than its enolic tautomer but for active methylene compounds the enol tautomer could be the more stable species; besides this, it has to be considered that it is not straightforward to *a priori* discard the less stable tautomers because it is in

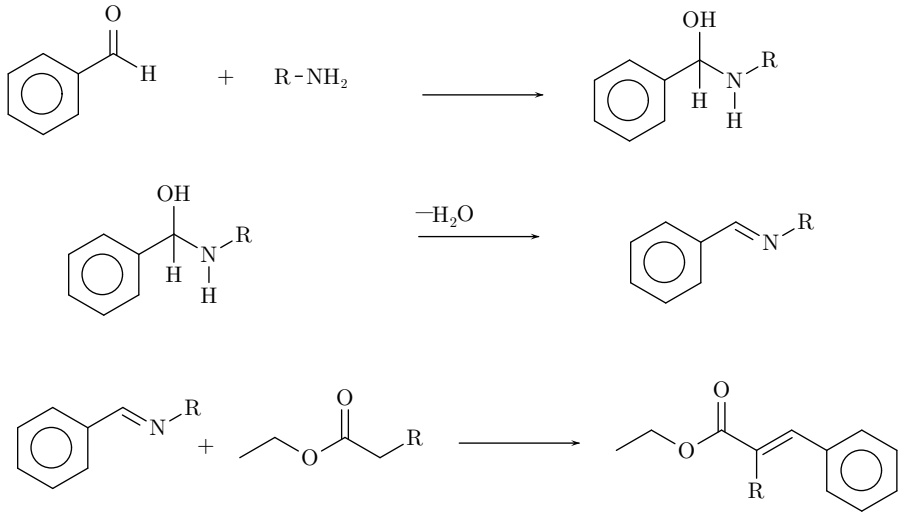

Figure 21.: Weak base catalyzed Knoevenagel condensation reaction steps. R is a generic electron–attractor group.

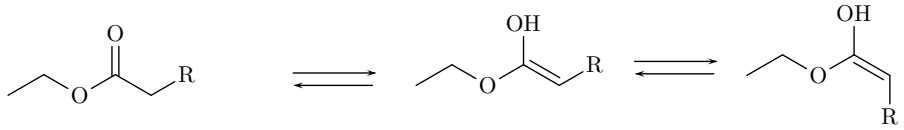

Figure 22.: Tautomeric equilibrium for the species containing α acid hydrogen.

principle possible that these species are more reactive. Moreover, considering that all these tautomers are in equilibrium it is not unlikely that the less stable species, present in a very small amount, reacts and then the tautomeric equilibrium is shifted toward the re–establishment of the less stable species; in this way the more stable species are always largely present while the active species are those present in smaller amounts.

4.2.2 *Is IRMOF-3 a weak or a strong base ?*

The investigation dealing with the energetics of the IRMOF-3 catalyzed Knoevenagel reaction was preliminary to the full characterization of the transition states of the cycle and was aimed at studying i) the classification of the IRMOF-3 as strong or weak base ii) the number and type of intermediates involved in the cycle, iii) the identification of the intermediate responsible of the deprotonation of the α hydrogen containing compound. All the intermediates were fully relaxed and characterized by a further frequency calculation within the harmonic approximation, moreover the basic properties characterization for all the nitrogen–containing intermediates was performed. The calculated properties are referred to the condensation reaction of benzaldehyde and ethyl cyanoacetate reported in Figure 23. In order to elucidate if

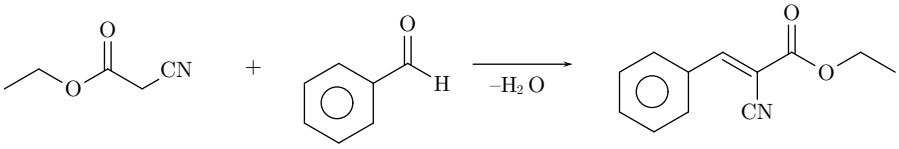

Figure 23.: Knoevenagel condensation between benzaldehyde and ethyl cyanoacetate.

the three considered aminic catalysts were behaving as strong or weak bases the energetics for the reactions [2] and [3] were calculated.

$$\text{R-NH}_2 + \text{C}_6\text{H}_5\text{COH} \rightarrow \text{R-NH-CH(OH)-C}_6\text{H}_5 \qquad [2]$$

$$\text{R-NH}_2 + \text{CN-CH}_2\text{COOCH}_2\text{CH}_3 \rightarrow \text{R-NH}_3{}^+ + \text{CN-CHCOOCH}_2\text{CH}_3{}^- \qquad [3]$$

The first reaction is a nucleophilic addition between the aminic group of the catalyst and the carbonylic group of the benzaldehyde molecule and is the starting point for the weak base catalyzed reaction mechanism; whereas, the second is the acid–base reaction between the aminic group of the catalysts and the acidic hydrogen of the ethyl cyanoacetate. As reported below, this is considered the first reaction of a strong base catalyzed Knoevenagel condensation. The energetics analysis of these two reactions permits the classification of the considered catalysts as a strong or a weak base. Table 5 reports the ΔE

Table 5.: ΔE values for the three investigated catalysts. The evaluated reactions are [2] and [3]. The energetics for the reaction [3] concerns all the three possible tautomers namely ketonic, *cis*–enolic and *trans*–enolic for the ethyl cyanoacetate designated respectively by the subscripts k, ce, and te.

ΔE/ kJmol^{-1}	Aniline	DM2AT	*f*-2A-1,4-BDC
ΔE[2]	4.3	7.9	19.6
ΔE_k[3]	549.3	539.4	496.3
ΔE_{ce}[3]	482.4	472.5	439.9
ΔE_{te}[3]	465.8	455.9	423.3

values for the two compared reactions, all the tautomers of the ethyl cyanoacetate were considered; as it is possible to notice the reaction involving two charged species requires a larger amount of energy than the reaction involving the formation of a tetrahedral addition intermediate. This finding concerns all the three analyzed catalysts. Two different energetics trends arose; in the case of the reaction [2] the energetics order is aniline<DM2AT<*f*-2A-1,4-BDC whereas in the case of the reaction [3] the energetics trend agree with the basicity trend reported in section 4.1.1. Even if at this stage of the discussion transition states are not taken into account, the difference in energy between the two compared pathways are large enough to point out

that all the three considered catalysts behave as weak bases in the Knoevenagel condensation. This hypothesis is supported by the experimental identification of imine species in Knoevenagel condensation, catalyzed by IRMOF-3 [26]. Concerning this, the experimental C=N IR band, isolated at 1645 cm^{-1} and characterizing the imine moiety, is correctly reproduced by the frequency calculations performed, by standard corrections, [163] on the *f*-2A-1,4-BDC imine derivative. The following step in the rationalization of the analyzed catalytic process was to figure out into a weak base catalyzed mechanism which species is the more basic. Three nitrogen–containing species are present in the catalytic mechanism, therefore, there are three molecules that can be responsible of the deprotonation of the ethyl cyanoacetate, namely the catalyst itself, the amino–alcoholic and the iminic intermediates formed respectively in the reaction [2] and [4]. Thermodynamic descriptors (PA and IB) and population analysis for these two species were calculated in order to build up a basicity scale between all the intermediates of the catalytic cycle.

$$\text{R-NH-C(OH)H-C}_6\text{H}_5 \rightarrow \text{R-N=CH-C}_6\text{H}_5 + \text{H}_2\text{O} \qquad [4]$$

In all the considered cases, reported in Table 6, the derivatives of

Table 6.: IB and PA calculated values of aniline, DM2AT and *f*-2A-1,4-BDC derivatives, formed in reactions [2] and [4].

R-NH_2 + $\text{C}_6\text{H}_5\text{CHO}$ → amino-alcohol [2]		
amino-alcoholic derivative	IB / $kJmol^{-1}$	PA / $kJmol^{-1}$
Aniline	925.3	955.6
DM2AT	926.2	956.4
f-2A-1,4-BDC	978.1	987.2
amino-alcohol → imine + water [4]		
iminic derivative	IB / $kJmol^{-1}$	PA / $kJmol^{-1}$
Aniline	954.8	982.6
DM2AT	970.1	1000.8
f-2A-1,4-BDC	1015.9	1030.1

f-2A-1,4-BDC are more basic than those of aniline and DM2AT and the trend is always the same. Among the considered nitrogen–containing species involved in the cycle, for all the three analyzed catalysts, the iminic derivatives are the more basic. These findings suggest that the eventual deprotonation step of the ethyl cyanoacetate will be carried out by the iminic derivative and corroborate the hypothesis of a weak based catalyzed reaction route for the three investigated catalysts. In order to understand the reason of the increased basicity also in this case, as in the section 4.1.1,below the structural features of the iminic derivatives were considered. The values reported in

Table 7.: Significant calculated structural parameters of aniline, DM2AT and *f*-2A-1,4-BDC protonated imine derivative. Numbering is coherent with that reported in Figure 18.

imine derivatives			
distance / pm	Aniline	DM2AT	*f*-2A-1,4-BDC
C3–N	142	142	142
N–H1	103	104	106
N–C4	132	132	132
H···O2	—	176	164
imine derivatives			
angle/ °	Aniline	DM2AT	*f*-2A-1,4-BDC
C2–C3–N–H1	-15.0	-8.6	-2.6

Table 7 clearly show the shortening of the hydrogen bonds and the flattening of the dihedral angles, involved in the 6–terms *quasi*–planar rings formation, when both basicity–strength and local molecular complexity increase. Hydrogen atoms individuating the reported dihedral angles are topologically equivalent. Their spatial properties are modified by hydrogen–bond interactions, occurring only in DM2AT and *f*-2A-1,4-BDC protonated imine derivatives, and in this change could lie the reason for the increased basicity. Nitrogen charges were also analyzed for the iminic protonated derivativess, following the partitioning–charge schemes previously presented. Charges resulted almost constant (-0.5 a.u.), irrespective of the employed method; hence the imine derivative basicity cannot be related to charge density variations, occurring on the imine nitrogen centres. Conversely, as already observed in analyzing the considered catalysts, a stabilization occurs for the DM2AT and *f*-2A-1,4-BDC protonated imine derivatives due to the formation of 6–terms *quasi*– planar rings, which involve hydrogen interactions of the protonated nitrogen centres with the oxygen of the carboxylic groups. As in the case of the catalysts, the formation of 6–terms rings seems to drive the relative basicity–strength.

4.3 DESCRIPTION AND ENERGETICS OF THE CYCLE

In order to summarize in a more compact view all the inferences and the findings exposed above, a full description of the step involved in the catalytic cycle is reported below. Energetics consideration and structural features characterizing the intermediates of the three catalysts will be also shown. In the following Cb and Ob will be representative of the carbonylic carbon and oxygen atoms of benzaldehyde whereas Cc and Hc will be respectively the carbon atom in–between the cyano group and the esteric group and the acidic hydrogen of the

ethyl cyanoacetate. The atom numbering employed in the following is coherent with that of Figure 18.

I STEP This step involves the nucleophilic addition of the catalyst aminic group to the carbonyl moiety of the benzaldehyde. Amino–alcohols are the resulting intermediates. These derivatives are product of two molecular processes: i) formation of a carbon nitrogen bond (Cb–N) and ii) transfer of an aminic hydrogen to the carbonyl oxygen of the benzaldehyde (Ob–H2). The three amino–alcoholic species are shown with their energetics in Figure 24 and are the products of the reaction [2]. The calculated energetics trend is aniline<DM2AT<*f*-2A-1,4-BDC. The reported energy values for the three catalysts show an increase according to the local complexity surrounding the aminic group. This, may suggest that there are steric hindrance effects that favor the analyzed reaction in the case of the aniline. Nevertheless, it is easy to notice that the difference in energy are very close for all the considered catalysts. An interesting issue, deriving from the investigation of the

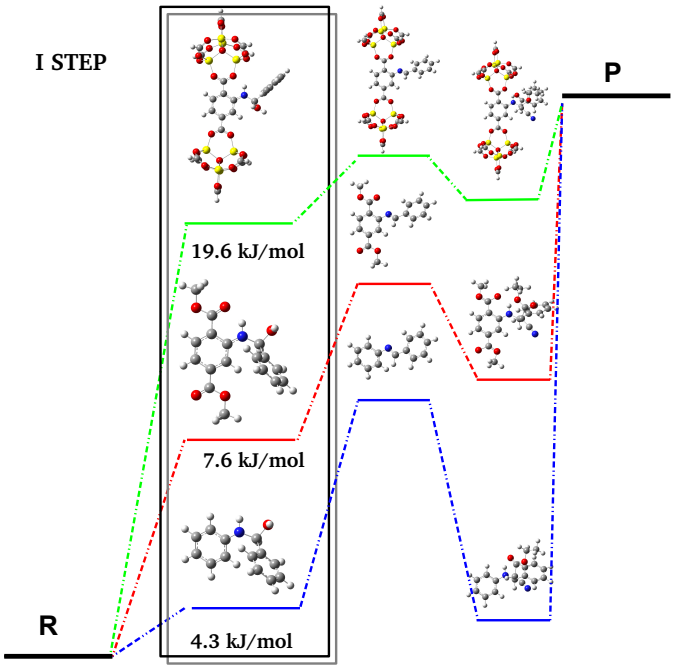

Figure 24.: Energetics for the I step [2] of the catalytic cycle. The intermediates for all the studied catalysts and their relative energy referred to reactants are reported. In blue, red and green are respectively detailed the energetics trend of the cycle catalyzed by aniline, DM2AT and *f*-2A-1,4-BDC.

energetics, is that in this step the stereospecificity of the reaction is not relevant. Calculations on the aniline amino–alcoholic derivatives (R) and (S) proved that both configurations have the same energy, therefore both the enantiomers were probable as products of the I step.

Thus, it has been assumed that the addition reaction of the I step was producing for the three investigated catalysts the same enantiomer. Another point considered at this stage of the study, concerns the break of the N–H1 bond of the catalyst during the formation of the amino–alcoholic intermediate. It was previously established that the basicity is linked to the stabilization of the conjugated acids of the catalysts, nevertheless, the N–H1 bond in the unprotonated species *f*-2A-1,4-BDC, should be more difficult to break than the N–H2; this, because of the partial interaction of the H1 with the oxygen of the inorganic vertex. In fact, calculations demonstrate that the amino–alcohol formed saving the H1···O2 interaction is 39.3 kJ mol $^{-1}$ more stable than the other.

II STEP In the second step of the catalytic cycle the amino–alcoholic derivative looses a molecule of water giving as product an iminic intermediate. In this step, H1 interacts with the alcoholic moiety of the amino–alcoholic derivative and the bond between the alcoholic group and Cb is broken forming a double bond Cb=N. All the iminic derivatives are (E)–isomers produced by the reaction [4]. The energet-

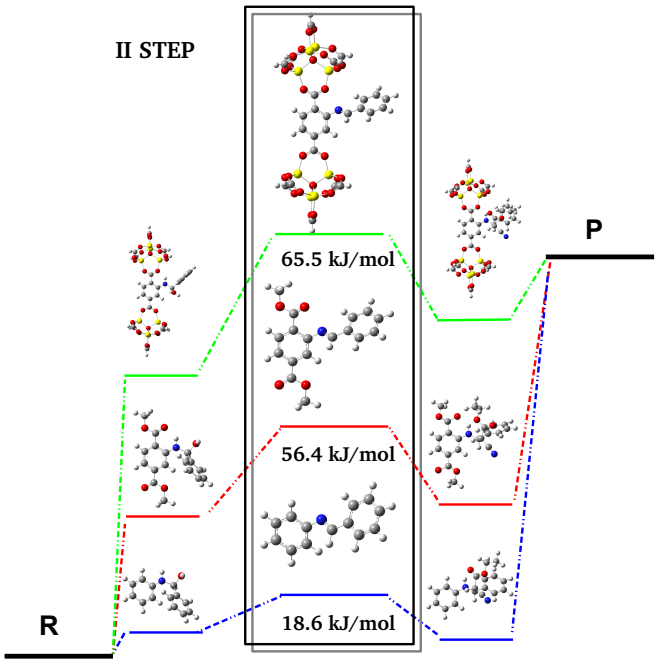

Figure 25.: Energetics for the II step [4] of the catalytic cycle. The intermediates for all the studied catalysts and their relative energy referred to reactants are reported. In blue, red and green are respectively shown the energetics trend of the cycle catalyzed by aniline, DM2AT and *f*-2A-1,4-BDC.

ics trend for the II step of the catalytic cycle, as shown in Figure 25, is aniline<DM2AT<*f*-2A-1,4-BDC. This trend is probably influenced by

the presence of the H1···O2 partial interaction in the amino–alcoholic intermediate. This influence is highlighted by the amount of energy required in order to form the iminic intermediates in the investigated cases; in fact, going from aniline to *f*-2A-1,4-BDC there is an increase in energy attributable to the break of this partial interaction present in the amino–alcoholic intermediates. Interestingly, the trend reported is opposite with respect of the amino–alcoholic derivatives basicity trend shown in Table 6. This finding agrees with the statement that H1···O2 interaction influences the amount of energy required for the formation of the iminic derivatives.

III STEP In this step of the catalytic cycle the iminic derivative reacts with the ethyl cyanoacetate. Two different pathways were analyzed for this step, the i) acid–base reaction between the iminic derivative and the ethyl cyanoacetate as shown in the reaction [5] and the ii) addition to the double Cb=N bond of the Cc–Hc bond of the ethyl cyanoacetate as reported in reaction [6]. The former pathway involves a deprotonation step whereas, the latter avoids the formation of charged species assuming the concerted formation of the Cb–Cc and N–Hc bonds.

$$\text{R-N=CH-C}_6\text{H}_5 + \text{CN-CH}_2\text{COOCH}_2\text{CH}_3 \rightarrow \text{R-NH-CH-C}_6\text{H}_5{}^+ + \text{CN-CHCOOCH}_2\text{CH}_3{}^- \quad [5]$$

$$\text{R-N=CH-C}_6\text{H}_5 + \text{CN-CH}_2\text{COOCH}_2\text{CH}_3 \rightarrow \text{R-NH-CH-(C}_6\text{H}_5\text{)-CH-(CN)-COOCH}_2\text{CH}_3 \quad [6]$$

Table 8 shows the calculated difference in energy for the two pathways. It is possible to notice that the formation of two charged species is strongly unliked in all the considered cases, therefore it has been assumed that the cycle proceeds trough reaction [6]. The molecular

Table 8.: Energy differences for the three considered catalysts referred to reactants. The presence of different possible tautomers for ethyl cyanoacetate is here explicitly taken into account.

	ΔE_k kJ mol^{-1} [5]	ΔE_{ce} kJ mol^{-1} [5]	ΔE_{te} kJ mol^{-1} [5]
Aniline	483.2	416.2	399.7
DM2AT	475.2	408.3	391.7
f-2A-1,4-BDC	483.7	416.8	400.2
	ΔE_c kJ mol^{-1}[6]	ΔE_{ce} kJ mol^{-1} [6]	ΔE_{te} kJ mol^{-1} [6]
Aniline	3.1	-64.8	-80.4
DM2AT	16.9	-50.1	-66.7
f-2A-1,4-BDC	43.3	-23.6	-40.2

process involves the hydrogen of the ethyl cyanoacetate, Hc, that interacts with the iminic nitrogen while the carbon Cc reacts with the iminic carbon. As in the I step, the addition may produce different

stereoisomers; it was established that this does not influence the energetics of the process. A degree of complexity is added to this analysis if all the possible ethyl cyanoacetate tautomers are considered. The two pathways reported above were checked for all the tautomers of ethyl cyanoacetate namely ketonic, *cis*–enolic and *trans*–enolic. The trend reported in the Table 8 reflects the stability order of the three tautomers; the less stable *trans*–enolic tautomer is also the species that gives origin to the most favorable pathway. However, these information should be intended as illustrative because considering that the energetics trends are not very different in the case of the three considered tautomers, the definitive evidence of a favorable pathway will arise only with the calculation of the transition states. Therefore, at this stage of the discussion, the tautomeric equilibrium will be taken into account implicitly and therefore the energetics order will be referred to the ketonic species for all the three studied catalysts. In the Figure 26 the energetics order referred to reactants for the III step of the catalytic cycle is reported. Aniline presents the lower energetics

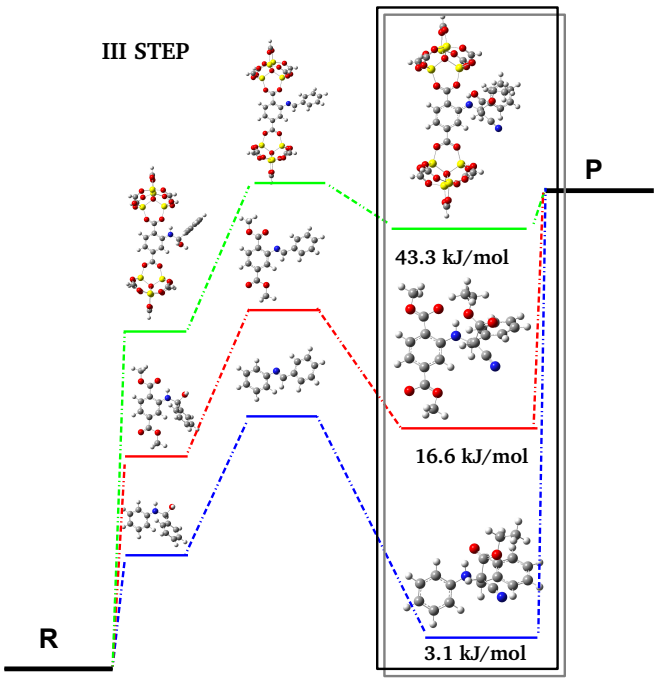

Figure 26.: Energetics for the III step [6] of the catalytic cycle. The intermediates for all the studied catalysts and their relative energy referred to reactants are reported. In blue, red and green are respectively reported the energetics trend of the cycle catalyzed by aniline, DM2AT and *f*-2A-1,4-BDC.

pathway followed by DM2AT and *f*-2A-1,4-BDC. However, if the single III step is considered (without the amount of energy deriving from the previous steps), and the ΔE between the intermediate of the II step

and that of the III step, is calculated the trends reported agree perfectly with the basicity order reported above for the iminic derivatives.

IV STEP The IV step was identified as that forming the product and re–establishing the catalyst as reported in the reaction [7]. The intermediate formed in the III step protonates the nitrogen atom of the catalyst, the Cb–N bond of the catalyst is broken and a carbon–carbon double bond is formed. The product, as experimentally reported for the Knoevenagel condensation of benzaldheyde and ethyl cyanoacetate, is the (E)-α-cyanocinnamate. The calculated ΔE referred to reactants is 59.8 kJ mol^{-1}.

$$\text{R-NH-CH-(C}_6\text{H}_5\text{)-CH-(CN)-COOCH}_2\text{CH}_3 \rightarrow \text{R-NH}_2 + \text{CH-(C}_6\text{H}_5\text{)=C-(CN)-COOCH}_2\text{CH}_3 \quad [7]$$

4.4 CONFINEMENT EFFECTS

The confinement effects were evaluated for energetics of the Knoevenagel condensation IRMOF-3 catalyzed. The calculations were performed within the QM/QM approach empolying the ONIOM extrapolation scheme as described in section 3.1; the model used for this issue was that reported in Figure 11b. In Figure 27 the trends for the models IRMOF-3c and *f*-2A-1,4-BDC are reported; it is evident that confinement effects, although present, play a minor role in driving the title reaction.

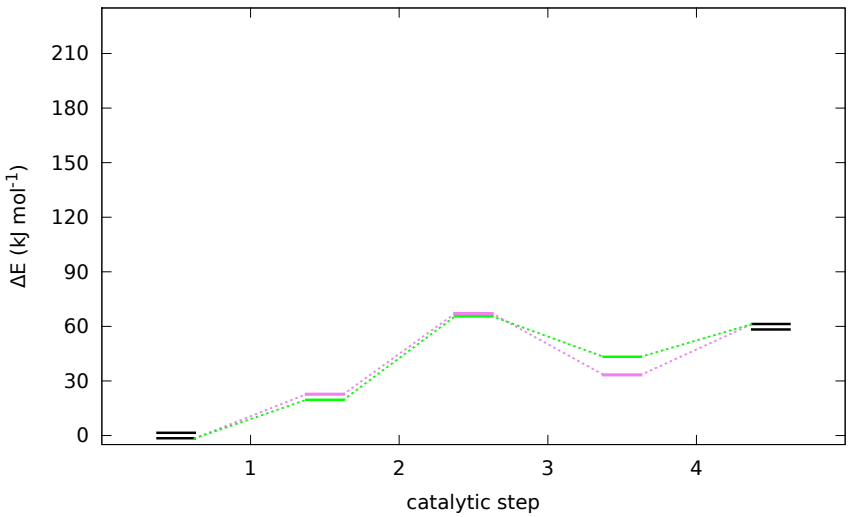

Figure 27.: Energetics trends for the Knoevenagel condensation involving IRMOF-3c and *f*-2A-1,4-BDC catalysts. In green and pink are respectively reported the trends of the cycle catalyzed by the *f*-2A-1,4-BDC and the IRMOF-3c models of the catalyst.

4.5 KINETIC ASPECTS OF THE CYCLE

In the previous sections energetic and structural aspects involved in the title study have been reported. However, the most important step of a kinetic study is obviously the search of the transition states involved in the catalytic cycle and its characterization. All the transition state calculations reported in this thesis are performed at the same level of theory of the intermediates. Transition states structures can be determined by searching for first–order saddle points on the potential energy surface (PES). Such a saddle point is a point where there is a minimum in all dimensions except one. Almost all quantum–chemical methods (DFT, MP2 etc.) can be used to find transition states. However, locating them is often difficult and there is no method guaranteed to find the right transition state. The transition state search is fundamental because it gives access to the calculation of the activation energy that is the main descriptor of the activity trends in catalysis. Therefore, in this section activity order will be shown and the considerations about the relationship between activity and basicity presented previously will become more founded. Moreover, the involvement of the inorganic vertex in IRMOF-3 catalysis will be introduced.

4.5.1 *Description of the transition states*

Here below, the main results of the transition states search are presented. The matter of discussion in the paragraphs below is focused on the relationship between structural descriptors and activity trends. Numbering, where used, is coherent with that reported in Figure 18 and the identificative letters of the atoms are the same reported in the section 4.3.

I STEP The transition states here reported concern the reaction [2], the involved intermediates and their energetics are shown in Figure 24. TS of the three investigated species, in this step, are very similar despite of the starting structural differences of the catalysts as shown in Figure 28. Table 9 shows calculated activation energies (E_a). From these, it is possible to notice that the E_a value increases with the local complexity surrounding the aminic group. Considering the basicity

Table 9.: Activation energies for the I step of the catalytic cycle referred to reactants.

R-NH_2 model species	E_a kJ mol^{-1}
Aniline	121.5
DM2AT	140.2
f-2A-1,4-BDC	146.5

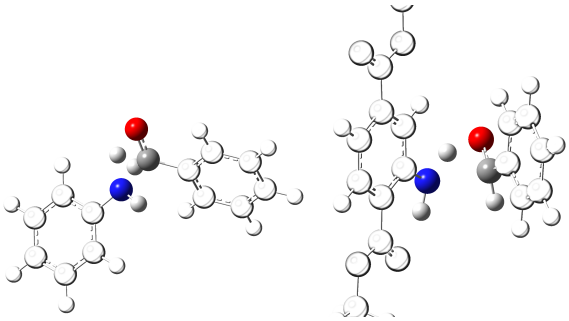

(a) I TS Aniline (b) I TS DM2AT

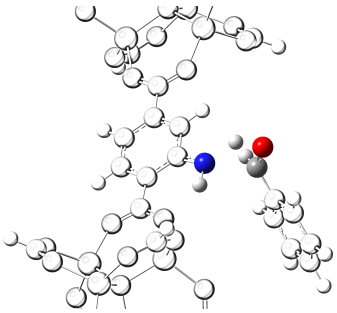

(c) I TS *f*-2A-1,4-BDC

Figure 28.: Transition states for the I step of the three investigated catalytic cycle. For clarity only the atoms involved in the molecular process are coloured.

trend found for the analyzed catalysts (see Table 2), it is evident that there is no correlation between activation energy trends and basicity. No immediate explanation for this trend was found because in principle the nucleophilicity of the aminic group should increase as the basicity. Nevertheless, a possible influence of the steric hindrance effects, as suggested in the section 4.3, still remains founded.

Table 10.: Significant calculated structural parameters in transition states and intermediates of the I step of the cycle catalyzed by aniline, DM2AT and *f*-2A-1,4-BDC. Vertibars separated calculated values respectively for the transition states and the intermediates formed in the considered catalytic step, namely the amino–alcoholic derivatives.

distance / pm	Aniline	DM2AT	*f*-2A-1,4-BDC
Cb–N	179 | 147	203 | 147	218 | 144
Ob–H1	130 | 97	116 | 97	108 | 97

In Table 10 structural features of the three considered catalyst models are reported. The two employed distances were considered reliable geometric descriptors for the formation of the analyzed transition states. The hypothesis that the explanation for the activation energies trend lies in the effects due to the growing sterical hindrance going

from aniline to *f*-2A-1,4-BDC through DM2AT is very probable. In fact, as it is possible to notice from Table 10 the Cb–N distance is larger for the transition state of *f*-2A-1,4-BDC followed by that of DM2AT and of aniline; therefore a correlation between the growing activation energy for this step and the difficulty of the benzaldehyde to approach the aminic group seems to be reliable. The shorter distance Ob–H1 for the *f*-2A-1,4-BDC transition state is in line with an endothermic reaction, where according to the Hammond postulate, a small reorganization of the molecular structures exists between the transition state and the following intermediate.

II STEP The transition states here reported refer to the reaction [4], the involved intermediates and their energetics are shown in Figure 25. The calculated TS structures of the II step for the three considered catalysts are reported in Figure 29 whereas, the activation energies for this step are shown in Table 11. The trend for the II step of the

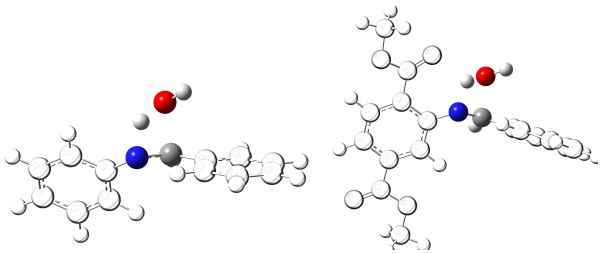

(a) II TS Aniline (b) II TS DM2AT

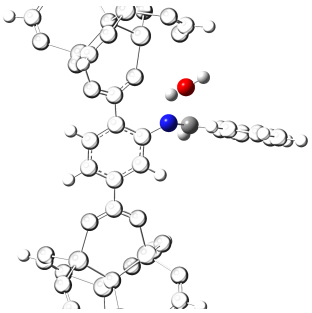

(c) II TS *f*-2A-1,4-BDC

Figure 29.: Transition states for the II step of the three investigated catalytic cycle. For clarity only the atoms involved in the molecular process are coloured.

catalytic cycle is aniline<DM2AT<*f*-2A-1,4-BDC. The explanation for such a trend can be found analyzing the structural features reported in Table 12.

In order to understand the activity trends some considerations about the variation of the structural features during the formation of the transition state have to be done. Obviously, the distance Cb–Ob increases for all the considered transition states because it is linkede to the removal of the water molecule, as well as the distance N–H1 that

Table 11.: Activation energies for the II step of the catalytic cycle referred to reactants.

R-NH_2 model species	E_a kJ mol^{-1}
Aniline	160.5
DM2AT	182.2
f-2A-1,4-BDC	194.7

Table 12.: Significant calculated structural parameters in II step TS of the cycle catalyzed by aniline, DM2AT and *f*-2A-1,4-BDC. Vertibars separate structural features of the intermediate preceding the TS and those of the analyzed transition state.

distance / pm	Aniline	DM2AT	*f*-2A-1,4-BDC
Cb–Ob	142 | 188	142 | 178	144 | 179
N–H1	102 | 129	103 | 136	102 | 135
angle / °	Aniline	DM2AT	*f*-2A-1,4-BDC
C2-C3-N-H1	-24.6 | -50.8	-11.9 | -50.9	-4.6 | -51.7

represents the progressive weakening of the bond between the aminic nitrogen and its hydrogen, H1. Nevertheless, the key point of this step is the change in the dihedral angle C2-C3-N-H1; in fact as it is possible to notice all the values of this parameters for the three catalysts, in the II transition states, approach to $\approxeq$ 50 °. In the intermediates preceding the transition states, these values are very different for each catalysts because in the case of the DM2AT and of the *f*-2A-1,4-BDC the aminic hydrogen, H1, is oriented by the H1···O2 partial interaction. This finding permits to infer that, as suggested in section 4.3, the increase of activation energy in this step may be related to the interaction H1···O2 present in DM2AT and *f*-2A-1,4-BDC and not in aniline.

III STEP The transition states here reported concern the reaction [5], the involved intermediates and their energetic are shown in Figure 26. As already recalled, the III step of the catalytic cycle involves the iminic derivative and the ethyl cyanoacetate; in section 4.2.1 it was put on evidence that the ethyl cyanoacetate could be present in the ketonic, *cis*–enolic and *trans*–enolic form. This equilibrium is influenced by the presence of the solvent and at this stage of the study solvents effects were not taken into account. Anyway, all the three tautomers were considered in order to understand their intrinsic reactivity towards the iminic derivatives; calculations suggest that the ketonic form is the more stable among the possible tautomers, nevertheless, in all the three considered cases no transition states were found for the ketonic or the *cis*–enolic tautomer; in fact, all the transitions states reported are those where the addition of the *trans*–enol to the imine takes place.

Table 13.: Activation energies for the III step of the catalytic cycle referred to reactants.

R-NH_2 model species	E_a kJ mol^{-1}
Aniline	192.6
DM2AT	220.7
f-2A-1,4-BDC	146.7

The absence of a *cis*–enolic transition state may be explained with steric hindrance arguments, but the absence of a ketonic transition state may be related to the fact that solvent is neglected, indeed, further investigations on this aspect are necessaries. The calculated activation energies shown in Table 13 are referred to the ketonic form, reacting with the iminic derivative, therefore, these values implicitly take into account the difference in energy between the ketonic and the *trans*–enolic tautomer. Additional investigations will be carried out on this aspect of the catalytic cycle. However, at this stage of the study the equilibrium between the tautomers is still taken into account in an implicit fashion. The activation energy order is *f*-2A-1,4-BDC< aniline<DM2AT; in order to explain this trend it is illustrative to analyze the structural features reported in Table 14 and the geometries in Figure 30. First of all, the distance Cb–Cc is very large in the case of the *f*-2A-1,4-BDC with respect of the values reported for aniline and DM2AT that are almost the same, conversely the distance N–Hc is shorter in the case of the *f*-2A-1,4-BDC and larger in the case of aniline and DM2AT. In all the considered cases the transition state is stabilized

Table 14.: Significant calculated structural parameters in transition states, for the III step of the cycle catalyzed by aniline, DM2AT and *f*-2A-1,4-BDC.

distance / pm	Aniline	DM2AT	*f*-2A-1,4-BDC
Cb–Cc	158	158	290
Hc–N	152	155	128

by a 6–terms ring and in the case of the *f*-2A-1,4-BDC an important finding arises: the transition state presents an interaction between the enolic oxygen and a Zn atom of the vertex (Zn–O distance 227 pm). It has to be stressed that different geometries were tested for this transition state and all of them gave as result the reported structure presenting a Zn–O interaction. This finding is very important because the Zn–O bond is in large amount responsible of the lower activation energy for the III step of the *f*-2A-1,4-BDC catalyzed cycle. Moreover, it is interesting to put on evidence that the activation energy trends for this step are almost in agreement with the basicity trends reported in the section 4.2.2 for the iminic derivatives.

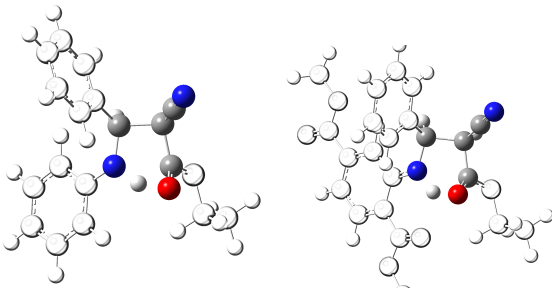

(a) III TS aniline (b) III TS DM2AT

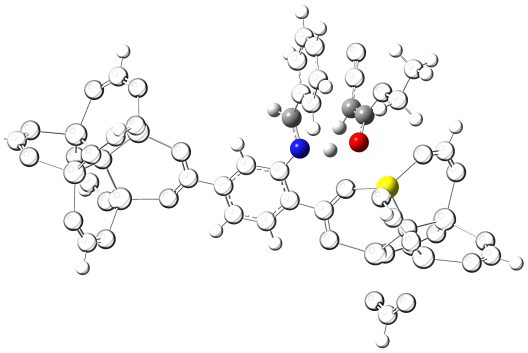

(c) III TS *f*-2A-1,4-BDC

Figure 30.: Transition states for the III step of the three investigated catalytic cycle. For clarity only the atoms involved in the molecular process are coloured.

Table 15.: Activation energies for the IV step of the catalytic cycle referred to reactants.

R-NH_2 model species	E_a kJ mol^{-1}
Aniline	140.2
DM2AT	165.1
f-2A-1,4-BDC	181.3

IV STEP The transition states here discussed concern the reaction [7]. The activation energy trends for the IV step are reported in the Table 15 and as it is possible to notice the order is aniline<DM2AT<*f*-2A-1,4-BDC. In the paper [200] it was reported for the IV step of the Knoevenagel condensation an activation energy of 204.7 kJ/mol, and as established this activation energy refers to the transition state without a Zn–O interaction. Recently a transition state with a Zn–O interaction was found, this is more stable and the calculated difference in energy between this two structures is 23.4 kJ mol^{-1}. This, demonstrates that the Zn–O interaction stabilizes the transition states and could be connected with the difference in activity between the catalysts. However, it is important to stress that this finding does not change the overall inferences exposed in the paper. In fact, still, no

direct connection between the increased basicity and the increased activity of IRMOF-3 has been found. The structure of the transition states of the three analyzed catalysts are reported in Figure 31. As

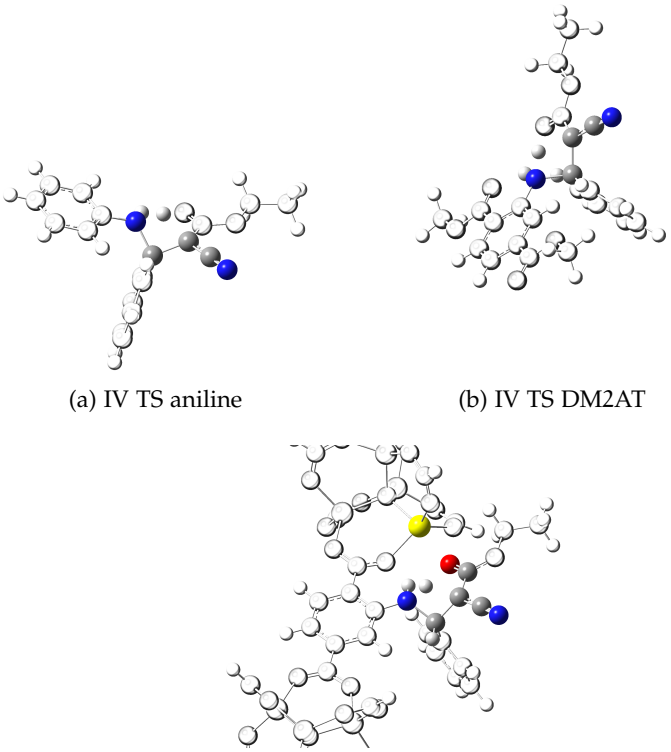

(a) IV TS aniline

(b) IV TS DM2AT

(c) IV TS *f*-2A-1,4-BDC

Figure 31.: Transition states for the IV step of the three investigated catalytic cycle. For clarity only the atoms involved in the molecular process are coloured.

Table 16.: Significant calculated structural parameters in transition states, for the IV step of the cycle catalyzed by aniline, DM2AT and *f*-2A-1,4-BDC. Vertibars separate structural features respectively of the IV transition states and of the intermediates preceding the TS.

distance / pm	Aniline	DM2AT	*f*-2A-1,4-BDC
Cb–N	153 | 145	153 | 144	151 | 145
N–Hc	128 | 208	125 | 253	129 | 268

in the case of the III transition state, aniline and DM2AT present very similar structural features as reported in Table 16, whereas the IV *f*-2A-1,4-BDC transition state presents a Zn–O interaction (distance Zn–O 222 pm) and therefore different structural descriptors. According to the Table 16 it seems that beyond the presence of the Zn–O interaction, one other cause is responsible of the energetic trend. In fact, if we analyze the change in the N–Hc distance it appears clear

that the activation energy increases in agreement with the increase of the distance N–Hc in the preceding intermediate.

4.6 DEACTIVATION ROUTE OF THE CATALYTIC CYCLE

Considering that no direct explanations have been found for the IRMOF-3 enhanced catalytic activity, the deactivation route for this catalytic cycle has been also considered. It has been taken into account the possibility that i) the carbonyl group of ethyl cyanoacetate reacts with the aminic group producing an amino–alcoholic intermediate and then ii) the resulting amino-alcoholic intermediate looses an ethanol molecule, producing an amide as shown in Figure 32. Full characterization of the intermediates and of the transition states for the three catalysts was carried out. This analysis was aimed at understanding if the difference in activity of these catalysts could be related to a deactivation route. It has to be put on evidence that experimentally no deactivation for the catalyst was detected.

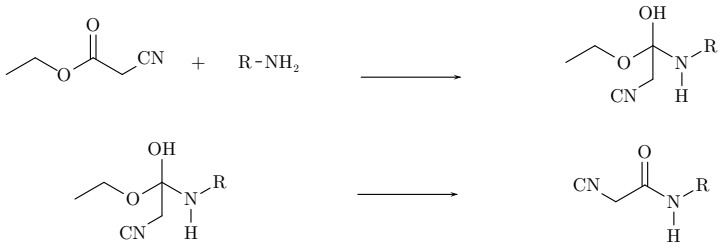

Figure 32.: Reactions involved in the deactivation route of the catalysts.

The results presented here are well in agreement with this finding, in fact, as shown in the Figure 33 and in Table 17 none of these catalysts present a lower activation energy with respect of their I step of the catalytic cycle. This, implies that none of the catalysts is

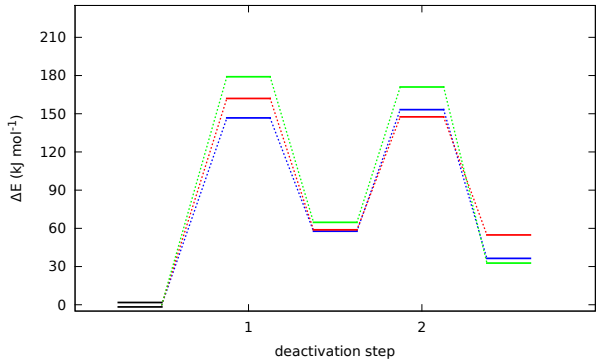

Figure 33.: Trend for deactivation route of aniline DM2AT and *f*-2A-1,4-BDC as catalysts in the Knoevenagel condensation. In blue, red and green are reported the trends respectively for aniline, DM2AT and *f*-2A-1,4-BDC.

affected by deactivation and therefore their experimental differences in activity can not be related to a diverse behaviour with respect of the deactivation. The trends reported here are quite similar to

Table 17.: Activation energies for the I and II step of the deactivation route of the catalytic cycle referred to reactants. Vertibars in the upper part of the Table separate respectively the activation energy values for the I step of the catalytic cycle and for the I step of the deactivation route.

R-NH_2 model species	E_a kJ mol^{-1}
Aniline	146.5 | 121.5
DM2AT	162.0 | 140.1
f-2A-1,4-BDC	179.0 | 158.1
R-NH_2 model species	E_a kJ mol^{-1}
Aniline	153.2
DM2AT	147.5
f-2A-1,4-BDC	171.1

those reported for the cycle where aniline presents almost the lower activation energy followed by DM2AT and *f*-2A-1,4-BDC.

4.7 SUMMARY OF THE CATALYTIC CYCLE AND CONFINEMENT EFFECTS

In order to analyze the confinement effects on the activation energies, the transition state search was performed with a QM/QM approach using the protocol reported in section 3.1 and the model IRMOF-3c. In the Figure 34 the activation energy trends are reported for all the species that were analyzed. As in the previous reported analysis, no particular confinement effects arise and the overall inferences for the considered catalysts remain unchanged. The IV step in dotted line is relative to the transitions state for the *f*-2A-1,4-BDC model without the Zn–O interaction whereas in solid line is reported the transition state with the Zn–O interaction. The confinement effect was evaluated for the IV transition step without Zn–O interaction. It is interesting to notice that the IRMOF-3c model reflects the trend found for the smaller model *f*-2A-1,4-BDC. Aniline and DM2AT present as rate-determining step the III step, whereas both the models of IRMOF-3 present as rate determining step the IV, when the structure of the transition state without Zn–O interaction is considered. Conversely, if the lower energy IV step is included in the investigation the rate–determining step for the *f*-2A-1,4-BDC catalyzed cycle is the II. The energies involved in the two steps, hypothesized to be rate determining, are respectively 192.6 and 194.7 kJ mol^{-1}. The catalytic cycle was fully analyzed and new unexpected findings arose. At this stage of the investigation, no

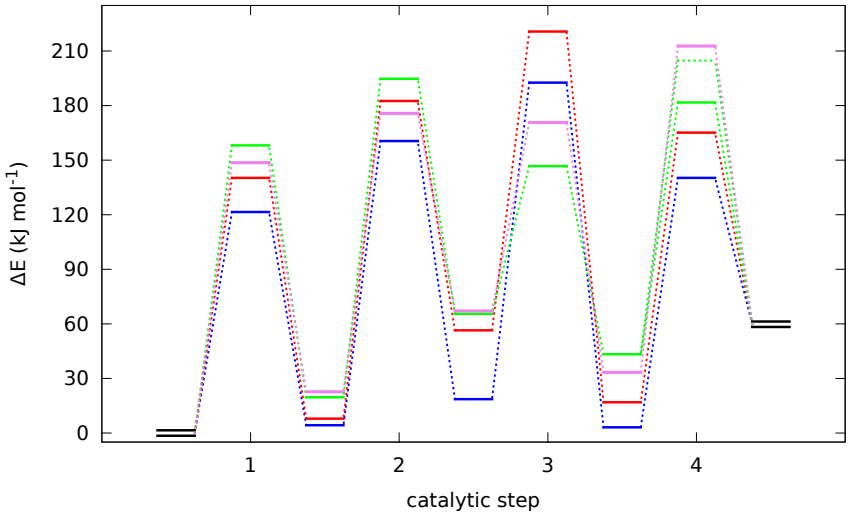

Figure 34.: Catalytic cycle for the three considered catalysts are shown, blue red and green represent respectively the trend for aniline, DM2AT and the *f*-2A-1,4-BDC model as catalysts whereas pink is used for the trend of IRMOF-3c model.

direct correlation between basicity and activity has been found and the enolic transition state found for the III step of all the evaluated catalysts poses new questions about the tautomeric equilibria of ethyl cyanoacetate. Moreover, the interaction with the saturated Zn atoms of the vertex in the III an IV step of the catalytic cycle catalyzed by IRMOF-3 opens new perspectives in the evaluation of the IRMOF-3 activity. It is interesting to recall, that experimental documented activity of saturated metallic vertex in MOF materials has been already reported in the literature.

4.8 CHANGING THE ACIDITY OF THE α HYDROGENS

In order to understand if the whole computational model was adaptable to other reactants, the effect of the substitution of the cyano group with the aceto group on the catalytic cycle was calculated. Full characterization of the intermediates and the transition states, involving the ethyl acetoacetate molecules, both for the cycle and the deactivation route was performed. The calculations were carried out for the three considered catalysts namely aniline, DM2AT and *f*-2A-1,4-BDC. Gascon et al. reported that IRMOF-3 shows a decrease in activity when ethyl acetoacetate is employed instead of ethyl cyanoacetate. In Figure 35a the catalytic cycle and the deactivation route for the reaction between the ethyl cyanoacetate and the benzaldheyde are reported whereas in Figure 35b the catalytic cycle and the deactivation route for the reaction between the ethyl acetoacetate and benzaldheyde are shown. Calculations are perfectly in agreement with the experimental

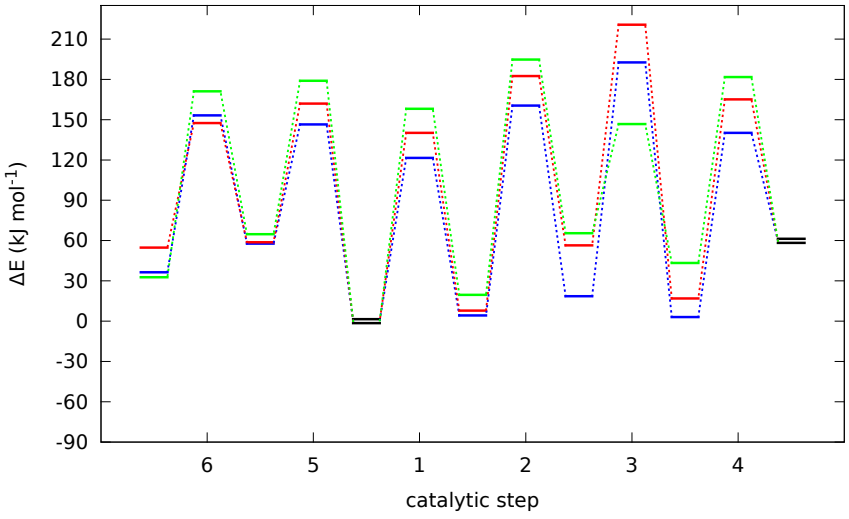

(a)

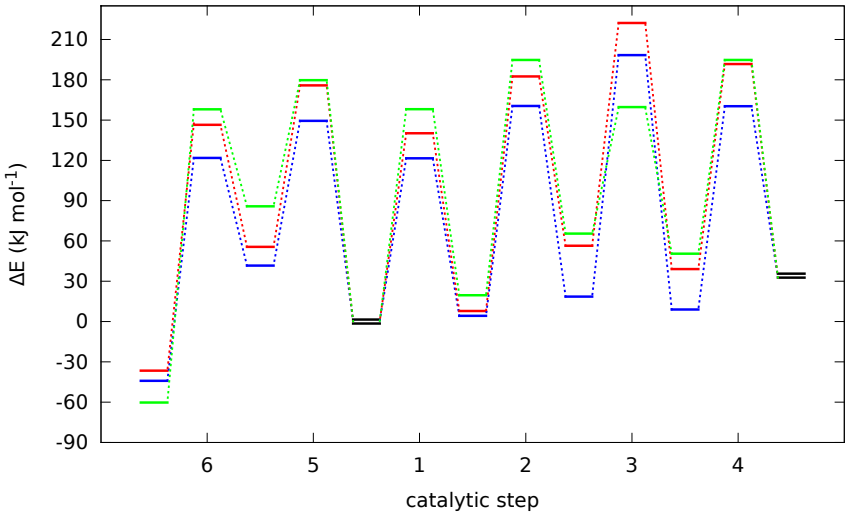

(b)

Figure 35.: Energetics trend for the catalytic cycle and deactivation route of ethyl cyanoacete 35a and ethyl acetoacetate 35b Knoevenagel condensation with benzaldheyde. Blue, red and green represent respectively the aniline, DM2AT and *f*-2A-1,4-BDC catalyzed cycle.

trend; in fact, as it is possible to notice in the Figure 35, the III and the IV step for the ethyl acetoacetate are higher in energy with respect of those of ethyl cyanoacetate and this, can explain the reported decreased activity of the IRMOF-3 [26]. Also in this case III and IV step catalyzed by the *f*-2A-1,4-BDC involved a Zn–O interaction.

4.9 WATER AS BYPRODUCT: EFFECTS ON THE REACTIVITY

Considering that i) no unambiguous information arises from the kinetic analysis of the cycle, ii) no deactivation occurs for the considered catalysts and iii) no strong confinement effects were found, in order to explain the increased activity of IRMOF-3, a poisoning mechanism of the catalyst was suggested and the cycle was formulated in a new overall view. In the second step of the catalytic cycle a water molecule is produced. The hypothesis is that in the case of aniline and DM2AT the water molecule blocks the aminic group and therefore the catalytic cycle. This, may be consistent with the multi–modes adsorptions suggesting an interpretation of the experimental findings, which shows an higher long–term activity of IRMOF-3 with respect of aniline but also a comparable starting activity of aniline with respect of IRMOF-3 [26]. This behaviour is in fact compatible with a progressive deactivation of aniline that indeed could be attributed to the formation of water–aniline complexes.

WATER AS POISON In the case of IRMOF-3 the catalytic amino groups embedded in its framework could be protected from aquation by the presence of the carboxylic groups and Zn-centres that could intercept and block the water molecules formed in the II step of the catalytic cycle; whereas in the case of aniline this possibility does not exist and the poisoning of the aminic group is very likely. To prove the soundness of this inference, BSSE and ZPE corrected adsorption energies (ΔE_{ads}) of one water molecule on different molecular moieties – namely, amino (H_2O/-NH_2), carboxylic (H_2O/-COO) and Zn–centre (H_2O/Zn) – characterizing aniline, DM2AT and IRMOF-3 models have been found out (see Table 18). The acronyms characterize the

Table 18.: BSSE and ZPE corrected adsorption energy of one water molecule on different moieties, characterizing aniline, DM2AT, *f*-2A-1,4-BDC and 2A- B species

	ΔE_{ads} / kJmol^{-1}		
model species	H_2O/-NH_2	H_2O/-COO	H_2O/Zn
aniline	-13.7	—	—
DM2AT	-16.9	—	—
f-2A-1,4-BDC	-16.7	-6.2	—
2A-B	—	—	-24.6

interaction modes of the water molecule with a aniline and aniline–like moieties; in particular, the optimized interacting fragments of Figure 36 are indicated as (H_2O/-NH_2)-*f*-2A-1,4-BDC (H_2O/-COO)-*f*-2A-1,4-BDC and (H_2O/Zn)-2A-B. The ΔE_{ads}(H_2O/Zn) value has been calculated, using the 2A-B corner model (see Figure 15), which is

obtained saturating one SBU by 2-amino-benzoate fragments. The $\Delta E_{ads}(H_2O/\text{-}NH_2)$ values are comparable, irrespective of the model system examined. In particular, considering the IRMOF-3 models, the $\Delta E_{ads}(H_2O/\text{-}NH_2)$ value is in–between that of $\Delta E_{ads}(H_2O/\text{-}COO)$ and of (H_2O/Zn), being the former and the latter, lower and higher, respectively. The corresponding optimized IRMOF-3 model structures, (H_2O/Zn)-2A-B, $(H_2O/\text{-}NH_2)$-*f*-2A-1,4-BDC and $(H_2O/\text{-}COO)$-*f*-2A-1,4-BDC), are reported in Figure 36. For the IRMOF-3 models, it is

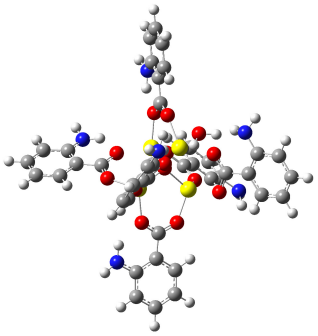

(a) (H_2O/Zn)-2A-B

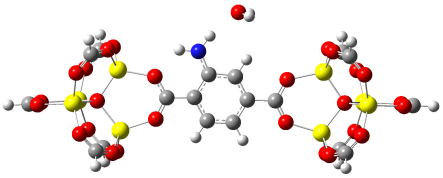

(b) $(H_2O/\text{-}NH_2)$-*f*-2A-1,4-BDC

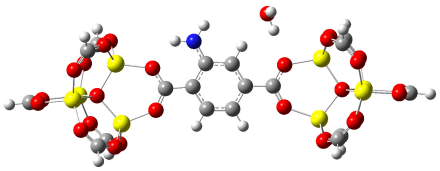

(c) $(H_2O/\text{-}COO)$-*f*-2A-1,4-BDC

Figure 36.: Optimized IRMOF-3 moieties, singly interacting with one water molecule; models (b) and (c) are obtained adsorbing one H_2O molecule either on the amino or on a carboxylic group of the *f*-2A-1,4-BDC fragment; model (a) is conversely obtained adsorbing one H_2O molecule on a Zn centre of a corner fragment (2A-B) builded, with a Zn_4O tetrahedral unit saturated by 2-amino substituted benzoate groups.

interesting to notice that the interaction strength of water with the Zn-centre is the largest one. At variance with the other two interaction modes, which occur trough H-bonds, the interaction of water with Zn-centres takes place by the oxygen atom.

WATER MOLECULE INVOLVEMENT IN THE CATALYTIC CYCLE

Considering that the Zn atom is the centre where the largest interaction strength was found and takin into account that catalysis at the metal centre in MOFs, even if saturated, has been reported in the literature it has been hypothesized that: water not even adsorbs on the Zn centre preventing the poisoning of the aminic sites but also

presents an active role in the catalytic cycle. Interestingly, there are analogies between the the water interaction with the inorganic vertex of IRMOF-3 and some zinc–based enzymes, as carboxypeptidase and carbonic anhydrase, that present a water molecule, coordinated to a Zn atom, involved in the catalytic cycle [201]. Therefore the catalytic cycle for the IRMOF-3 catalysts has been modified on the ground of this hypothesis. Following this, in the II step a water molecule is lost by the amino–alcoholic intermediate. At this stage of the catalytic cycle the Zn centre is very close to the molecule so it was hypothesized, on the ground of the calculations shown in the previous paragraph, that the water molecule may adsorb on the Zn atoms (Figure 37). In fact, the stabilization produced by this interaction, calculated with respect of the situation where the resulting imine and the water molecule are distant, is of -27 kJ mol^{-1}. The calculated interaction energy between the water molecule and the iminic intermediate has been corrected for the BSSE. This finding suggests that probably, the water Zn coordi-

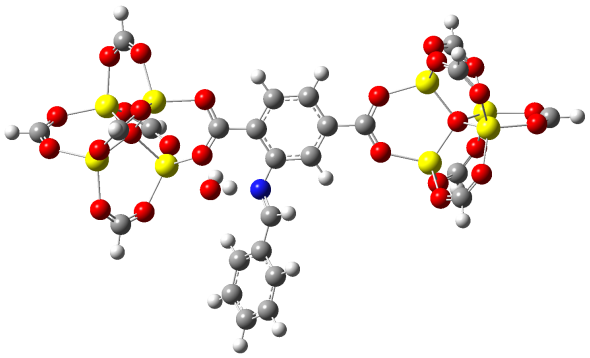

Figure 37.: Optimized structure of iminic intermediate with a water molecule adsorbed on the Zn atom of the inorganic vertex.

nated molecule, not only may be considered as a poison but also as an interactive species in the catalytic cycle. This outcome poses new question, in fact, the water may be considered as a new acidic catalytic centre and at the same time it could interfere with the *f*-2A-1,4-BDC catalyzed cycle even if it does not poison the aminic site; in fact, as reported above the Zn atom is crucial in the III and IV step of the catalytic cycle and this means that ethyl cyanoacetate has to move away water molecules from the Zn atom before reacting with the iminic derivative. Moreover, the presence of this acidic sites suggests the possibility that the water coordinated to the Zn atom may catalyze the keto–enolic conversion of the ethyl cyanoacetate. Considering this new unexpected findings further investigation on this aspects of the catalytic cycle will be carried out.

4.10 KEY POINTS

The information obtained by the performed calculations can be resumed into nine key points:

- characterization of the basic properties of IRMOF-3;
- elucidation of the relationship between the experimental proved increased basicity of IRMOF-3 and the structural features of the catalyst;
- individuation of a reasonable mechanism for the Knoevenagel condensation;
- computational characterization of all the intermediates hypothesized for the cycle catalyzed by aniline DM2AT and for the two IRMOF-3 models namely *f*-2A-1,4-BDC and IRMOF-3c;
- characterization of the transition states structures of the catalytic cycle;
- analysis of the deactivation route;
- comparison between the ethyl cyanoacetate and the ethyl acetoacetate as reactants;
- evaluation of the confinement effects;
- role of the water as poison and as active species in the catalytic cycle.

5

CONCLUSIONS AND FUTURE DEVELOPMENTS

> The ice age is coming, the sun is zooming in. Engines stop running and the wheat is growing thin. A nuclear error, but I have no fear.
>
> The Clash "London Calling"

In this doctoral thesis, molecular modeling was employed in order to elucidate the behaviour as catalyst of the IRMOF-3. It has been proved, already experimentally, that this catalyst is active in the Knoevenagel condensation of benzaldheyde and ethyl cyanoacetate, and it was established that it is more active than aniline. This study was aimed at understanding the structural features of IRMOF-3 responsible of the increased activity. This phenomenon was considered linked to electronic and steric effects that may influence the chemistry of the aromatic aminic moieties framed in the IRMOF-3 structure. Aniline and DM2AT were chosen to model the effect of an increasing local complexity, surrounding basic sites of interest for the IRMOF-3 systems. Different quantum mechanical methods were used in order to rationalize the IRMOF-3 behaviour as catalyst and various model sizes of IRMOF-3 were tested. Benchmark calculations were carried out in order to employ the best model in terms of accuracy and computational cost ratio. According to the obtained results it was demonstrated that structural features do not change appreciably with the increase of the model and also employing a QM/QM approach the structural parameters are not influenced. *f*-2A-1,4-BDC and IRMOF-3c have been selected as model for the title investigation. Thermodynamic properties as PA and IB have been calculated for this solid. It was stated that there is a relationship between the increased basicity of the aminic group framed into IRMOF-3 with respect of aniline and the reason of this lies in the formation of a 6–term *quasi*–planar ring in the protonated form that stabilizes the conjugate acid of IRMOF-3. Imines obtained by IRMOF-3 fragments are the most basic species involved in the cycle and the reason of their increased basicity lies, again, in the formation of intra–molecular O–H hydrogen bonds, originating 6–term *quasi*–planar rings. A reasonable mechanism for the Knoevenagel condensation catalyzed by IRMOF-3, was found between various hypothesized pathways. Full characterization of the intermediates and transition states involved in the catalytic cycle and in the deactivation route was performed. Moreover, also the reaction between benzaldheyde and ethyl acetoacetate was considered and it was found

a good agreement between the calculated and the experimental trend. Confinement effects were considered and it was stated that no further information are added to the investigation employing a QM/QM approach. At variance with literature results, the basicity of the starting catalysts and of the corresponding derivatives seems to not play a fundamental role in characterizing the different catalytic cycles related to the benzaldehyde and ethyl cyanoacetate condensation. The energy trends, characterizing both the condensation catalytic cycles and the relative deactivation paths of IRMOF-3, DM2AT and aniline, clearly display that the increased activity of IRMOF-3 can not be related to confinement effects and/or to energy differences, characterizing given steps involved in the catalytic process. Both the unexpected findings of the latter two points suggest that other local occurrences should drive the Knoevenagel condensation. One by-product occurring in the cycles is, in fact, water that is able to poison the aminic site, resulting in its deactivation. This effect, unlike the case of simpler phenylaminic species, can be avoided in the IRMOF-3 applications because its framework Zn-centres interact more strongly with the produced water molecules. The increased activity of IRMOF-3 can be, thus, explained by a lower deactivation of the catalyst caused by the produced water molecules. Interesting findings about the role of the inorganic vertex involvement in the catalytic process arise. In fact, the interaction with the Zn atom of the vertex seems to be fundamental in the stabilization of the transition states of IRMOF-3 and in the prevention of the poisoning of the aminic group. However, further investigations about the role of the inorganic vertex have to be carried out, because it is reliable that the adsorbed water on the vertex may be involved in the catalysis of the tautomeric equilibrium of ethyl cyanoacetate. In addition to this, will be deserved particular attention to studies about the solvent effects, with implicit and explicit approaches .

A

DENSITY FUNCTIONAL THEORY

There has been enormous growth in DFT since the early 1990s. The reason for this is simple. Correlated methods based on the 4N–dimensional many-electron wavefunction scale poorly with the system size and they require high angular momentum basis function to describe the electron–electron cusp [ref]. DFT, on the other hand, is a formally exact theory based on the one–electron density, which depends on just three spatial coordinates and one spin coordinate. It is therefore computationally much simpler and –because the wavefunction is not explictly modeled– the high angular momentum functions are much less important, allowing more modest basis sets to be used. It follows that DFT offers the possibility of high quality calculations at low computational cost. The key idea in DFT is to express the electronic energy as a functional of the electron density. A functional is a mathematical object that takes as its argument a function and which returns a number, in an analogous way to a function which takes a number as its argument and equally returns a number. Density functional theory has its conceptual roots in the Thomas–Fermi model and early DFT models found a widespread use in the solid–state physics community where the enormous system size required to mimic the properties of a solid required simplier approaches than those based on the wavefunction. DFT was rigorous founded in the 1964 by the two Hohenberg–Kohn theorems [14]. The approach of Hohenberg and Kohn was to formulaye density functional theory as an exact theory of many–body systems. The formulation applies to any system of interacting particles in an external potential , including any problem of electrons and fixed nuclei, where the hamiltonian can be written. However, they provide no guidance for constructing the functionals, and no exact functionals are known for any system of more than one electron. According to Martin *"DFT would remain a minor curiosity today if it were not for the ansatz made by Khon and Sham, which has provided a way to make useful, approximate ground state functionals for real systems of many electrons"* [202] The most fundamental difference between DFT and the molecular orbital (MO) theory can be recognized in the trivial observation that DFT optimizes an electron density while MO theory optimizes a wave function. So, to determine a particular molecular property using DFT, we need to know how that property depends on the density, while to determine the same property using a wave function, we need to know the correct quantum mechanical operator. As there are more well–characterized operators then there are generic property functionals of density, wave functions clearly have broader

utility. Anyway, the formal scaling behaviour of DFT is in principle no worse than N^3 where N is the number of basis functions used to represent the Kohn–Sham (KS) orbitals [13]. This is better than Hartree–Fock (HF) by a factor of N, and very substantially better than other methods that like DFT, also include electron correlation. As a rule, for programs that use approximately the same routines and algorithms to carry out HF and DFT calculations, the cost of a DFT calculation on a moderately sized molecule, is double of that of the HF calculation with the same basis set. According to Cramer *"one area where DFT enjoys a clear advantage over HF is in its ability to use basis functions that are not necessarily contracted Gaussians"*[203]. One of the most interesting possibility is the use of plane waves as basis set in periodic infinite systems. Even in cases where contracted, gaussian–type orbitals (GTOs) are chosen as basis sets, DFT offers the advantage that convergence with respect to basis set size tends to be more rapid than for MO techniques. Thus polarized valence double–ζ are quite adequate for a wide variety of calculation and very good convergence in many properties can be seen at the level of employing polarized triple–ζ basis sets. According to Cramer *"DFT functionals present certain pathological failures but the general picture for DFT is really quite bright"* [203].

A.1 RIGOROUS FUNDATION

A.1.1 *The Hohenberg–Kohn Existence Theorem*

The first Hohenberg–Kohn theorem demonstrates that the ground state properties of a many–electron system are uniquely determined by an electron density that depends on only 3 spatial coordinates. The many–electron Hamiltonian is given by:

$$\hat{H} = \hat{T} + \hat{V}_{ne} + \hat{V}_{ee} = -\sum_{i}^{N} \frac{1}{2}\nabla_i^2 + \sum_{i}^{N} v(\mathbf{r}_i) + \sum_{i<j}^{N} \frac{1}{r_{ij}} \tag{A.1}$$

where the first term is the many–electron kinetic energy operator, the second term is the nuclear–electron attraction operator and the final term is the electron–electron repulsion operator. The external potential due to the nuclei is given by

$$v(\mathbf{r}_i) = \sum_{A} \frac{Z_A}{r_{A_i}} \tag{A.2}$$

The proof of this theorem is presented in the following. Let there be two external potentials $v_1(\mathbf{r})$ and $v_2(\mathbf{r})$ arising from the same electron density $\rho(\mathbf{r})$. This implies that two different external potentials may be consistent with the same ground–state density. There will be two Hamiltonians $\hat{H}_1$ and $\hat{H}_2$ with the same ground state density, but

different wavefunctions Ψ_1 and Ψ_2. Evaluating the expectation value of $\hat{H}_1$ employing Ψ_2 and using the variational principle

$$\begin{aligned} E_1^0 &< \langle \Psi_2 \mid \hat{H}_1 \mid \Psi_2 \rangle \\ &= \langle \Psi_2 \mid \hat{H}_2 \mid \Psi_2 \rangle + \langle \Psi_2 \mid \hat{H}_1 \mid \Psi_2 \rangle - \langle \Psi_2 \mid \hat{H}_2 \mid \Psi_2 \rangle \\ &= \langle \Psi_2 \mid \hat{H}_2 \mid \Psi_2 \rangle + \langle \Psi_2 \mid \hat{H}_1 - \hat{H}_2 \mid \Psi_2 \rangle \\ &= E_2^0 + \int \rho(\mathbf{r})[v_1(\mathbf{r}) - v_2(\mathbf{r})]d\mathbf{r} \end{aligned} \tag{A.3}$$

The reasoning can be equally applied to the operator $\hat{H}_2$ and the wavefunction Ψ_1

$$\begin{aligned} E_2^0 &< \langle \Psi_1 \mid \hat{H}_2 \mid \Psi_1 \rangle \\ &= \langle \Psi_1 \mid \hat{H}_1 \mid \Psi_1 \rangle + \langle \Psi_1 \mid \hat{H}_2 \mid \Psi_1 \rangle - \langle \Psi_1 \mid \hat{H}_1 \mid \Psi_1 \rangle \\ &= \langle \Psi_1 \mid \hat{H}_1 \mid \Psi_1 \rangle + \langle \Psi_1 \mid \hat{H}_2 - \hat{H}_1 \mid \Psi_1 \rangle \\ &= E_1^0 + \int \rho(\mathbf{r})[v_2(\mathbf{r}) - v_1(\mathbf{r})]d\mathbf{r} \end{aligned} \tag{A.4}$$

Adding the two expression and considering the assumption that the ground–state densities associated with wavefunctions 1 and 2 were the same, permits to eliminate the integrals as they must sum to zero. The overall result is

$$E_1^0 + E_2^0 < E_2^0 + E_1^0 \tag{A.5}$$

which is a contraddiction. It follows that there can not be two different external potentials associated with the same density. The external potential is therefore determined by the density. The density also defines the number of electrons N and therefore all the components of the Hamiltonian $\hat{H}$. Thus, the electronic energy can be written as a functional of the density

$$E[\rho] = V_{ne}[\rho] + T[\rho] + V_{ee}[\rho] \tag{A.6}$$

where $T[\rho]$ is the kinetic energy, $V_{ee}[\rho]$ is the electron–electron interaction energy and $V_{ne}[\rho]$ is the nuclei–electron interaction energy.

A.1.2 *The Hohenberg–Kohn Variational Theorem*

The second Hohenberg–Kohn theorem establishes a variational principle based on the electron density, thus providing a method for its calculation. Assume that there is some well–behaved candidate density that integrates to the proper number of electrons, N. In that case, the first theorem indicates that this density $\bar{\rho}$ determines its own external potential $\bar{v}$ and hence its own wavefunction $\bar{\Psi}$. Using this wavefunction in the usual variational principle

$$\langle \bar{\Psi} \mid \hat{H} \mid \bar{\Psi} \rangle = \int \bar{\rho}(\mathbf{r})v(\mathbf{r})d\mathbf{r} + T[\rho] + V_{ee}[\rho] = E[\bar{\rho}] \geqslant E[\rho] \tag{A.7}$$

A.1.3 *Kohn–Sham self consistent Field methodology*

As a self–consistent method, the Kohn–Sham approach involves independent particles but an interacting density. The Kohn–Sham approach is to replace the difficult interacting many–body system obeying the hamiltonian A.1 with a different auxiliary system that can be solved more easily. There are no compulsory prescriptions for choosing the simpler auxiliary system, therefore Kohn and Sham state an *ansatz* assuming that the ground state density of the original interacting system is equal to that of some chosen non–interacting system. This leads to independent–particle equations for the non–interacting system that can be considered exactly soluble with all the difficult many–body terms incorporated into an exchange–correlation functional of the density. By solving the equations one finds the ground state density and energy of the original interacting system with the accuracy limited only by the approximations in the exchange–correlation functional. Kohn and Sham's idea was to introduce orbitals into the problem, allowing the kinetic energy to be computed accurately, leaving just a small residual correction. The electronic energy can be written exactly as

$$E[\rho] = \int \rho(\mathbf{r})v(\mathbf{r}) + F[\rho] \tag{A.8}$$

where $F[\rho]$ is

$$F[\rho] = T[\rho] + V_{ee}[\rho] \tag{A.9}$$

Kohn and Sham defined

$$F[\rho] = T_s[\rho] + J[\rho] + E_{XC}[\rho] \tag{A.10}$$

where $J[\rho]$ is the classical Hartree repulsion of the density with itself

$$J[\rho] = \frac{1}{2}\int\int \frac{\rho(\mathbf{r_1})\rho(\mathbf{r_2})}{r_{12}} d(\mathbf{r_1})d(\mathbf{r_2}) \tag{A.11}$$

and $T_s[\rho]$ is the kinetic energy of a system of non–interacting electrons with density ρ. Cosidering the two definitions of $F[\rho]$ it follows that

$$E_{XC} = T[\rho] - T_s[\rho] + V_{ee}[\rho] - J[\rho] \tag{A.12}$$

Minimising the Khon–Sham energy expression

$$E = \int \rho(\mathbf{r})v(\mathbf{r}) + T_s[\rho] + J[\rho] + E_{XC}[\rho] \tag{A.13}$$

with respect to the density gives the Euler equation

$$\mu = v_{eff}(\mathbf{r}) + \frac{\partial T_s[\rho]}{\partial \rho(\mathbf{r})} \tag{A.14}$$

where the effective potential is

$$v_{eff} = v(\mathbf{r}) + \frac{\partial J[\rho]}{\partial \rho(\mathbf{r})} + \frac{\partial E_{XC}[\rho]}{\partial \rho(\mathbf{r})} \tag{A.15}$$

The Hamiltonian for a system of non–interacting electrons moving in an external potential $v_{eff}(\mathbf{r})$ is

$$\hat{H} = -\sum_{i}^{N} \frac{1}{2}\nabla_i^2 + \sum_{i}^{N} v_{eff}(\mathbf{r}_i) \tag{A.16}$$

This operator is separable and so the exact wavefunction is simply a single determinant constructed from orbitals that are the solutions to

$$(-\frac{1}{2}\nabla_i^2 + v_{eff}(\mathbf{r}))\phi_i(\mathbf{r}) = \epsilon_i\phi_i(\mathbf{r}) \tag{A.17}$$

Considering that the density of the non–interacting system is identical to the density of the real system, it follows that

$$\rho(\mathbf{r}) = \sum_{i}^{N} \phi_i^2(\mathbf{r}) \tag{A.18}$$

while the kinetic energy of the non interacting system is given by

$$T_s[\rho] = \sum_{i}^{N} \langle \phi_i \mid -\frac{1}{2}\nabla^2 \mid \phi_i \rangle \tag{A.19}$$

The Kohn–Sham procedure can therefore be summarized just solving the following equations

$$(-\frac{1}{2}\nabla_i^2 + v_{eff}(\mathbf{r}))\phi_i(\mathbf{r}) = \epsilon_i\phi_i(\mathbf{r})$$

where

$$v_eff = v(\mathbf{r}) + \frac{\partial J[\rho]}{\partial \rho(\mathbf{r})} + \frac{\partial E_{XC}[\rho]}{\partial \rho(\mathbf{r})}$$

Then evaluate the electron density using

$$\rho(\mathbf{r}) = \sum_{i}^{N} \phi_i^2(\mathbf{r})$$

and the total electronic energy using

$$E = \int \rho(\mathbf{r})v(\mathbf{r}) + T_s[\rho] + J[\rho] + E_{XC}[\rho]$$

where

$$T_s[\rho] = \sum_{i}^{N} \langle \phi_i \mid -\frac{1}{2}\nabla^2 \mid \phi_i \rangle$$

Key point of this discussion is that Kohn–Sham theory is formally exact; if the exact exchange–correlation energy is used then the exact density and electronic energy of the real, interacting system are obtained. In practical calculations of course, the exchange–correlation energy must be approximated. It contains the difference between the exact electron–electron repulsion energy $V_{ee}[\rho]$ and the Coloumb energy $J[\rho]$, together with the difference between the exact kinetic energy $T[\rho]$ and non–interacting kinetic energy $T_s[\rho]$.

A.1.4 *Exchange and Correlation Functionals*

The fundamental difficulty in DFT is that it is not possible to *a priori* know how to write the exchange–correlation energy E_{XC}, which includes exchange, correlation and small kinetic component. There are many categories of approximations, including

- The local density approximation (LDA) where the energy is expressed as the integral of a function of just the density,

$$E_{XC} = \int F(\rho)\mathbf{dr} \tag{A.20}$$

- Generalised gradient approximation (GGA) where the energy is expressed as an integral of a function of the density and its gradient

$$E_{XC} = \int F(\rho, \nabla(\rho))\mathbf{dr} \tag{A.21}$$

- Meta GGAs, where higher order derivatives are introduced

$$E_{XC} = \int F(\rho, \nabla(\rho), \nabla^2(\rho))\mathbf{dr} \tag{A.22}$$

- Hybrid functionals, which combines a GGA functional with a fraction of exactly computed exchange, evaluated using Kohn–Sham orbitals

$$E_{XC} = \int F(\rho, \nabla(\rho))\mathbf{dr} + \xi E_X^0 \tag{A.23}$$

Perdew has referred to the hierarchy of approximations developed during the last two decades as the "Jacob's ladder of DFT" [204]. Some key comparisons between functionals performances are in the three points below

- For a given average level of accuracy, hybrid and meta-GGA DFT methods are obviously the most efficient, showing mean unsigned errors almost equal in quality to the much more expensive multilevel correlated methods. However, the maximum absolute errors are larger with the former methods than the latter, indicating a slightly lowere generality even in the most current generation of functionals.

- Hybrid and meta–GGA DFT functionals usually offer some improvement over coorresponding pure DFT functionals.

- Increasing the basis set size does not always improve the accuracy of the DFT models.

B

CURRICULUM

Scuole

- Twelfth European Summerschool in Quantum Chemistry 2009 svoltasi all'Hotel Torre Normanna, nel periodo 6-19 Settembre 2009

Seminari tenuti su richiesta dell'Università ospite

- Computational Study of L-Arabinose hydrogenation on Ru nanoparticles: preliminary results, 23-09-2010, Lappeenranta University of Technology Finland
- Computational Study of L-Arabinose hydrogenation on Ru nanoparticles, 18-11-2010, Åbo Akademi Turku Finland

Comunicazioni a congresso

- Sorrento, 5-10 Luglio 2009, *Theoretical Modelling of IRMOF-3: a computational approach on a hetereogeneous basic catalyst*, R. Cortese, D. Duca, F. Ferrante XXIII Congresso nazionale SCI
- Pisa, 12 Febbraio 2010, *IRMOF-3: A computational study on a heterogeneous basic catalyst*, R. Cortese, D. Duca Winter Modeling
- Glasgow, 28 Agosto-2 Settembre 2011, *IRMOF-3 and Knoevenagel condensation: A computational study*, R. Cortese, D. Duca Europacat X
- Lecce, 11-16 Settembre 2011, *IRMOF-3* Zn_4O *vertices: role in Knoevenagel condensation*, R. Cortese, D. Duca XXIV Congresso nazionale SCI

Comunicazioni orali a congresso

- Lecce, 11-16 Settembre 2011, *L-Arabinose adsorption on a Ru cluster*, R. Cortese, D. Yu Murzin, D. Duca XXIV Congresso nazionale SCI

Articoli

- N. Armata, G. Baldissin, G. Barone, R. Cortese, V. D'Anna, F. Ferrante, S. Giuffrida, G. Li Manni, A. Prestianni, T. Rubino, D. Duca, Top. Catal., 2009, 52, 444–455.
- N. Armata, G. Baldissin, G. Barone, R. Cortese, V. D'Anna, F. Ferrante, S. Giuffrida, G. Li Manni, A. Prestianni, T. Rubino, D. Duca, Top. Catal., 2009, 52, 431–443.

- R. Cortese, D.Duca Phys. Chem. Chem. Phys. 13, 2011, 15995–16004.
- R. Cortese, V. Sifontes–Herrera, D. Yu. Murzin, D. Duca submitted J. Chem. Inf. Mod.
- N. Armata, R. Cortese, R. Triolo, D. Duca submitted J. Phys. Chem. A
- R. Cortese, D. Duca "in preparation"

Varie

- Vincitrice Gadolin Scholarship presso la Åbo Akademi
- Collaborazione alla traduzione e alla cura dell'edizione italiana, "Chimica Inorganica" G. L. Miessler, D. A. Tarr PICCIN, della IV edizione inglese del testo "Inorganic Chemistry" G. L. Miessler, D. A. Tarr Prentice Hall
- Contributo "Modeled Catalytic Properties of MOF–based compounds" su richiesta dell'editore J. Jianwen al libro "Metal-Organic Frameworks: Materials Modeling towards Engineering Applications" Pan Stanford
- Partecipazione al progetto europeo POLYCAT

Periodi all'estero

- 15/05/2010-30/11/2010 Åbo Akademi Turku Finland

BIBLIOGRAPHY

[1] S. C. Tang, T. E. Paxson, and L. Kim, "Heterogenization of homogeneous catalysts-The immobilization of transition metal complexes on ion-exchange resins," *J. Mol. Cat.*, vol. 9, pp. 313–321, 1980.

[2] M. Peuckert and W. Keim, "Heterogenization of homogeneous nickel-based ethylene oligomerization catalysts," *J. Mol. Cat.*, vol. 22, pp. 289–295, 1984.

[3] J. M. Thomas and T. W. J., *Principle and Practice of Heterogeneous Catalysis*. Wiley-VCH, 1997.

[4] R. A. van Santen, P. W. N. M. van Leeuwen, J. A. Moulijn, and B. A. M. Averill, *Catalysis an Integrated Approach*. Elsevier, 1999.

[5] R. R. and F. Schüth, "Design of solid catalysts for the conversion of biomass," *Energy Environ. Sci.*, vol. 2, pp. 610–626, 2009.

[6] R. A. van Santen and M. Neurock, *Molecular Heterogeneous Catalysis*. Wiley-VCH, 2006.

[7] J. K. Nørskov, T. Bligaard, J. Rossmeisl, and C. H. Christensen, "Towards the computational design of solid catalysts," *Nature Chemistry*, vol. 1, pp. 37–46, 2009.

[8] L. J. Broadbelt and R. Q. Snurr, "Applications of molecular modeling in heterogeneous catalysis research," *Appl. Catal. A: Gen.*, vol. 200, pp. 23–46, 2000.

[9] I. Langmuir, "Chemical Reaction on Surfaces," *Trans. Faraday Soc.*, vol. 17, pp. 62–65, 1921.

[10] H. S. Taylor, "A Theory of the Catalytic Surface," *Proc. Roy. Soc. A*, vol. 108, pp. 105–111, 1925.

[11] N. I. Levine, *Quantum Chemistry*. Prentice Hall, 1999.

[12] W. Khon and L. J. Sham, "Self-Consistent equations including exchange and correlation effects," *Phys. Rev. A*, vol. 140, pp. 1133–1138, 1965.

[13] W. Kohn and L. S. Sham, "Phys. rev.," *Self–Consistent Equations Including Exchange and Correlation Effects*, vol. 140, pp. A1133–A1138, 1965.

[14] P. Hohenberg and W. Kohn, "Inhomogeneous Electron Gas," *Phys. Rev. B*, vol. 136, pp. B864–B871, 1964.

[15] N. Armata, G. Baldissin, G. Barone, R. Cortese, V. D'Anna, F. Ferrante, S. Giuffrida, G. Li Manni, A. Prestianni, T. Rubino, and D. Duca, "Structural and Kinetic DFT Characterization of Materials to Rationalize Catalytic Performance," *Top. Catal.*, vol. 52, pp. 444–455, 2009.

[16] G. Barone, G. Casella, S. Giuffrida, and D. Duca, "H-ZSM-5 modified zeolite: quantum chemical models of acidic sites," *J. Phys. Chem. C*, vol. 111, pp. 13033–13043, 2007.

[17] I. Czekaj, J. Wambach, and O. Kröcher, "Modelling Catalyst Surfaces Using DFT Cluster Calculations," *Int. J. Mol. Sci.*, vol. 10, pp. 4310–4329, 2009.

[18] M. Svensson, S. Humbel, R. D. J. Froese, T. Matsubara, S. Sieber, and K. Morokuma, "ONIOM: a multilayered integrated MO + MM method for geometry optimizations and single point energy predictions. A test for Diels-Alder reactions and $Pt(P(t{-}Bu)_3)_2$ + H_2 oxidative addition," *J. Phys. Chem.*, vol. 100, pp. 19357–19363, 1996.

[19] D. Loffreda, "Theoretical insight of adsorption thermodynamics of multifunctional molecules on metal surfaces," *Surf. Science*, vol. 600, pp. 2103–2112, 2006.

[20] M. Calatayuda, "Ethylene glycol interaction on alkaline earth oxides: A periodic DFT study," *Catal. Today*, vol. 152, pp. 88–92, 2010.

[21] G. C. Maitland, M. Rigby, E. B. Smith, and W. A. Wakeham, *Intermolecular Forces: Their Origin and Determination*. Clarendon Press, 1981.

[22] A. R. Leach, *Molecular Modeling: Principles and Applications*. Pearson Education EMA, 2001.

[23] J. L. Soto and A. L. Myers, "Monte Carlo studies of adsorption in molecular sieves," *Mol. Phys.*, vol. 42, pp. 971–983, 1981.

[24] W. G. B. and J. S. Rowlinson, "Computer simulations of fluids in zeolites X and Y," *J. Chem. Soc, Faraday Trans. 2*, vol. 85, pp. 765–781, 1989.

[25] J. A. Dumesic, D. F. Rudd, L. M. Aparicio, J. E. Rekoske, and A. A. Trevino, *The Microkinetics of Heterogeneous Catalysis*. American Chemical Society, 1993.

[26] J. Gascon, U. Aktay, M. D. Hernandez-Alonso, G. P. M. van Klink, and F. Kapteijn, "Amino-based metal-organic frameworks as stable, highly active basic catalysts," *J. Catal.*, vol. 261, pp. 75–87, 2009.

[27] J. H. Rayner and H. M. Powell, "Structure of molecular compounds. part X. Crystal structure of the compound of benzene with an ammonia-nickel cyanide complex," *J. Chem. Soc.*, pp. 319–328, 1952.

[28] R. Baur and G. Schwarzenbach, "Neue Einschlussverbindungen vom Typus des Nickelcyanid-Ammoniak-Benzols," *Helv. Chim. Acta*, vol. 43, pp. 842–847, 1960.

[29] W. P. Griffin, "Cyanide complexes of the transition metals," *Q. Rev., Chem. Soc.*, vol. 16, pp. 188–207, 1962.

[30] R. D. Billard and G. Wilkinson, "Triethylenetetramine complexes of cobalt(III) and rhodium(III)," *J. Chem. Soc.*, pp. 3193–3200, 1963.

[31] K. V. Krishnamurty, G. M. Harris, and V. S. Sastri, "Chemistry of the metal carbonato complexes," *Chem. Rev.*, vol. 70, pp. 171–197, 1970.

[32] T. Iwamoto, T. Nakano, M. Morita, T. Miyoshi, M. T., and Y. Sasaki, "The Hofman-type clathrate: $M(NH_3)2\,M\prime(CN)_4$," *Inorg. Chim. Acta*, vol. 2, pp. 313–316, 1968.

[33] R. A. Walton, "The reactions of metal halides with alkyl cyanides," *Q. Rev., Chem. Soc.*, vol. 19, pp. 126–143, 1965.

[34] M. B. and M. J. Zaworotko, "From Molecules to Crystal Engineering: Supramolecular Isomerism and Polymorphism in Network Solids," *Chem. Rev.*, vol. 101, pp. 1629–1658, 2001.

[35] S. L. James, "Metal-organic frameworks," *Chem. Soc. Rev.*, vol. 32, pp. 276–288, 2003.

[36] K. Biradha, M. Sarkar, and L. Rajput, "Crystal engineering of coordination polymers using 4,4′-bipyridine as a bond between transition metal atoms," *Chem. Commun.*, vol. 40, pp. 4169–4179, 2006.

[37] N. L. Rosi, M. Eddaoudi, J. Kim, M. O'Keeffe, and O. M. Yaghi, "Advances in the chemistry of metal-organic frameworks," *CrystEngComm*, vol. 4, pp. 401–404, 2002.

[38] G. K. H. Shimizu, "Assembly of metal ions and ligands with adaptable coordinative tendencies as a route to functional metal-organic solids," *J. Solid State Chem.*, vol. 178, pp. 2519–2526, 2005.

[39] A. K. Cheetham, C. N. R. Rao, and R. K. Feller, "Structural diversity and chemical trends in hybrid inorganic-organic framework materials," *Chem. Commun.*, vol. 46, pp. 4780–4795, 2006.

[40] M. J. Rosseinsky, "Recent developments in metal-organic framework chemistry: design, discovery, permanent porosity and flexibility," *Microporous Mesoporous Mater.*, vol. 73, pp. 15–30, 2004.

[41] A. Y. Robin and K. M. Fromm, "Coordination polymer networks with O- and N-donors: What they are, why and how they are made," *Coord. Chem. Rev.*, vol. 250, pp. 2127–2157, 2006.

[42] M. J. Zaworotko, "Molecules to Crystals, Crystals to Molecules ... and Back Again?," *Cryst. Growth Des.*, vol. 7, pp. 4–9, 2007.

[43] R. Robson, "Design and its limitations in the construction of bi- and poly-nuclear coordination complexes and coordination polymers (aka MOFs): a personal view," *Dalton Trans.*, vol. 38, pp. 5113–5131, 2008.

[44] B. F. Hoskins and R. Robson, "Infinite polymeric frameworks consisting of three dimensionally linked rod-like segments," *J. Am. Chem. Soc.*, vol. 111, pp. 5962–5964, 1989.

[45] B. F. Hoskins and R. Robson, "Design and construction of a new class of scaffolding-like materials comprising infinite polymeric frameworks of 3D-linked molecular rods. a reappraisal of the zinc cyanide and cadmium cyanide structures and the synthesis and structure of the diamond-related frameworks $[N(CH_3)_4][CuIZnII(CN)_4]$ and CuI[4,4′,4″,4‴-tetracyanotetraphenylmethane]$BF_4 \cdot xC_6H_5NO$," *J. Am. Chem. Soc.*, vol. 112, pp. 1546–1554, 1990.

[46] M. Fujita, M. Tominaga, A. Hori, and B. Therrien, "Coordination assemblies from a Pd(II)-Cornered Square Complex," *Acc. Chem. Res.*, vol. 38, pp. 369–378, 2005.

[47] P. J. Stang and B. Olenyuk, "Self-Assembly, Symmetry, and Molecular Architecture: Coordination as the Motif in the Rational Design of Supramolecular Metallacyclic Polygons and Polyhedra," *Acc. Chem. Res.*, vol. 30, pp. 502–518, 1997.

[48] M. Fujita, K. Umemoto, M. Yoshizawa, N. Fujita, T. Kusukawaand, and K. Biradha, "Molecular paneling via coordination," *Chem. Commun.*, vol. 6, pp. 509–518, 2001.

[49] A. F. Wells, "The geometrical basis of crystal chemistry. Part 1," *Acta Crystallogr.*, vol. 7, pp. 535–544, 1954.

[50] A. F. Wells, "The geometrical basis of crystal chemistry. Part 2," *Acta Crystallogr.*, vol. 1954, pp. 545–554, 7.

[51] J. J. Perry IV, J. A. Perman, and M. J. Zaworotko, "Design and synthesis of metal-organic frameworks using metal-organic

polyhedra as supermolecular building blocks," *Chem. Soc. Rev.*, vol. 38, pp. 1400–1417, 2009.

[52] G. B. Gardner, D. Venkataraman, J. S. Moore, and S. Lee, "Spontaneous assembly of a hinged coordination network," *Nature*, vol. 374, pp. 792–795, 1995.

[53] O. M. Yaghi, G. Li, and H. Li, "Selective binding and removal of guests in a microporous metal-organic framework," *Nature*, vol. 378, pp. 703–706, 1995.

[54] M. Kondo, T. Yoshitomi, K. Seki, H. Matsuzaka, and S. Kitagawa, "Three-Dimensional Framework with Channeling Cavities for Small Molecules: [M(4, 4′bpy)$_3$(NO$_3$)$_4$]x(H2O)n(M = Co, Ni, Zn)," *Angew. Chem., Int. Ed. Engl.*, vol. 36, pp. 1725–1727, 1997.

[55] Y. O. M. and H. Li, "Hydrothermal Synthesis of a Metal-Organic Framework Containing Large Rectangular Channels," *J. Am. Chem. Soc.*, vol. 117, pp. 10401–10402, 1995.

[56] O. M. Yaghi, D. A. Richardson, G. Li, E. Davis, and T. L. Groy, "Open-Framework Solids with Diamond-like Structures Prepared from Clusters and Metal-Organic Building Blocks," *Mater. Res. Soc. Symp. Proc.*, vol. 371, pp. 15–19, 1995.

[57] S. Noro, S. Kitagawa, M. Kondo, and K. Seki, "A New, Methane Adsorbent, Porous Coordination Polymer [CuSiF$_6$(4, 4′bipyridine)$_2$]n," *Angew. Chem., Int. Ed.*, vol. 39, pp. 2082–2084, 2000.

[58] S. Shimomura, S. Horike, and S. Kitagawa, "Chemistry and application of porous coordination polymers," *Stud. Surf. Sci. Catal.*, vol. 170B, pp. 1983–1990, 2007.

[59] J. Maddox, "Crystals from first principles," *Nature*, vol. 335, pp. 201–202, 1988.

[60] G. M. J. Schmidt, "Photodimerization in the solid state," *Pure Appl. Chem.*, vol. 27, pp. 647–678, 1971.

[61] G. U. Desiraju, *Crystal Engineering: The design of Organic Solids*. Elsevier, 1989.

[62] F. C. Hawthorne, "Structural aspects of oxide and oxysalt crystals," *Acta Cryst.*, vol. b50, pp. 481–510, 1994.

[63] O. M. Yaghi, M. O'Keeffe, N. W. Ockwig, H. K. Chae, M. Eddaoudi, and J. Kim, "Reticular synthesis and the design of new materials," *Nature*, vol. 423, pp. 705–714, 2003.

[64] M. Eddaouddi, D. Moler, H. Li, B. Chen, T. Reineke, M. O'Keeffe, and O. Yaghi, "Modular Chemistry: Secondary Building Units as a Basis for the Design of Highly Porous and Robust Metal-Organic Carboxylate Frameworks," *Acc. Chem. Res*, vol. 34, pp. 319–330, 2001.

[65] D. J. Tranchemontagne, J. L. Mendoza-Cortés, M. O'Keeffe, and O. M. Yaghi, "Secondary building units, nets and bonding in the chemistry of metal-organic frameworks," *Chem. Soc. Rev.*, vol. 38, pp. 1257–1283, 2009.

[66] M. Eddaoudi, H. L. Li, and O. M. Yaghi, "Highly Porous and Stable Metal-Organic Frameworks: Structure Design and Sorption Properties," *J. Am. Chem. Soc.*, vol. 122, pp. 1391–1397, 2000.

[67] A. P. Côtè, A. I. Benin, N. W. Ockwig, M. O'Keeffe, A. J. Matzger, and O. M. Yaghi, "Porous, Crystalline, Covalent Organic Frameworks," *Science*, vol. 310, pp. 1166–1170, 2005.

[68] F. Gandara, A. de Andres, B. Gomez-Lor, E. Gutierrez-Puebla, M. Iglesias, M. A. Monge, D. M. Proserpio, and N. Snejko, "A Rare-Earth MOF Series: Fascinating Structure, Efficient Light Emitters, and Promising Catalysts," *Cryst. Growth Des.*, vol. 8, pp. 378–380, 2008.

[69] A. Mantion, L. Massuger, P. Rabu, C. Palivan, L. B. McCusker, and A. Taubert, "Metal-Peptide Frameworks (MPFs): Bioinspired Metal Organic Frameworks," *J. Am. Chem. Soc.*, vol. 130, pp. 2517–2526, 2008.

[70] Z. Park, K. S. an Ni, A. P. Côtè, J. Y. Choi, R. D. Huang, F. J. Uribe-Romo, H. K. Chae, M. O'Keeffe, and O. M. Yaghi, "Exceptional chemical and thermal stability of zeolitic imidazolate frameworks," *Proc. Natl. Acad. Sci.*, vol. 103, pp. 10186–10191, 2006.

[71] G. Ferey, C. Mellot-Draznieks, C. Serre, F. Millange, J. Dutour, S. Surble, and I. Margiolaki, "A Chromium Terephthalate-Based Solid with Unusually Large Pore Volumes and Surface Area," *Science*, vol. 309, pp. 2040–2042, 2005.

[72] S. S. Y. Chui, S. M. F. Lo, J. P. H. Charmant, A. G. Orpen, and I. D. Williams, "A Chemically Functionalizable Nanoporous Material $[Cu_3(TMA)_2(H_2O)_3]n$," *Science*, vol. 283, pp. 1148–1150, 1999.

[73] M. O'Keeffe, M. A. Peskov, S. J. Ramsden, and O. M. Yaghi, "The Reticular Chemistry Structure Resource (RCSR) Database of, and Symbols for, Crystal Nets," *Acc. Chem. Res.*, vol. 41, pp. 1782–1789, 2008.

[74] N. W. Ockwig, O. Delgado-Friedrichs, M. O'Keeffe, and O. M. Yaghi, "Reticular Chemistry: Occurrence and Taxonomy of Nets and Grammar for the Design of Frameworks," *Acc. Chem. Res.*, vol. 38, pp. 176–182, 2005.

[75] S. Kitagawa, R. Kitaura, and S. Noro, "Functional Porous Coordination Polymers," *Angew. Chem., Int. Ed.*, vol. 43, pp. 2334–2375, 2004.

[76] H. Furukawa, J. Kim, N. W. Ockwig, M. O'Keeffe, and O. M. Yaghi, "Control of Vertex Geometry, Structure Dimensionality, Functionality, and Pore Metrics in the Reticular Synthesis of Crystalline Metal-Organic Frameworks and Polyhedra," *J. Am. Chem. Soc.*, vol. 130, pp. 11650–11661, 2008.

[77] K. Biradha, H. Hongo, Yoshito, and M. Fujita, "Open Square-Grid Coordination Polymers of the Dimensions 20 $\times$ 20 å: Remarkably Stable and Crystalline Solids Even after Guest Removal," *Angew. Chem., Int. Ed.*, vol. 39, pp. 3843–3845, 2000.

[78] C. J. Kepert and M. J. Rosseinsky, "Zeolite-Like Crystal Structure of an Empty Microporous Molecular Framework," *Chem. Commun.*, pp. 375–376, 1999.

[79] N. L. Rosi, M. Eddaouddi, J. Kim, M. O'Keeffe, and O. M. Yaghi, "Advances in the chemistry of metal-organic frameworks," *CrystEngComm*, vol. 4, pp. 401–404, 2002.

[80] O. M. Rowsell, J. L. C. Yaghi, "Metal-organic frameworks: a new class of porous materials," *Microporous Mesoporous Mater.*, vol. 73, pp. 3–14, 2004.

[81] K. Biradha, "Are "secondary building units" the true building blocks in crystal engineering of coordination polymers?," *Current Science*, vol. 92, pp. 584–585, 2007.

[82] A. Ramanan and M. S. Whittingham, "How Molecules Turn into Solids: the Case of Self-Assembled Metal-Organic Frameworks," *Cryst. Growth Des.*, vol. 6, pp. 2419–2421, 2006.

[83] S. Natarajan and P. Mahata, "Non-carboxylate based metal-organic frameworks (MOFs and related aspects," *Curr. Opin. Solid State Meter. Sci.*, vol. 13, pp. 46–53, 2009.

[84] A. Clearfield, "Metal phosphonate chemistry," *Prog. Inorg. Chem.*, vol. 47, pp. 371–510, 1998.

[85] J. Liang and G. H. K. Shimizu, "Crystalline zinc diphosphonate metal-organic framework with three-dimensional microporosity," *Inorg. Chem.*, vol. 46, pp. 5229–5236, 2007.

[86] S. Konar, J. Zon, A. V. Prosvirin, K. R. Dunbar, and A. Clearfield, "Synthesis and characterization of four metal-organophosphonates with one- two- and three-dimensional structures," *Inorg. Chem.*, vol. 46, pp. 5229–5236, 2007.

[87] B. Liu, B. L. Li, Y. Z. Li, Y. Chen, S. S. Bao, and L. M. Zheng, "Lanthanide diruthenium (II,III) compounds showing layered ad Pt-S type open framework structures," *Inorg. Chem.*, vol. 46, pp. 8524–8532, 2007.

[88] Y. S. Ma, Y. Song, and L. M. Zheng, "Nature of the ln^{III}-co^{II} magnetic interactions in compounds $[Ln_2Co_3(C_5H_4NPO_3)_6]4\,H_2O$," *Inorg. Chim. Acta*, vol. 361, pp. 1363–1371, 2008.

[89] Y. S. Ma, H. Li, J. J. Wang, S. S. Bao, R. Cao, and Y. Z. Li, "Three-dimensional lanthanide(III)-copper(II) compounds based on an unsymmetrical 2-pyriylphosphonate ligand: an experimental and theoretical study," *Chem. Eur. J.*, vol. 13, pp. 4759–4769, 2007.

[90] S. R. Miller, G. M. Pearce, P. A. Wright, F. Bonino, S. Chavan, and S. Bordiga, "Structural transformations and adsorption of fuel related gases of structurally responsive nickel phosphonate metal-organic framework, Ni-STA-12," *J. Am. Chem. Soc.*, vol. 10, pp. 1124–1131, 2008.

[91] N. Zheng, J. Zhang, X. Bu, and P. Feng, "Cadmium-porphyrin coordination networks: rich coordination modes and three-dimensional four connected $CdSO_4$ and (3,5)-connected hams nets," *Cryst. Growth Des.*, vol. 7, pp. 2576–2581, 2007.

[92] S. Muniappan, S. Lipstman, S. George, and I. Goldberg, "Porphyrin framework solids. synthesis and structure of hybrid coordination polymers of tetra(carboxyphenyl)porphyrins and lanthanide-bridging ions," *Inorg. Chem.*, vol. 46, pp. 5544–5554, 2007.

[93] E. Y. Choi, P. M. Barron, R. W. Novotney, C. Hu, Y. U. Kwon, and W. A. Choe, "A mixed-linker porhyrin framework with CdI_2-type topology.," *CrystEngComm*, vol. 10, pp. 824–826, 2008.

[94] Y. Diskin-Posoner and I. Goldberg, "From porphyrin sponges to porphyrin sieves: a unique crystalline lattice of aquazinc tetra(4-carboxyphenyl)porphyrin with nanosized channels," *Chem. Commun.*, pp. 1961–1962, 1999.

[95] Y. Diskin-Posoner, S. Dahal, and I. Goldberg, "Crystal engineering of Metalloporphyrin Zeolite Analogues," *Angew. Chem. Int. Ed.*, vol. 39, pp. 1288–1292, 2000.

[96] A. Phan, C. J. Doonan, F. J. Uribe-Romo, C. B. Knobler, M. O'Keeffe, and O. M. Yaghi, "Synthesis, Structure, and Carbon

Dioxide Capture Properties of Zeolitic Imidazolate Frameworks," *Acc. Chem. Res.*, vol. 43, pp. 58–67, 2010.

[97] B. Wang, A. P. Côtè, H. Furukawa, M. O'Keeffe, and O. M. Yaghi, "Colossal Cages in Zeolitic Imidazolate Frameworks as Selective Capture Dioxide Reservoirs," *Nature*, vol. 453, pp. 207–212, 2008.

[98] H. Li, M. Eddaoudi, M. O'Keeffe, and O. M. Yaghi, "Design and synthesis of an exceptionally stable and highly porous metal-organic framework," *Nature*, vol. 402, pp. 276–279, 1999.

[99] J. N. Van Niekerk and Schoening, "A new type of copper complex as found in the crystal structure of cupric acetate, $Cu_2(CH_3COO)_4\ 2\,H_2O$," *Acta Cryst.*, vol. 6, pp. 227–232, 1953.

[100] G. M. Brown and R. Chidambaram, "Dinuclear copper(II) acetate monohydrate: a redetermination of the structure by neutron-diffraction analysis," *Acta Cryst. B*, vol. B 29, pp. 2393–2403, 1973.

[101] S. I. Vagin, A. K. Ott, and B. Rieger, "Paddle-Wheel Zinc Carboxylate Clusters as Building Units for Metal-Organic Frameworks," *Chemie Ingenieur Technik*, vol. 79, pp. 767–780, 2007.

[102] F. A. Cotton, C. Y. Liu, and C. A. Murillo, "Systematic Preparation ofMo_{24}^{+} Building Blocks for Supramolecular Assemblies," *Inorg. Chem.*, vol. 43, pp. 2267–2276, 2004.

[103] S. Takamizawa, E. Nakata, T. Saito, T. Okamura, and N. Ueyama, "Microporous solid based solely upon an intermolecular NH...O and nh... Cl hydrogen bond network," *Inorg. Chem. Commun.*, vol. 6, pp. 1239–1242, 2003.

[104] G. F. Liu, Z. P. Qiao, H. Z. Wang, X. M. Chen, and G. Yang, "Synthesis, structures and photoluminescence of three terbium(III) dicarboxylate coordination polymers," *New J. Chem.*, vol. 26, pp. 791–795, 2002.

[105] H. Koyama and Y. Saito, "The Crystal Structure of Zinc Oxyacetate, $Zn_4O(CH_3COO)_6$," *Bull. Chem. Soc. Jpn.*, vol. 27, pp. 112–114, 1954.

[106] F. Tulinsky, C. R. A. Worthington, and E. Pignataro, "Basic beryllium acetate. I. The collection of intensity data," *Acta Cryst.*, vol. 12, pp. 623–626, 1959.

[107] P. Jaitner, C. Rieker, and K. Wurst, "Aggregation of carbamato ligands around the $[Co_4O]_6^+$ core. synthesis and structure of the cluster $[Co_4O(O_2CNC_9H_{18})_6]$ prepared by a novel oxo-transfer reaction of the nitroxyl free radical 2,2,6,6-tetramethylpiperidin-1-oxyl with $[Co_2(CO)_8]$," *Chem. Commun.*, pp. 1245–1246, 1997.

[108] M. Eddaoudi, J. Kim, N. Rosi, D. Vodak, J. Watcher, M. O'Keeffe, and O. M. Yaghi, "Systematic Design of Pore Size and Functionality in Isoreticular MOFs and Their Application in Methane Storage," *Science*, vol. 295, pp. 469–472, 2002.

[109] N. L. Rosi, J. Eckert, M. Eddaoudi, D. T. Vodak, J. Kim, M. O'Keeffe, and O. M. Yaghi, "Hydrogen Storage in Microporous Metal-Organic Frameworks," *Science*, vol. 300, pp. 1127–1129, 2003.

[110] J. L. C. Rowsell, A. R. Millward, K. S. Park, and O. M. Yaghi, "Hydrogen Sorption in Functionalized Metal-Organic Frameworks," *J. Am. Chem. Soc.*, vol. 126, pp. 5666–5667, 2004.

[111] A. R. Millward and O. M. Yaghi, "Metal-Organic Frameworks with Exceptionally High Capacity for Storage of Carbon Dioxide at Room Temperature," *J. Am. Chem. Soc.*, vol. 127, pp. 17998–17999, 2005.

[112] J. L. C. Rowsell and O. M. Yaghi, "Strategies for Hydrogen Storage in Metal-Organic Frameworks," *Angew. Chem. Int. Ed. Engl.*, vol. 44, pp. 4670–4679, 2005.

[113] S. Ma, D. Sun, J. M. Simmons, C. D. Collier, D. Yuan, and H. Zhou, "Metal-Organic Framework from an Anthracene Derivative Containing Nanoscopic Cages Exhibiting High Methane Uptake," *J. Am. Chem. Soc.*, vol. 130, pp. 1012–1016, 2008.

[114] H. K. Chae, D. K. Siberio-Pèrez, J. Kim, Y. Go, M. Eddaouddi, A. J. Matzger, M. O'Keeffe, and O. M. Yaghi, "A route to high surface area, porosity and inclusion of large molecules in crystals," *Nature*, vol. 427, pp. 523–527, 2004.

[115] H. Li, M. Eddaouddi, O. M. Groy, and O. M. Yaghi, "Establishing Microporosity in Open Metal-Organic Frameworks: Gas Sorption Isotherms for Zn(BDC) (BDC = 1,4-Benzenedicarboxylate)," *J. Am. Chem. Soc.*, vol. 120, pp. 8571–8572, 1998.

[116] U. D. of Energy, "Multi-year research, development and demonstration plan: Planned program activities for 2003-2010: Technical plan." http://www.eere.energy.gov/hydrogenandfuelcells/mypp/pdfs/storage.pdf.

[117] J. L. Roswell, A. R. Millward, K. S. Park, and O. M. Yaghi, "Hydrogen Sorption in Functionalized Metal-Organic Frameworks," *J. Am. Chem. Soc.*, vol. 126, pp. 5666–5667, 2004.

[118] A. R. Millward and O. M. Yaghi, "Metal-Organic Frameworks with Exceptionally High Capacity for Storage of Carbon Dioxide

at Room Temperature," *J. Am. Chem. Soc.*, vol. 127, pp. 17998–17999, 2005.

[119] R. Banerjee, A. Phan, B. Wang, C. Knobler, H. Furukawa, M. O'Keeffe, and O. M. Yaghi, "High-Throughput Synthesis of Zeolitic Imidazolate Frameworks and Application to CO_2 Capture," *Science*, vol. 319, p. 939, 2008.

[120] R. Banerjee, H. Furukawa, D. Britt, C. Knobler, M. O'Keeffe, and O. M. Yaghi, "Control of the Pore Size and Functionality in Isoreticular Zeolitic Imidazolate Frameworks as Selective Carbon Dioxide Reservoirs," *Nature*, vol. 453, pp. 207–212, 2008.

[121] M. Fujita, Y. J. Kwon, S. Washizu, and K. Ogura, "Preparation, Clathration Ability, and Catalysis of a Two-Dimensional Square Network Material Composed of Cadmium(II) and 4,4'-Bipyridine," *J. Am. Chem. Soc.*, vol. 116, pp. 1151–1152, 1994.

[122] J. Y. Lee, O. K. Farha, J. Roberts, K. A. Scheidt, S. T. Nguyen, and J. T. Hupp, "Metal-organic framework materials as catalysts," *Chem. Soc. Rev.*, vol. 38, pp. 1450–1459, 2009.

[123] S. H. Cho, B. Ma, S. T. Nguyen, J. T. Hupp, and T. E. Albrecht-Schmitt, "A metal-organic framework material that functions as an enantioselective catalyst for olefin epoxidation," *Chem. Commun.*, pp. 2563–2565, 2006.

[124] M. H. Alkordi, Y. Liu, R. W. Larsen, J. F. Eubank, and M. Eddaoudi, "Zeolite-like Metal-Organic Frameworks as Platforms for Applications: On Metalloporphyrin-Based Catalysts," *J. Am. Chem. Soc.*, vol. 130, pp. 12639–12641, 2008.

[125] C. D. Wu, A. Hu, L. Zhang, and W. Lin, "A Homochiral Porous Metal-Organic Framework for Highly Enantioselective Heterogeneous Asymmetric Catalysis," *J. Am. Chem. Soc.*, vol. 127, pp. 8940–8941, 2005.

[126] S. S. Chui, S. M. Lo, J. P. Charmant, A. G. Orpen, and I. D. Williams, "A Chemically Functionalizable Nanoporous Material $[Cu_3(TMA)_2(H_2O)_3]n$," *Science*, vol. 283, pp. 1148–1150, 1999.

[127] O. K. Farha, K. L. Mulfort, and J. T. Hupp, "An Example of Node-Based Postassembly Elaboration of a Hydrogen-Sorbing, Metal-Organic Framework Material," *Inorg. Chem.*, vol. 47, pp. 10223–10225, 2008.

[128] S. Horike, M. Dinca, K. Tamaki, and J. R. Long, "Size-Selective Lewis Acid Catalysis in a Microporous Metal-Organic Framework with Exposed Mn_2^+ Coordination Sites," *J. Am. Chem. Soc.*, vol. 130, pp. 5954–5855, 2008.

[129] A. Corma, H. Garcìa, and F. X. Llabrés i Xamena, "Engineering Metal Organic Frameworks for Heterogeneous Catalysis," *Chem. Rev.*, vol. 110, pp. 4606–4655, 2010.

[130] F. X. Llabres i Xamena, A. Abad, A. Corma, and H. Garcìa, "MOFs as catalysts: Activity, reusability and shape-selectivity of a Pd-containing MOF," *J. Catal.*, vol. 250, pp. 294–298, 2007.

[131] U. Ravon, M. E. Domine, C. Gaudillere, A. Desmartin-Chomel, and D. Farrusseng, "MOFs as acid catalysts with shape selectivity properties," *New J. Chem.*, vol. 32, pp. 937–940, 2008.

[132] J. S. Seo, D. Whang, H. Lee, S. I. Jun, J. Oh, Y. J. Jeon, and K. Kim, "A homochiral metal–organic porous material for enantioselective separation and catalysis," *Nature*, vol. 404, pp. 982–986, 2000.

[133] M. M uller, S. Hermes, K. K ahler, M. W. E. van den Berg, M. Muhler, and R. A. Fischer, "Loading of MOF-5 with Cu and ZnO Nanoparticles by Gas–Phase Infiltration with Organometallic Precursor: Properties of Cu/ZnO@MOF as Catalyst for Methanol Synthesis," *Chem. Mater.*, vol. 20, pp. 4576–4587, 2008.

[134] B. Smit and T. L. M. Maesen, "Molecular Simulations of Zeolites: Adsorption, Diffusion, and Shape Selectivity," *Chem. Rev.*, vol. 108, pp. 4125–4184, 2008.

[135] J. Hafner, "*Ab-initio* simulations of materials using VASP: Density-functional theory and beyond," *J. Comput. Chem.*, vol. 29, pp. 2044–2078, 2008.

[136] J. Hafner, L. Benco, and T. Bucko, "Acid–based Catalysis in Zeolites Investigated by Density-Functional Methods," *Top. Catal.*, vol. 37, pp. 41–54, 2006.

[137] M. Tafipolsky, S. Amirjalayer, and R. Schmid, "Atomistic theoretical models for nanoporous hybrid materials," *Microporous Mesoporous Mater.*, vol. 129, pp. 304–318, 2010.

[138] T. Mueller and G. Ceder, "A Density Functional Theory Study of Hydrogen Adsorption in MOF-5," *J. Phys. Chem. B*, vol. 2005, pp. 17974–17983, 109.

[139] F. M. Mulder, T. J. Dingemans, M. Wagemaker, and G. J. Kearley, "Modelling of hydrogen adsorption in the metal organic framework MOF-5," *Chem. Phys.*, vol. 317, pp. 113–118, 2005.

[140] B. Civalleri, F. Napoli, Y. Noel, C. Roetti, and R. Dovesi, "Ab-initio prediction of materials properties with CRYSTAL: MOF-5 as a case study," *Cryst. Eng. Com.*, vol. 8, pp. 364–371, 2006.

[141] Y. Gao and X. C. Zeng, "Ab initio Study of Hydrogen Adsorption on Benzenoid Linkers in Metal–Organic Framework Materials," *J. Phys.: Condens. Matter*, vol. 19, pp. 386220–386225, 2007.

[142] C. F. Braga and R. L. Longo, "Structure of Functionalized Porous Metal–Organic Frameworks," *J. Mol. Struct.–Theochem*, vol. 716, pp. 33–38, 2005.

[143] T. Sagara, J. Klassen, J. Ortony, and E. Ganz, "Binding energies of hydrogen molecules to isoreticular metal–organic framework materials," *J. Chem. Phys.*, vol. 123, pp. 1944730–1944734, 2005.

[144] Q. Yang and C. Zhong, "Understanding Hydrogen Adsorption in Metal–Organic Frameworks with Open Metal Sites: A Computational Study," *J. Phys. Chem. B*, vol. 110, pp. 655–658, 2006.

[145] S. S. Han, J. L. Mendoza-Cortes, and W. A. I. Goddard, "Recent advances on simulation and theory of hydrogen storage in metal-organic frameworks and covalent organic frameworks," *Chem. Soc. Rev.*, vol. 38, pp. 1460–1476, 2009.

[146] Q. Yang, C. Zhong, and J. F. Chen, "Computational Study of co2 Storage in Metal-Organic Frameworks," *J. Phys. Chem. C*, vol. 112, pp. 1562–1569, 2008.

[147] C. Zheng, D. Liu, Q. Yang, C. Zhong, and J. Mi, "Computational Study on the Influences of Framework Charges on CO2 Uptake in Metal-Organic Frameworks," *Ind. Eng. Chem. Res.*, vol. 48, pp. 10479–10484, 2009.

[148] S. Keskin, J. Liu, R. B. Rankin, J. K. Johnson, and D. S. Sholl, "Progress, Opportunities, and Challenges for Applying Atomically Detailed Modeling to Molecular Adsorption and Transport in Metal-Organic Framework Materials," *Ind. Eng. Chem. Res.*, vol. 48, pp. 2355–2371, 2009.

[149] G. Garberoglio, A. I. Skoulidas, and J. K. Johnson, "Adsorption of Gases in Metal Organic Materials:Comparison of Simulations and Experiments," *J. Phys. Chem. B*, vol. 109, pp. 13094–13103, 2005.

[150] Q. Yang and C. Zhong, "Molecular Simulation of Adsorption and Diffusion of Hydrogen in Metal-Organic Frameworks," *J. Phys. Chem. B*, vol. 109, pp. 11862–11864, 2005.

[151] M. P. Allen and D. J. Tildesley, *Computer Simulation of Liquids*. Oxford University Press, 1987.

[152] D. Frenkel and B. Smit, *Understanding Molecular Simulation: From Algorithms to Applications*. Accademic Press, 2002.

[153] C. Møller and M. S. Plesset, "Note on an approximation treatment for many-electron systems," *Phys. Rev.*, vol. 46, pp. 618–622, 1934.

[154] O. Hüber, A. Gl oss, M. Fichtner, and W. Klopper, "On the Interaction of Dihydrogen with Aromatic Systems," *J. Phys. Chem. A*, vol. 108, pp. 3019–3023, 2004.

[155] T. Sagara, J. Klassen, and E. Ganz, "Computational study of hydrogen binding by metal-organic framework-5," *J. Chem. Phys.*, vol. 121, pp. 12543–12548, 2004.

[156] S. Hamel and M. Côtè, "First-principles study of the rotational transitions of H_2 physisorbed over benzene," *J. Chem. Phys.*, vol. 121, pp. 12618–12626, 2004.

[157] K. Sillar, A. Hofmann, and J. Sauer, "Ab Initio Study of Hydrogen Adsorption in MOF-5," *J. Am. Chem. Soc.*, vol. 131, pp. 4134–4150, 2009.

[158] R. N. Devi, M. Edgar, J. Gonzalez, D. P. Slawin, D. P. Tunstall, P. Grewal, P. A. Cox, and P. A. Wright, "Structural Studies and Computer Simulation of the Inclusion of Aromatic Hydrocarbons in a Zinc 2,6-Naphthalene Dicarboxylate Framework Compound," *J. Phys. Chem. B*, vol. 108, pp. 535–543, 2004.

[159] S. Hamel, T. V., and M. Côtè, "Fullerene in a Metal-Organic Matrix: Design of the electronic structure," *Pys. Rev. Lett.*, vol. 95, pp. 146403–146407, 2005.

[160] S. Choomwattana, T. Maihom, P. Khongpracha, M. Probst, and J. Limtrakul, "Structures and Mechanisms of the Carbonylene Reaction between MOF-11 encapsulated formaldehyde and propylene: An ONIOM Study," *J. Phys. Chem.*, vol. 112, pp. 10855–10861, 2008.

[161] C. F. Braga and R. L. Longo, "Conformational analysis of protonated cyclo-[(S)-phenylalanyl-(S)-histidyl] and its complex with benzaldehyde within metal-organic frameworks (MOFs)," *J. Braz. Chem. Soc.*, vol. 19, pp. 321–329, 2008.

[162] M. J. Frisch, G. W. Trucks, H. B. Schlegel, G. E. Scuseria, M. A. Robb, J. R. Cheeseman, J. A. Montgomery Jr., T. Vreven, K. N. Kudin, J. C. Burant, J. M. Millam, S. S. Iyengar, J. Tomasi, V. Barone, B. Mennucci, M. Cossi, G. Scalmani, N. Rega, G. A. Petersson, H. Nakatsuji, M. Hada, M. Ehara, K. Toyota, R. Fukuda, J. Hasegawa, M. Ishida, T. Nakajima, Y. Honda, O. Kitao, H. Nakai, M. Klene, X. Li, J. E. Knox, H. P. Hratchian, J. B. Cross, V. Bakken, C. Adamo, J. Jaramillo, R. Gomperts, R. E. Stratmann, O. Yazyev, A. J. Austin, R. Cammi, C. Pomelli, J. W.

Ochterski, P. Y. Ayala, K. Morokuma, G. A. Voth, P. Salvador, J. J. Dannenberg, V. G. Zakrzewski, S. Dapprich, A. D. Daniels, M. C. Strain, O. Farkas, D. K. Malick, A. D. Rabuck, K. Raghavachari, J. B. Foresman, J. V. Ortiz, Q. Cui, A. G. Baboul, S. Clifford, J. Cioslowski, B. B. Stefanov, G. Liu, A. Liashenko, P. Piskorz, I. Komáromi, R. L. Martin, D. J. Fox, T. Keith, M. A. Al-Laham, C. Y. Peng, A. Nanayakkara, M. Challacombe, P. M. W. Gill, B. Johnson, W. Chen, M. W. Wong, C. Gonzalez, and J. A. Pople, *Gaussian 03, Revision D.02*. Gaussian, Inc., Wallingford CT, 2005.

[163] J. B. Foresman and Æ. Frisch, *Exploring Chemistry with Electronic Structure Methods*. Gaussian Inc., 1996.

[164] S. Dapprich, I. Komároni, K. Byun, K. Morokuma, and M. J. Frisch, "A new ONIOM implementation in Gaussian98. Part I. The calculation of energies, gradients, vibrational frequencies and electric field derivatives," *J. Mol. Struct. (THEOCHEM)*, vol. 461–462, pp. 1–21, 1999.

[165] M. J. S. Dewar, E. G. Zoebisch, E. F. Healy, and J. J. P. Stewart, "Development and use of quantum mechanical molecular models. 76. AM1: a new general purpose quantum mechanical molecular model," *J. Am. Chem. Soc.*, vol. 107, pp. 3902–3909, 1985.

[166] J. J. P. Stewart, "Optimization of parameters for semiempirical methods I. method," *J. Comput. Chem.*, vol. 10, pp. 209–220, 1989.

[167] J. J. P. Stewart, "Optimization of parameters for semiempirical methods II. applications," *J. Comput. Chem.*, pp. 221–264, 1989.

[168] A. Becke, "Density-functional exchange-energy approximation with correct asymptotic behavior," *Phys. Rev. A*, vol. 38, pp. 3098–3100, 1988.

[169] J. Perdew, "Density-functional approximation for the correlation energy of the inhomogeneous electron gas," *Phys. Rev. B*, vol. 33, pp. 8822–8824, 1986.

[170] A. D. Becke, "Density-functional thermochemistry. III. The role of exact exchange," *J. Chem. Phys.*, vol. 98, pp. 5648–5652, 1993.

[171] P. J. Stephens, J. F. Devlin, C. F. Chabalowsky, and M. J. Frisch, "Ab-initio calculation of vibrational absorption and circular dichroism spectra using density-functional force fields," *J. Phys. Chem.*, vol. 98, pp. 11623–11627, 1994.

[172] V. Barone and C. Adamo, "Exchange functionals with improved long-range behavior and adiabatic connection methods without adjustable parameters: The mpw and mpw1pw models," *J. Chem. Phys.*, vol. 108, pp. 664–675, 1988.

[173] A. Becke, "Density-functional thermochemistry .4. a new dynamical correlation functional and implications for exact-exchange mixing," *J. Chem. Phys.*, vol. 104, pp. 1040–1046, 1996.

[174] P. J. Hay and W. R. Wadt, "Ab initio effective core potentials for molecular calculations. Potentials for the transition metal atoms Sc to Hg," *J. Chem. Phys.*, vol. 82, pp. 270–284, 1985.

[175] P. J. Hay and W. R. Wadt, "Ab initio effective core potentials for molecular calculations. Potentials for the transition main group elements Na to Bi," *J. Chem. Phys.*, vol. 82, pp. 284–299, 1985.

[176] P. J. Hay and W. R. Wadt, "Ab initio effective core potentials for molecular calculations. potentials for K to Au including the outermost core orbitals," *J. Chem. Phys.*, vol. 82, pp. 299–311, 1985.

[177] P. C. Hariharan and J. A. Pople, "The influence of polarization functions on molecular orbital hydrogenation energies," *Theor. Chim. Acta*, vol. 28, pp. 213–222, 1973.

[178] M. M. Francl, W. J. Petro, W. J. Hehre, J. S. Binkley, D. J. Gordon, M. S.; De Frees, and J. A. Pople, "Self-consistent molecular orbital methods. XXIII. a polarization-type basis set for second-row elements," *J. Chem. Phys.*, vol. 77, pp. 3654–3665, 1982.

[179] S. F. Boys and F. Bernardi, "The calculation of small molecular interactions by the differences of separate total energies. Some procedures with reduced errors," *Mol. Phys.*, vol. 19, pp. 553–566, 1970.

[180] R. A. van Santen, "The cluster approach to molecular heterogeneous catalysis," *J. Mol. Cat. A: Chem.*, vol. 115, pp. 405–419, 1997.

[181] G. Barone, N. Armata, A. Prestianni, T. Rubino, D. Duca, and D. Yu. Murzin, "Confined but-2-ene catalytic isomerization inside H-ZSM-5 models: A DFT study," *J. Chem. Theory Comput.*, vol. 5, pp. 1274–1283, 2009.

[182] T. Yildirim and M. R. Hartman, "Direct Observation of Hydrogen Adsorption Sites and Nanocage Formation in Metal-Organic Frameworks," *Phys. Rev. Lett.*, vol. 95, pp. 215504–215508, 2005.

[183] M. Head-Gordon, J. A. Pople, and M. J. Frisch, "MP2 energy evaluation by direct methods," *Chem. Phys. Lett.*, vol. 153, pp. 503–506, 1988.

[184] M. J. Frisch, M. Head-Gordon, and J. A. Pople, "Semi-direct algorithms for the MP2 energy and gradient," *Chem. Phys. Lett.*, vol. 166, pp. 281–289, 1990.

[185] R. S. Mulliken, "Electronic population analysis on LCAO-MO molecular wave functions. i," *J. Phys. Chem.*, vol. 23, pp. 1833–1831, 1955.

[186] P. O. Löwdin, "On the Nonorthogonality Problem," *Adv. Quantum Chem.*, vol. 5, pp. 185–199, 1970.

[187] P. O. Löwdin, "The nonorthogonality problem connected with the use of atomic wave functions in the theory of molecules and crystals," *J. Chem. Phys.*, vol. 18, pp. 365–375, 1950.

[188] K. Morokuma, "Why Do Molecules Interact ? The Origin of Electron Donor-Acceptor Complexes, Hydrogen Bonding, and Proton Affinity," *Acc. Chem. Res.*, vol. 10, pp. 294–300, 1977.

[189] J. P. Foster and F. Weinhold, "Natural hybrid orbitals," *J. Am. Chem. Soc.*, vol. 102, pp. 7211–7218, 1980.

[190] F. L. Hirshfeld, "Bonded-atom fragments for describing molecular charge densities," *Theor. Chim. Acta*, vol. 44, pp. 129–138, 1977.

[191] A. D. Becke and K. E. Edgecombe, "A simple measure of electron localization and molecular systems," *J. Chem. Phys*, vol. 92, pp. 5397–5404, 1990.

[192] P. F. Zou and R. F. W. Bader, "Variational principle and path integrals for atoms in molecules," *Int. J. Chem.*, vol. 43, pp. 677–699, 1992.

[193] U. C. Singh and P. A. Kollman, "An approach to computing electrostatic charges for molecules," *J. Comp. Chem.*, vol. 5, pp. 129–145, 1984.

[194] C. M. Breneman and K. B. Wiberg, "Determining atom-centered monopoles from molecular elctrostatic potentials. The need for high sampling density in formamide conformational analysis," *J. Comp. Chem.*, vol. 11, pp. 361–373, 1990.

[195] I. Rodriguez, G. Sastre, A. Corma, and S. Iborra, "Catalytic Activity of Proton Sponge: Application to Knoevenagel Condensation Reactions," *J. Catal.*, vol. 183, pp. 14–23, 1999.

[196] A. Corma, S. Iborra, I. Rodriguez, and F. Sanchez, "Immobilized Proton Sponge on Inorganic Carriers: The Synergic Effect of the Support on Catalytic Activity," *J. Catal.*, vol. 211, pp. 208–215, 2002.

[197] D. Kim, T. B. Lee, S. B. Choi, J. H. Yoon, J. Kim, and S. Choi, "A density functional theory study of a series of functionalized metal-organic frameworks," *Chem. Phys. Lett.*, vol. 420, pp. 256–260, 2006.

[198] A. Corma, V. Fornes, R. M. Martin-Aranda, and F. Rey, "Determination of base properties of hydrotalcites: Condensation of benzaldehyde with ethyl acetoacetate," *J. Catal.*, vol. 134, pp. 58–65, 1992.

[199] M. Climent, A. Corma, V. Fornés, A. Frau, R. Guil-Lopez, I. S., and J. Primo, "Aluminophosphates Oxynitrides as Base Catalysts: Nature of the Base Sites and Their Catalytic Implications," *J. Catal.*, vol. 163, pp. 392–398, 1996.

[200] R. Cortese and D. Duca, "A DFT study of IRMOF-3 catalyzed Knoevenagel condensation," *Phys. Chem. Chem. Phys.*, vol. 13, pp. 15995–16004, 2011.

[201] D. W. Christianson and W. N. Lipscomb, "Carboxypeptidase A," *Acc. Chem. Res.*, vol. 22, pp. 62–69, 1989.

[202] R. M. Martin, *Electronic Structure*. Cambridge University Press, 2004.

[203] C. J. Cramer, *Essential of Computational Chemistry*. WILEY, 2004.

[204] J. P. Perdew and K. Schmidt, "Jacob's ladder of density functional approximations for the exchange–correlation energy," *AIP Conference Proceedings*, vol. 577, pp. 1–20, 2001.